Synthesis of novel backbone functional polymers

Daniel C. Lee

A dissertation

submitted in partial fulfillment of the

requirements for the degree of

Doctor of Philosophy

University of Washington

2020

Reading Committee:

Suzie H. Pun, Chair

Cole A. DeForest

David S. Ginger Jr.

Matthew R. Golder

Program Authorized to Offer Degree:

Bioengineering

University of Washington

Abstract

Synthesis of novel backbone functional polymers

Daniel C. Lee

Chair of the Supervisory Committee:

Suzie H. Pun

Department of Bioengineering

Due to their synthetic versatility, high processability, relatively low material costs, and useful properties, polymers are ubiquitous in modern life, from yoga mats and backpacks to construction materials and medical supplies. In many of these applications, polymers are used as plastics, for their thermal and oxidative stability, and chemical inertness. Over the last few decades, however, there have been many advances in functional polymers: polymers designed to play active roles in a variety of applications, such as stress sensing and targeted drug delivery. This thesis describes the work done in the synthesis, characterization, and use of three different polymers whose functions are derived from the polymer backbone. In Chapter 3, vinyl-addition polynorbornenes are explored for their intrinsic mechanochemical reactivity, a property that is unique to polymers of high molecular weight. In Chapter 4, anionic poly(cyclopentadienylene vinylene)s are explored

for their charge transport properties along the polymer backbone (and between them). In Chapter 5, polymers with reversible molecular recognition pairs are explored for the stimuli-responsive folding and unfolding behaviors of their backbones.

TABLE OF CONTENTS

LIST OF FIGURES

LIST OF TABLES

ACRONYMS AND INITIALISMS

ATRP	atom transfer radical polymerization
CP	π-conjugated polymer
CPE	π-conjugated polyelectrolyte
CycEE	cyclic enol ether
CycP	cyclic polymer
CH	conductive hydrogel
CM	cardiomyocyte
CTA	chain transfer agent
DSC	differential scanning calorimetry
DMA	dynamic mechanical analysis
ED-ROMP	entropy driven ring opening metathesis polymerization
Đ	dispersity
EVE	ethyl vinyl ether
FTO	fluoride doped tin oxide
G2	Grubbs II generation catalyst
G3	Grubbs III generation catalyst
GmMA	glycerol monomethacrylate
GPC	gel permeation chromatography
macro-CTA	macro chain transfer agent
MALDI-TOF/MS	matrix assisted laser desorption ionization mass spectrometry
NMR	nuclear magnetic resonance
oxy-endo CycEE	cyclic enol ether with the oxygen endo to the ring
oxy-exo CycEE	cyclic enol ether with the oxygen exo to the ring
polySTAT	engineered hemostatic polymer
TGA	thermal gravimetric analysis
M_n	number average molecular weight
M_w	weight average molecular weight
RAFT	reversible addition-fragmentation chain-transfer polymerization
RDRP	reversible-deactivation radical polymerization

ROMP	ring opening metathesis polymerization
ROP	ring opening polymerization
SANS	small angle neutron scattering
T_g	glass transition temperature
T_d	temperature for decomposition onset
THF	tetrahydrofuran
TMAB	tetramethoxyazobenzene
TMAB-MA	tetramethoxyazobenzene methacrylate
TMAB-TEG	tetramethoxyazobenzene triethylene glycol
qPCR	quantitative polymerase chain reaction
VA-PNB	vinyl addition polynorbornene

ACKNOWLEDGEMENTS

Thank you, AJ B. and Suzie H. P., for being exemplary role models and mentors. I appreciated that you granted me incredible flexibility to pursue my academic interests and grounded me when I got *too* excited. I truly believe my graduate school experience working both *for* and *with* you have prepared me well for my future career. I would like to specially thank Suzie for graciously adopting me into your group, supporting my request for a fume hood in CHB, and trusting me, a novice Punion, to execute on a high-risk project.

Thank you, David S. G. and Matt R. G., for letting me use your space in CHB, involving me in your group research, and serving on my committee. Providing a fume hood and a desk in CHB have saved me over 100 hours of walking back and forth from the NMR spectrometers. I will forever be grateful and owe a large portion of my success in graduate school to your generosity.

Thank you, Buzzy M. and Loch H., for making my experiences with purchasing, traveling, and shipping so easy. I was only able to achieve so much in graduate school because of all the work you do in the background for us students.

Thank you, Adrienne M. R., Martin S., and Rajan K. P., for making it so easy, fun, and informative to use the various instruments you oversee. Your friendliness, approachability, and willingness to go above and beyond the request made me feel very welcome and willing to learn more about the instruments and associated techniques.

Thank you, Alex N. P., Fan L., Meilyn R. S., and Trey P., for agreeing to be my experimental mentees as I struggled to find my mentor identity. I learned so much from working with you (both how to be a good mentor and about myself) and I hope you got a lot out of our meetings. My future graduate students owe you a lot.

Thank you, Bob J. L., Drew L. S., and Gary W. L., for teaching me everything I know about cells, listening to me complain, and mentoring me in patience, kindness, professionalism, career development, and navigating work relationships.

Thank you, Ty D. J. and Dylan C. S., for all the fun nights. I'm glad we still regularly met for nachos despite our increasingly busy schedules. We've come a long way since we started 4 years ago!

Thank you, Brock E. L., for being a dear friend and my science sounding board. My best ideas have always come from arguing chemistry with you. I will always cherish the memories of us sharing a fume hood and the late nights in the lab.

Lastly, thank you, Fischer and Miguel, for lifting me up during the tough times, laughing with me during the good times, coaching me through the confusing times, and supporting my work, always. I will always value your input on the tough crosswords.

DEDICATION

Chapter 1. THREE APPROACHES TO POLYMER SYNTHESIS

There are three ways I think about polymer synthesis. These three ways are not mutually exclusive, are all useful in certain situations, and are all limiting in their own way.

One way is to group polymers by their polymerization method. For example, polymers made by reversible-deactivation radical polymerizations (RDRP) would be in one category and polymers made by ring-opening metathesis polymerization (ROMP) would be in another. This is the most practical view of polymer synthesis for three reasons (and this viewpoint is the one I adopted for my review[1]). First, polymers made by the same method are similar; polymers made by RDRP have hydrogenated aliphatic backbones, and polymers made by ROMP have residual alkenes in the backbone. Second, from a practical standpoint, academic labs that do not specialize in polymer methodology can still become proficient at certain polymerization systems by accumulating reagents for and knowledge of the nuances of said polymerization, allowing them to make and use polymers in ways never imagined by a polymer methodology lab. Lastly, many people have adopted this viewpoint and published detailed reviews for each polymerization type, resulting in a vast field of utility-based information about each polymerization. Not sure if reversible addition-fragmentation chain-transfer polymerization (RAFT) will fit your needs? Have you read *The Handbook of RAFT Polymerization*[2] or *50th Anniversary Perspective: RAFT Polymerization-A User Guide*?[3] However, this approach to thinking of polymers is limiting in two ways. First, becoming accustomed to thinking about polymer synthesis through existing mechanisms limits the potential creativity of researchers. Second, it fails to capture the complexity of monomers that are amenable to multiple types of polymerization. For example, norbornene can be polymerized into vinyl-addition type polymers as well as ROMP polymers.[4] Conversely, the same polymers can be made by different polymerization methods.[5]

A second way of thinking of polymer synthesis is to group polymers by their constituent monomers. This is useful for two reasons because polymer nomenclature is such that they are named by the monomer with which they are made. Specifically, polymethacrylates, made by methacrylates, are identical regardless of whether they were made by atom transfer radical polymerization (ATRP) or reversible addition-fragmentation chain-transfer polymerization (RAFT). This way of thinking is limiting because it fails to properly describe polymers that are reacted post-polymerization into a different polymer,[6–13] and situations in which a single monomer can be polymerized by a single method into different polymers based on changes made to the initiator.[14]

A third way of thinking of polymer synthesis is to group polymers by function. This is the unifying theme of the thesis. This approach is the least defined, the least useful, but (I believe) the most interesting. Polymerization methods, monomer classes, and other practical considerations for synthesis are secondary. There are many "functions" that can be achieved with the use of polymers. Functions that arise from polymer backbones are unique to polymers and the most interesting to me. My three main projects (Chapters 3, 4, 5) look at polymer properties that can be defined by some function along the axis of the polymer backbone. In Chapter 3, I explore an intrinsically mechanochemically active polymer backbone. Mechanochemistry is a property unique to polymers with high degrees of polymerization and works along the axis of the polymer backbone. In Chapter 4, I synthesize, characterize, and use π-conjugated polymers which exhibit charge transport along the polymer backbone (and between them). In Chapter 5, I synthesize and characterize folding polymers which change their end-to-end distance in response to stimuli.

This approach to polymer synthesis, however, is also limiting. Designing backbone-derived functions often requires thinking about a single polymer chain in a vacuum. However, polymer

chains rarely exist as single chains and thus translation of single-chain technologies into useful devices and systems can be difficult. For example, polymer films, even of nanometer thickness, still require accounting for interpolymer interactions to optimize properties such as surface morphology. Single-chain technologies can be deployed in solution but would require ultra-dilute conditions, making them difficult to scale due to volume limitations.

Chapter 2. USING MORE THAN ONE POLYMERIZATION IN THE SYNTHESIS OF A SINGLE POLYMER[1]

2.1 ABSTRACT

Block copolymers with unique architectures and those that can self-assemble into supramolecular structures are used in medicine as biomaterial scaffolds and delivery vehicles for cells, therapeutics, and imaging agents. To date, much of the work relies on controlling polymer behavior by varying the monomer side chains to add functionality and tune hydrophobicity. Although varying the side chains is an efficient strategy to control polymer behavior, changing the polymer backbone can also be a powerful approach to modulate polymer self-assembly, rigidity, reactivity, and biodegradability for biomedical applications. There have been many developments in the syntheses of polymers with segmented backbones, but these developments have not been widely adopted as strategies to address the unique constraints and requirements of polymers for biomedical applications. In this review, we highlight dual polymerization strategies for the synthesis of backbone-segmented block copolymers to facilitate their adoption for biomedical applications.

2.2 INTRODUCTION

Recent advancements in polymerization techniques have afforded the ability to control, with unprecedented precision, the composition, sequence, molecular weight, size distribution, and mechanical and chemical properties of polymers. In turn, the precision synthesis of polymers has enabled the development of highly tunable materials for use in tissue engineering, drug delivery, and biomaterial implants. As of 2017, there were 8 polymeric micelle systems in clinical trials for

evaluation as cancer treatments.[15] Polymeric systems are also used in FDA-approved platforms for prolonged drug delivery.[16] While there has been tremendous progress in both basic polymer science and translation into biomedical applications, there remain many unsolved challenges that can potentially be addressed with new monomers, sequences, or polymeric architectures. Block copolymers (BCPs), polymers with distinct repeat units connected by covalent bonds, are particularly interesting as their behaviors differ from a physical blend of the homopolymers.

The development of reversible-deactivation radical polymerization (RDRP) and other polymerizations such as ring-opening metathesis polymerization (ROMP) with "living" characteristics have enabled chemists to synthesize BCPs using a single polymerization by sequential addition of monomer to a growing polymer chain end. These advancements in polymer synthesis have vastly expanded the potential for polymer structures.[17] Polymer with unique architectures such as block, star, comb, brush, knot and cyclic polymers (Figure 2.1, upper) have been shown to affect the mechanical properties of biomaterials and affect administration route, biodistribution, and cargo loading of polymeric drug delivery systems.[18–23] Star polymers with internal hydrophobic blocks are used to encapsulate poorly-soluble drugs, followed by hydrophilic blocks that ensure hydration and prevent aggregation.[24] Star polymers have also been used for imaging and diagnosis.[25] Comb and brush polymers have been designed to contain hydrophobic regions to encapsulate and deliver paclitaxel,[26] doxorubicin,[27] and imaging agents, or to incorporate cationic monomers to complex with nucleic acids for gene delivery applications.[28,29] Cyclic polymers have longer circulation times compared to their linear analogs[21,30] and have been used as a multimacroinitiator in the synthesis of sunflower polymers for drug and nucleic acid delivery.[22,31] Other single-molecule polymeric structures, such as hyperbranched polymers and dendrimers, have made an impact in tumor targeting.[19,23]

Some of these polymeric architectures, as well as linear amphiphilic polymers, allow for self-assembly into supramolecular structures.[32,33] These supramolecular structures (Figure 2.1, lower) contain regions of hydrophobicity and regions of hydrophilicity with controlled sizes that can be designed by the user to sequester drugs, protect proteins from the immune system, adsorb to surfaces in the presence of a stimulus, and perform many tasks not possible with prior tools. Micelles that contain a hydrophobic core have been used to store hydrophobic cargo such as chemotherapeutics, hormones, and imaging agents in both academic and clinical settings.[15,34] Micellar structures can also utilize stimulus-responsive bonds to improve the stability of drug-micelle complexes[35], or crosslinked cores to prolong stability *in vivo*.[36] Polymeric micelles have medical applications beyond drug delivery, and have been studied extensively as diagnostic agents.[37,38]

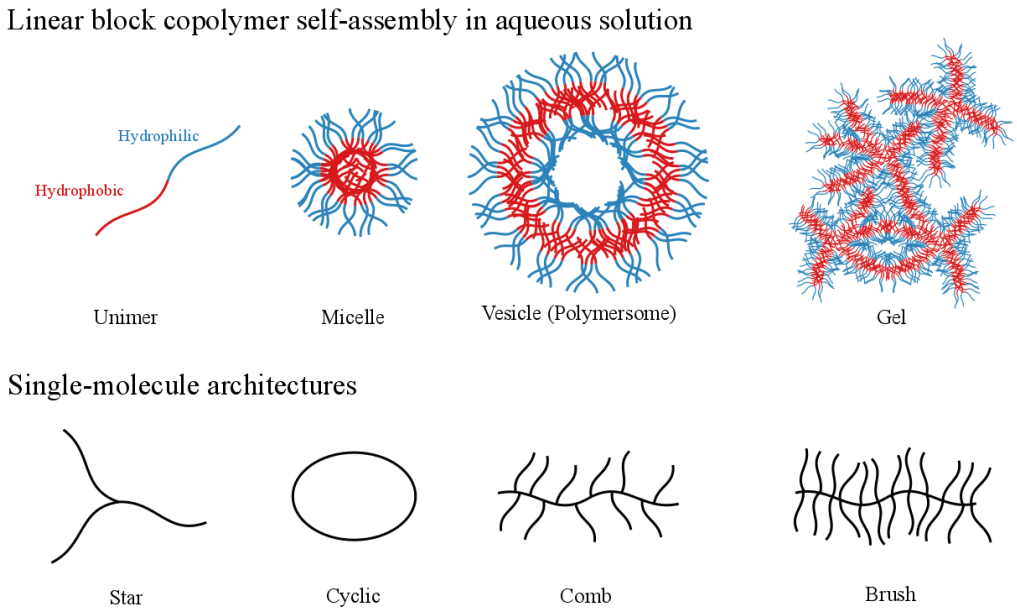

Figure 2.1. Polymers structures often used for biological applications. Above, amphipathic polymers can form supramolecular structures including spherical micelles, vesicles, and gels. Below, single-molecule structures including stars with various numbers of arms arm, cyclic polymers, comb polymers, and brush polymers have been used with success for the delivery of therapeutics and diagnostics.

Polymeric micelles have medical applications beyond drug delivery, and have been studied extensively as diagnostic agents.[37,38] Polymersomes, bi-layer vesicles consisting of polymer building blocks,[39] have also been used to deliver hydrophobic chemotherapeutics such as doxorubicin and paclitaxel,[40] and hydrophilic molecules such as genes[41] and proteins.[42] Polymersomes exhibit prolonged circulation in the body due to diminished opsonization compared to liposomes and slower kinetics of disassembly below the CMC due to the greater molecular weight of the building blocks.[39,43,44] Stimuli responsive polymersomes have been developed to increase the precision of drug release. For example, reduction-sensitive polymersomes are used for intracellular delivery of cargo in response to higher intracellular concentrations of reducing agents such as glutathione compared to the extracellular environment.[45] There are multiple excellent reviews on stimuli-responsive polymersomes with potential stimuli including pH, temperature, redox potential, light, and others.[46–48][49]

Gels made with polymers with side chains that promote gelation at varied temperatures such as hydroxyethyl methacrylate (HEMA) or n-isopropylacrylamide (NIPAM) can be made to be sensitive to temperature and pH.[50] Notably, temperature-sensitive BCPs with lower critical solution temperature (LCST) between room temperature and physiological temperature have been used as injectable materials since they are liquid upon injection, but can gel within the body.[51] This form of polymeric system is used in an FDA-approved platform for sustained drug delivery.[16] Additionally, self-assembled structures can be aggregated to form larger, irregular structures. One such example is that of micellar agglomerates which start as a multimodal population of nanoscale micelles, but after an increase in temperature undergo a phase transition forming macroscale gels.[52]

In these applications, the polymer behavior is often manipulated by modifying the polymer side chains and not the polymer backbone. While the monomer side chains of BCPs heavily dictate the behavior and properties of BCPs, the polymer backbone can also be used to impart biodegradability, reactivity,[40] as well as other behaviors and properties that cannot be achieved by changing the monomer side chains. For example, the polymer backbone of guanidinium side chain containing polymers has been shown to affect the cellular uptake of siRNA and proteins differently.[53] Additionally, some approaches to synthesize backbone segmented BCPs allow for the inclusion of stimuli responsive moieties between polymer blocks.[54,55]

The ability to segment the BCP backbone into different repeats is a powerful tool to further engineer the behavior and properties of polymeric materials. Because a polymerization is multiple turnovers of the same reaction, it results in a repetitive backbone structure. For example, radical polymerization of vinyl groups results in an aliphatic backbone and ring opening polymerization of cyclic electrophilic monomers results in a backbone with electrophilic repeats.

One effective approach to achieve BCPs with segmented backbone structures is to employ more than one polymerization. To date, there have been many developments in these dual polymerization approaches, but these developments have not been widely adopted as strategies to address the unique constraints and requirements of polymers used in biomedical applications. For this review, dual polymerizations include any approaches that use more than one unique polymerization, even if the polymer is isolated between polymerizations. We highlight useful synthetic strategies to facilitate the exploration of backbone-segmented BCPs in biomedical applications. Eventually, further developments in polymer synthesis will enable more feasible permutations of backbones and side chains, expanding the potential repertoire of highly engineerable materials for biomedical applications.

In this review, we focus on syntheses of backbone segmented polymers by the use two or more polymerization systems. We start with a description of BCPs and their applications, followed by an overview of each polymerization method individually, and then a survey of different polymerizations that have been combined in the synthesis of unique BCPs. Although viable options for synthesizing BCPs, polymer-polymer couplings and conjugation with poly(ethylene glycol) exceed the scope of this review.

2.3 Controlled Polymerization Techniques

2.3.1 *Atom Transfer Radical Polymerization (ATRP)*

ATRP is a proven strategy for the precision synthesis of polymers for biomaterials.[56] ATRP is a reversible-deactivation radical polymerization (RDRP) technique pioneered by Matyjaszewski and coworkers in 1994 that utilizes a transition metal complex to reduce the number of active chain ends in solution.[57] ATRP is well-studied and developed for broad monomer scope and tunable kinetics,[58] and results in a non-biodegradable polymer backbone whose behavior can be dictated by the monomer side chains. Many functionalized methacrylates and acrylates compatible with ATRP are commercially available. Additionally, methacryloyl chloride and related compounds are also commercially available, allowing for in-house synthesis of custom monomers. For example, cyclodextrin-functionalized methacrylates have been made for ATRP.[59] Commercially available compounds such as α-bromoisobutyryl bromide allow for synthesis of custom initiators.

ATRP has three potential drawbacks for biomedical applications. One drawback is that ATRP has limited functional group tolerance. Vinyl monomers with charged side groups are difficult to polymerize by ATRP. ATRP can be successful in water, but must be carefully designed to control initiation and minimize catalyst degradation.[60,61] Another drawback is that the aliphatic polymer backbone is not biodegradable. One final drawback is the residual levels of copper in polymers

made by ATRP may be toxic at concentrations as low as 5 ppb.[62] To mitigate this last drawback, there have been many advances over the past 20 years minimizing the use of copper in ATRP including reverse ATRP, activators regenerated by electron transfer (AGET) ATRP, initiators for continuous activator regeneration (ICAR) ATRP, and supplemental activators and reducing agents (SARA) ATRP, electrochemical ATRP (eATRP), photoinduced electron transfer ATRP, organocatalyzed ATRP and sonication-induced ATRP.[56,63] Reverse and eATRP are mentioned later in this review. Unlike conventional ATRP, in which Cu(I) is introduced to initiate the polymerization, in reverse and eATRP Cu(II) is reduced *in situ* to produce Cu(I). In reverse ATRP, a thermal radical initiator is used to reduce Cu(II) to Cu(I); in eATRP, electrodes can be used to reduce the copper resulting in the active species.

2.3.2 *Reversible Addition-Fragmentation Chain Transfer (RAFT)*

RAFT is a robust polymerization strategy for a wide variety of vinyl monomers. RAFT maintains a low concentration of active chain end species by degenerative transfer onto a chain transfer agent (CTA).[64] Since its introduction by Chiefari *et al*. in 1998,[65] RAFT has been widely adopted for the synthesis of polymers for biomedical applications due to its wide functional group tolerance, tunable kinetics, and ease of use. Like ATRP, RAFT results in a non-biodegradable polymer backbone whose behavior can be dictated by the monomer side chains. RAFT can be used to polymerize methacrylates, acrylates, methacrylamides, acrylamides, vinyl esters, and vinyl amides.[3] Methacryloyl chloride and related compounds are commercially available starting materials for the synthesis of custom RAFT monomers. Additionally, many CTAs are commercially available.

Of the three drawbacks mentioned for ATRP, RAFT overcomes both the limited functional group tolerance and the use of a copper catalyst. Due to the broad functional group compatibility

of RAFT, monomers with polar side chains can be polymerized in aqueous and organic solvents. RAFT has been used to polymerize monomers with pendant biomolecules.[66–68] RAFT polymerization has been performed on the surface of biologics, including living cells,[69] and has been shown to work in complex solvents like wine.[70] Additionally, RAFT polymerizations do not use a metal catalyst, eliminating the need for metal removal and further purification.

While the use of RAFT CTAs over ATRP has its advantages, it comes with its own limitations. RAFT CTAs are expensive to purchase and difficult to synthesize. Additionally, some CTAs are hydrolytically unstable.[71]

2.3.3 *Ring Opening Polymerization (ROP)*

ROP is a diverse class of polymerizations for cyclic electrophilic monomers such as N-carboxyanhydrides (NCAs), lactides, lactams, polycarbonates, and related compounds. Aside from water-sensitive condensation reactions, ROP is the most common way to synthesize polymers with biodegradable polyester or polyamide backbones. Biodegradability, and the subsequent potential for biocompatibility has led to the use of ROP-synthesized polymers in many biomedical applications.[72]

The synthetic approaches to ROP are more varied than the previously mentioned polymerizations. ROP can be catalyzed by acids, bases, organometallic complexes, and enzymes.[73–79] Because alcohol and amine groups are common nucleophiles used to initiate ROP, drugs with these heteroatoms can be used to initiate ROP. For example, regioselective activation of a hydroxyl group in paclitaxel can be used to initiate ROP of lactide.[80] Polylactones, polylactides, and polyNCAs/polypeptides are common in biomedical applications due to their biocompatibility and biodegradability. Blocks of ROP polymers are commonly used to make up the core of self-assembled structures since high molecular weight polyesters are hydrophobic.

However, ROPs have limited functional group tolerance. Because ROPs require a nucleophile to open the ring of the electrophilic cyclic monomers, other heteroatoms like water or free alcohols can interfere with the polymerization, making polymerization difficult in some laboratory conditions. This sensitivity also makes functionalizing ROP monomers difficult; it is more common to functionalize the side chains post-polymerization, however specific chemistries are required to effect efficient functionalization of ROP polymer side chains.[81]

2.3.4 *Ring Opening Metathesis Polymerization (ROMP)*

ROMP of strained cyclic monomers is a useful strategy for the synthesis of functionalized polymers. Many different transitional metal metathesis catalysts have been developed, each with its own advantages, but it was the commercial production of ruthenium-based metathesis catalysts that made ROMP feasible for bioapplications due to its functional group tolerance.[82,83] ROMP backbones are olefinic and often hydrophobic, but the olefins can be further reacted to make the polymers biodegradable; for example, the olefins in the ROMP backbone of poly(oxanobornene) were reacted to make alginic acid mimics.[84] ROMP has broad functional group tolerance and has been used to make polymers with peptides, imaging agents, and therapeutics.[85–89]

Due to use of Ru catalysts for ring closing metathesis in commercial pharmaceutical synthesis, there has been extensive work in modifying Grubbs' ruthenium-based catalysts for metatheses in aqueous and organic solvents.[90–92] Additionally, there are many commercially available ROMP monomers and catalysts. Custom ROMP monomers can also be synthesized by thermally cracking commercially available dicyclopentadiene, and reacting cyclopentadiene with functionalized alkenes, resulting in a functionalized norbornene molecule. Ru ROMP catalysts are often extremely active and can be used to polymerize macromonomers with both synthetic polymers and large bioactive molecules as side chains.[83,93]

There are two main disadvantages to ROMP. First is that Ru transition metal complexes are toxic, and thus the International Conference on Harmonization guidelines limit permissible ruthenium exposure.[94] While there has been recent advances in ruthenium purification, these strategies are energy intensive.[90–92] Another drawback is that commercially available catalysts for ROMP are expensive. This problem is compounded by the fact that unlike the ring closing metathesis commonly used by the pharmaceutical industry, in ROMP, the [Ru] species acts as the initiator and is thus attached to the polymer chain, preventing it from being easily recycled in a catalytic cycle.

2.4 Strategies for Dual Polymerizations

Developments in RDRPs and other living polymerizations have made sequence-controlled synthesis of BCPs easier by allowing one-pot techniques such as sequential monomer addition. Employing multiple polymerizations for the synthesis of segmented backbone polymers offers an additional level of control over polymer behavior and characteristics. For example, combining hydrophobic biodegradable poly(lactic acid) with hydrophilic nonbiodegradable poly(HEMA) may confer new pharmacokinetic properties to the polymer. This section reviews works that use two or more different polymerizations in the synthesis of a single material and is organized by three main approaches:

1. The use of orthogonal polymerizations (often in a single pot)
2. Post-polymerization functionalization with a new initiator motif
3. Post-polymerization functionalization with a new monomer motif

Figure 2.2 has a schematic road map for using dual polymerizations to synthesize BCPs with different architectures.

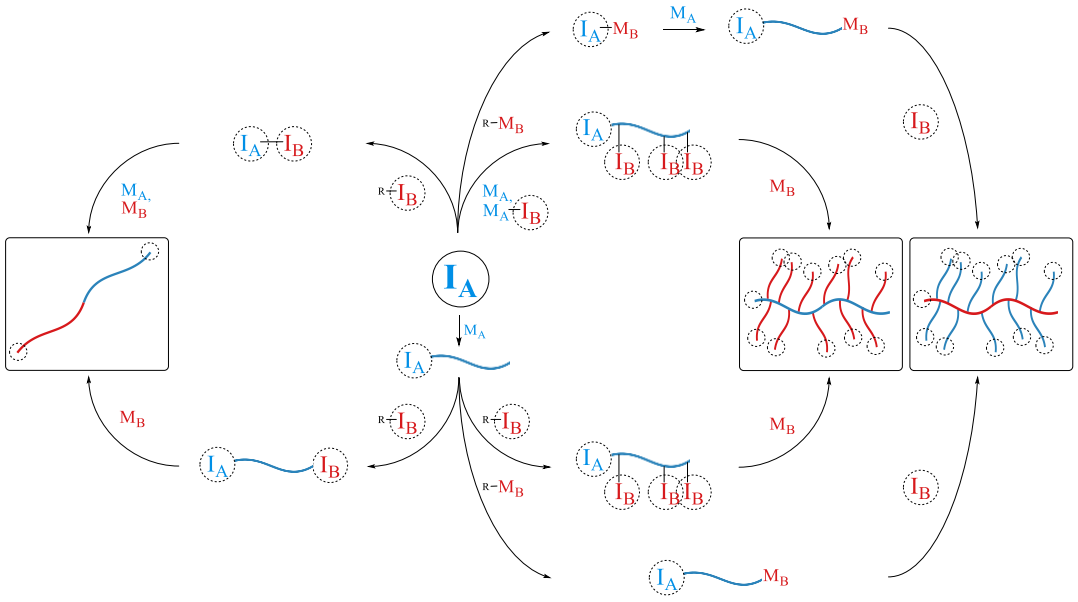

Figure 2.2. Schematic road map for using dual polymerizations to synthesize BCPs with different architectures.

2.4.1 *Orthogonal Polymerizations in One Pot*

One approach to the synthesis of BCPs is the use of two or more orthogonal polymerizations. A successful pairing of two orthogonal polymerizations for the synthesis of BCPs allows a one-pot polymerization and removes the need for intermediate deprotection or purification. However, orthogonal polymerization systems must be carefully selected as the reagents and conditions necessary for one polymerization may interfere with or initiate the second polymerization, resulting in loss of polymerization control. For example, small levels of acrylates can cause early irreversible termination of ROMP;[95] some CTA_{RAFT} are susceptible to aminolysis and may be incompatible with the use of strong bases or substituted amines, both of which are commonly used for ROP and the latter of which are used as ligands in ATRP.[71]

The use of orthogonal polymerizations can be further broken down into two approaches. The first approach involves the use of a single difunctional initiator I_A-I_B in which I_A only reacts in

polymerization system A and I_B only reacts in polymerization system B. As there is a thorough review on this topic published in 2006, this section focuses on developments in this approach since 2006.[96]

The second approach involves the polymerization of an inimer M_A-I_B, a monomer that contains both the monomer motif for polymerization A (M_A) and an initiator motif for polymerization B (I_B); initiator I_B does not polymerize monomer M_A and only polymerizes monomer M_B in a subsequent polymerization.

2.4.1.1 The Use of a Single Difunctional Initiator

2.4.1.1.1 *ROP-RAFT Initiator-Chain Transfer Agent I_{ROP}-CTARAFT (inifers)*

Combining ROP with radical polymerizations is useful for biomedical applications. ROP can be used to make biodegradable blocks while the radical polymerization can be used to make stable blocks for prolonged circulation. Many difunctional ROP-RAFT inifers (I_{ROP}-CTA_{RAFT}) in which one end contains an alcohol or amine (I_{ROP}) and the other contains a trithiocarbonate, dithiobenzoate, or xanthogenate (CTA_{RAFT}) have been used to make block copolymers. These inifers have been used to copolymerize a variety of vinyl monomers with many cyclic ester monomers with dispersities lower than 1.1.[97–101] These polymerizations can be done in one pot, simultaneously or sequentially, suggesting that the polymerizations are orthogonal. The incorporation efficiency of RAFT monomer and ROP monomer into the final polymer can be adjusted by changing the monomer feed ratio or catalyst loading. Additionally, this strategy has been used to incorporate thiols in the RAFT chain and subsequently attach biologically relevant molecules for cell adhesion or metal chelators for imaging applications.[99]

Due to the relatively low reactivity of the alcohols and the mild conditions for RAFT, water and free alcohols do not significantly hydrolyze CTA_{RAFT} within the timeframe of the

polymerization. In fact, some common RAFT monomers have pendant alcohol groups. Unlike alcohols, however, primary and secondary amines must be protected as they are reactive enough to aminolyze the CTA under common polymerization conditions, leading to early irreversible termination of the RAFT chain end and poor control over molecular weight distribution.[71] The Zhang group used an inifer (I_{ROP}-CTA_{RAFT}) for amine-initiated ROP of N-carboxyanhydride and RAFT of NIPAM and found their polymerization resulted in block copolymers of lower dispersity if the ROP-initiating amine was protected during RAFT.[102]

2.4.1.1.2 *ROP-ATRP Difunctional Initiators I_{ROP}-I_{ATRP}*

Many difunctional ROP-ATRP initiators (I_{ROP}-I_{ATRP}) in which one end contains an alcohol or amine (I_{ROP}) and the other contains a substituted halide (I_{ATRP}) have been used to make block copolymers.[103–106] These polymerizations can be done simultaneously or sequentially in a single pot, making it an attractive option in the synthesis of block copolymers. This combination is robust and synthetically accessible as α-bromoisobutyryl bromide and related compounds are commercially available and can be reacted with multivalent alcohols to synthesize I_{ROP}-I_{ATRP}. Because these conjugation reactions can be carried out under mild conditions, stimuli-responsive linkages can also be incorporated. For example, I_{ROP}-I_{ATRP} connected by a disulfide linkage was synthesized by coupling chemistry and used to grow p(lactic acid)-*block*-p(OEGMA) (Figure 2.3).[107] The amphiphilic polymers were used to make micelles which were found to be non-toxic to HeLa cervical cancer cells and, upon introduction of dithiothreitol, cleave at the disulfide linkage that covalently bound the hydrophobic and hydrophilic blocks, resulting in disassembly of the micelle.

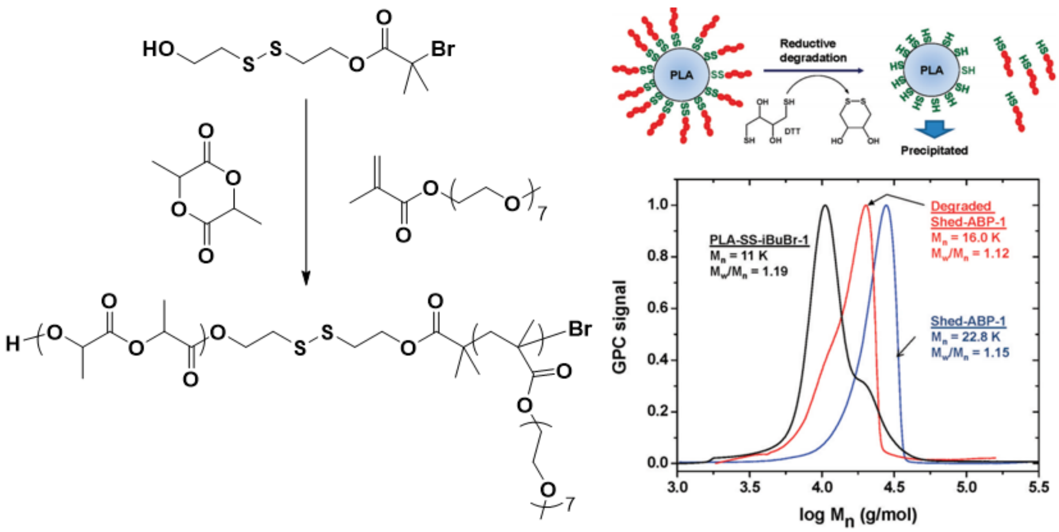

Figure 2.3. ROP/RAFT from a single difunctional initiator. The polymer has been used to make stimuli responsive micelles. Reprinted with permission from Sourkohi, B. K. *et al.* Biodegradable Block Copolymer Micelles with Thiol-Responsive Sheddable Coronas. *Biomacromolecules* **12,** 3819–3825 (2011). Copyright 2018 American Chemical Society.

One interesting application of I_{ROP}-I_{ATRP} is the incorporation of a radical generator in the middle of a difunctional initiator. The Chang group showed simultaneous ROP and reverse ATRP by the use of an I_{ROP}-azo-I_{ROP} initiator in which the azo bond disassociates upon heating and produces two active radical chains.[108] The addition of Cu(II) allowed the control of the radical chain end via reverse ATRP and resulted in polymers with lower dispersity when compared to the polymerization done without Cu(II). When the reaction is heated to 90 ˚C, only the reverse ATRP polymerization proceeds. But heating the polymerization to >110 ˚C in the presence of the $Sn(oct)_2$ resulted in simultaneous ROP and reverse ATRP.

As mentioned in the ROP-RAFT section, there are potential concerns of reagents in one polymerization negatively affecting the second polymerization. However, it is also possible to use a single non-monomer reagent for both polymerizations. We found this to be common for the ROP-

ATRP combination. For example, a tin species can be used both as a catalyst for ROP and a reductant for copper in reverse ATRP;[109] a substituted amine can be used both as a catalyst for ROP and a ligand for copper in ATRP.[110,111] The use of shared substituted amines between ROP and ATRP has also been demonstrated when the ROP was mediated by lipase Novozym 435.[112] PMDETA and dNbpy, common copper ligands in ATRP, can also be used to coordinate metal ions in solution which would otherwise coordinate to the histidine in the lipase active site and prevent the enzyme-catalyzed ROP.

In a particularly interesting use of enzyme-mediated ROP, the Meijer group used Novozym 435 to make an enantiomerically rich p((S)-4-methyl-caprolactone).[113] (S)-caprolactone was found to be more active towards polymerization by Novoyzm 435; to prevent the (R) enantiomer from polymerizing at low concentrations of (S)-caprolactone, a Ni species was intentionally introduced into the polymerization to deactivate the lipase to prevent polymerization of the less active enantiomer once most of the (S)-caprolactone was polymerized. The Ni species also acted as a reductant for subsequent ATRP.

2.4.1.1.3 *ATRP-RAFT I_{ATRP}-CTA_{RAFT}*

Difunctional ATRP-RAFT inifers have been synthesized and used to perform simultaneous and sequential ATRP and RAFT. These difunctional inifers have been made with a stimuli-responsive linker which upon application of the specified stimulus can result in cleavage of the diblock copolymer. Thiol/redox sensitive difunctional inifers connected by a disulfide linkage have been used to make polymeric micelles with sheddable coronas; these polymers have been used for more efficient gene transfection of neurons when decorated with the Tet1 peptide.[54] Acid-cleavable diblock copolymers have also been made with the potential for application in nanofabrication and stimuli-responsive micelles.[55]

Because ATRP and RAFT both require the generation of a radical active chain end which is often mediated by a third species, there is significant potential for overlap; the use of a single organic photocatalyst for PET-RAFT and O-ATRP has recently been published.[114,115] The RAFT/ATRP combination has even been used to polymerize the same monomer.[114] Despite their similarities, however, difunctional I_{ATRP}-CTA_{RAFT} inifers can be used to polymerize different monomers on their respective chain ends. For example, pairs such as acrylate/styrene and methacrylate/acrylate have been used to make BCPs with ATRP and RAFT.[54,55,114–117]

2.4.1.1.4 ***ROMP-ATRP I_{ROMP}-I_{ATRP}***

The main consideration when employing ROMP-ATRP is the difference in polymerization kinetics between the two approaches. Because ROMP is generally much faster than any other living polymerization, ROMP must be slowed down in dual polymerizations by the addition of bulky monomers or low ring strain monomers. An active ROMP chain end with no ROMP monomer available can result in chain transfer which results in sequence scrambling and high dispersities. If this condition is met, it is possible to do dual ROMP-ATRP. In one example, a modified Grubbs catalyst (I_{ROMP}-I_{ATRP}) was used to synthesize poly(butadiene)-*block*-poly(methyl methacrylate).[118]

2.4.1.2 Polymerizing an initiator monomer M_A-I_B (inimer)

In this section, we review the use of an inimer (M_A-I_B) in which a single molecule has a monomer motif polymerizable in polymerization A (M_A) and an orthogonal initiator motif that does not react in the first polymerization (I_B). These pendant initiators (I_B) can be used to initiate subsequent polymerizations. This approach often results in a polymer with many initiating side chains, making it an attractive method to synthesize polymers with unique architectures. In all the examples described, while the first polymerization used for inimer M_A varied, the pendant initiator

(I_B) was almost always I_{ATRP}.[27,119–124] This may be because I_{ATRP}-functionalized monomers are easy to synthesize for the reasons described previously. To our knowledge, there are no examples of a monomer containing a pendant CTA_{RAFT} for subsequent RAFT, perhaps due to the relative cost and synthetic complexity of CTA_{RAFT} compared to I_{ATRP}.

The inimer approach has been used to make dendritic nanoparticles. The Guan group synthesized a hydrophobic core which was first synthesized by chain walking polymerization of ethene and a vinyl functionalized ATRP initiator.[120] ATRP was then used to grow a hydrophilic block with OEGMA which was terminated with an NHS ester functionalized acrylate. The terminal NHS were used to conjugate fluorescein and ovalbumin to demonstrate bioconjugation and the potential for this system in biomedical applications such as protein delivery and imaging.

Bottle-brush polymers with high grafting densities can also be synthesized by the inimer approach. In one example, RAFT was used to copolymerize a styrene and a maleimide-containing monomer, the latter of which was functionalized with both I_{ROP} and I_{ATRP} for their respective polymerizations.[27] In a different approach, a norbornene monomer functionalized with an I_{ROP} and an I_{ATRP} were polymerized by ROMP and then ROP and ATRP were subsequently initiated off the side chains.[119] The order of polymerization using this inimer can also be switched.[121]

The inimer approach has also been used to make structurally tailored and engineered macromolecular gels whose material properties can be modified by the application of a site-specific stimulus.[122] The Matyjaszewski group copolymerized an acrylate, a diacrylate, and an acrylate inimer M_{RAFT}-I_{ATRP} by RAFT, resulting in an initial gel. The gel was then dried and subsequently soaked in a DMF solution of copper and ATRP monomer. The gel was then irradiated to initiate ATRP from the pendant I_{ATRP}. A wide variety of monomers were used and yielded

segmented materials with hard and soft regions with different hydrophobic character, depending on which sections were irradiated for ATRP (Figure 2.4).

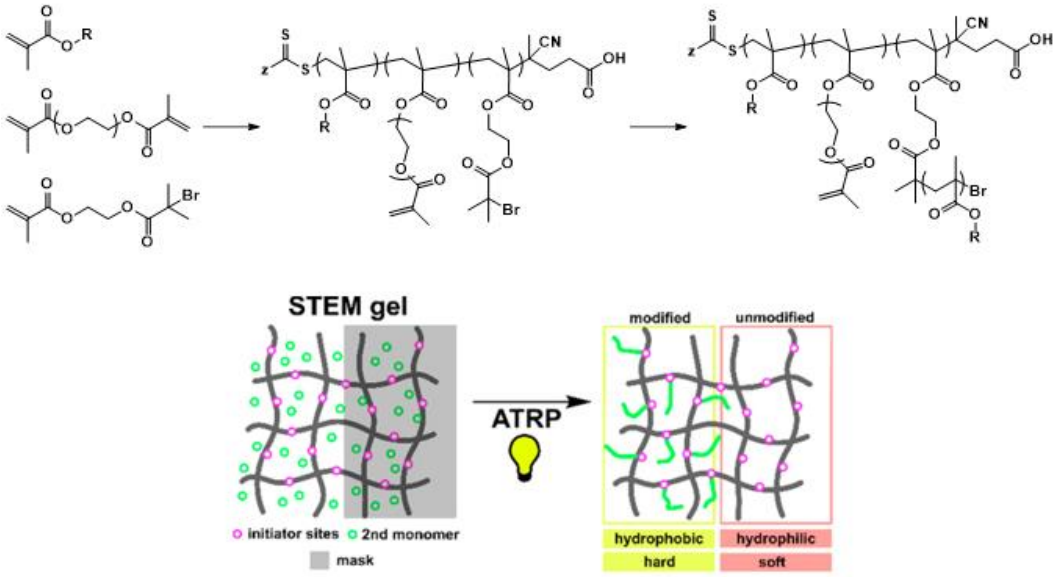

Figure 2.4. RAFT/ATRP combination by polymerizing an inimer. This approach has been used to reinforce gels with a second polymerization. Reprinted with permission from Cuthbert, J. *et al*. Transformable Materials: Structurally Tailored and Engineered Macromolecular (STEM) Gels by Controlled Radical Polymerization. *Macromolecules* 2018, *51*, 3808–3817. Copyright 2018 American Chemical Society.

In another example, three different controlled radical polymerization mechanisms were combined by the inimer approach. A TEMPO-functionalized acrylate and an I_{ATRP}-functionalized acrylate were polymerized by RAFT. The pendant initiators were then subsequently initiated, forming bottle-brush structures.[123]

2.4.2 *Post-Polymerization Modification with I_B*

Polymers can be further modified post-polymerization by conjugating a new initiator (I_B) to the polymer chain end or on monomer side chains. If a new initiator were conjugated onto the chain end, a block copolymer could be synthesized; if a new initiator were conjugated onto a

monomer side chain, a comb or bottle-brush polymer could be synthesized. In this section, we review works that use post-polymerization functionalization of a polymer with a new initiator motif or use secondary reactions to activate a latent initiator into an active one.

2.4.2.1 Post-Polymerization Functionalization/Activation with New I_B

2.4.2.1.1 *Post-Polymerization Functionalization with I_{ATRP}*

Pendant alcohols on monomer side chains or chain ends can be easily functionalized to form an I_{ATRP}.[22,125–130] Commercially-available α-bromoisobutyryl bromide can be reacted with the pendant alcohols of a polymer at room temperature for a few hours with excess triethylamine with good conversion. One limitation of post-polymerization functionalization by this method is that a hydrophilic polymer may not be soluble in suitable organic solvents like THF or DCM. In this case, an inimer as discussed in the previous section is a suitable alternative.

Pendant I_{ATRP} has been used to make block copolymers and bottle-brush polymers with low dispersities. In one example,[129]beta-cyclodextrin alcohols were used to initiate ROP of caprolactone. The hydrophobic PCL block was capped with an ATRP initiator to polymerize a second, amine containing cationic block (Figure 2.5). These cationic cyclodextrin-based star polymers could deliver nucleic acids to R264.7 cells, a macrophage cell line, with similar efficiencies as commercial agent Lipofectamine with comparible or decreased toxicity. A similar strategy of conjugating I_{ATRP} to chain ends was used to develop tri-block materials which form gels at physiological temperature for potential injectable administration.[130]

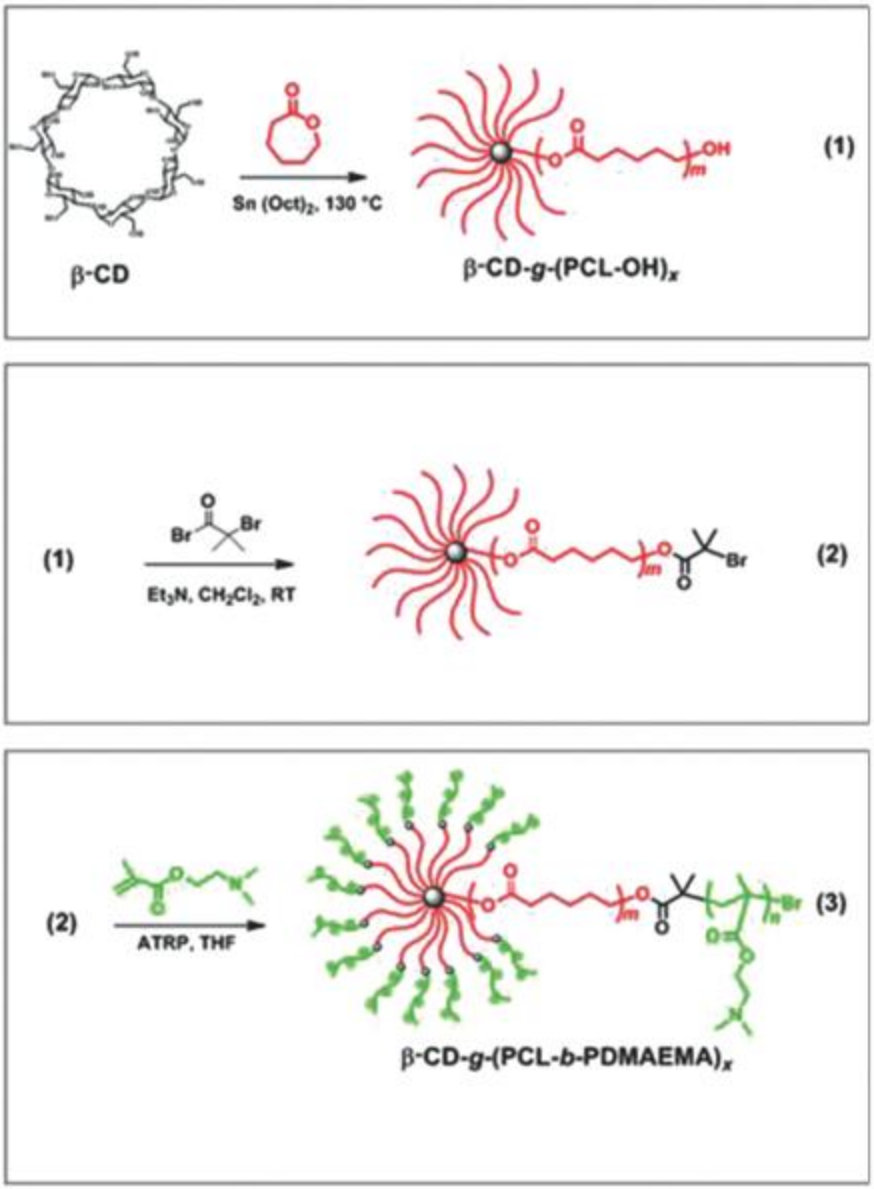

Figure 2.5. ROP/ATRP by end capping a polymer with a new initiator. This approach has been used to make carriers for gene delivery. Cheng, H.; Fan, X.; Wu, C.; Wang, X.; Wang, L.-J.; Loh, X. J.; Li, Z.; Wu, Y.-L. Cyclodextrin-Based Star-Like Amphiphilic Cationic Polymer as a Potential Pharmaceutical Carrier in Macrophages. *Macromol. Rapid Commun.* **2018**, *1800207*, e1800207.

Another approach is to functionalize a ROMP polymer chain end with an I_{ATRP} by terminating ROMP with a symmetric *cis*-alkene with an I_{ATRP}.[131] Additionally, an asymmetric enol ether

functionalized with an I_{ATRP} can be used to cap the polymer; however it was found that this is not as efficient because there is a probability that the chain end is functionalized with the enol ether group as opposed to the I_{ATRP}.

2.4.2.1.2 *Post-Polymerization Functionalization with a CTA_{RAFT}*

The RDRP of a monomer that also contains a pendant CTA_{RAFT} risks generating a hyperbranched structure and thus is difficult to use in the synthesis of block copolymers. However, it is possible to functionalize the polymer side chains and chain ends with CTA_{RAFT} after the initial polymerization. In one example, Bolton and Rzayev use RAFT to copolymerize a methacrylate with a pendant I_{ATRP} and a methacrylate with a protected alcohol.[124] After I_{ATRP} was used to grow some side chain polymers, the protected alcohol was deprotected post-polymerization and used to conjugate on CTA_{RAFT} for subsequent RAFT.

2.4.2.1.3 *Post-Polymerization Functionalization with I_{ROP}*

One common approach to the synthesis of polypeptides is the ROP of N-carboxyanhydrides (NCA) initiated by a primary amine. There is a more detailed review specifically on the synthesis of biohybrid block copolymers,[132] but this section highlights the use of dual polymerization for the synthesis of peptide-polymer copolymers. Due to the high heteroatom content of NCAs which may be incompatible with other polymerization methods, it is common to use other polymerizations first, followed by terminal functionalization with an amine for subsequent ROP of NCA monomers. This strategy was utilized in the development of non-toxic pH-responsive micelles which release prednisone more quickly at low pH.[133]

There are many ways to functionalize different polymer chain ends with amines.[133,134] Specifically for polymers synthesized by ATRP, the halide on the polymer chain end can be a useful reactive site for the introduction of amines. One approach is to replace the halogen chain

end of ATRP with an amine and use that to directly initiate ROP of NCA. The use of a multivalent amine allows for the synthesis of miktoarm star polymers.[135,136] The Deming group further reacted their amine terminated polymer to incorporate a nickelacycle end group which was then used to initiate an ROP of NCA.[137]

A difunctional initiator that contains a protected amine may also be used. After the first polymerization, the amine is deprotected and used to initiate ROP of NCA. As discussed above, an unprotected amine can result in higher polymer dispersities due to RAFT CTA aminolysis,[102,138] or act as a ligand for Cu and will interfere with ATRP.

2.4.2.1.4 *Post-Polymerization Functionalization/Activation with/of I_{ROMP}*

While it is more common to perform ROMP before other polymerizations, it is also possible to conjugate on an I_{ROMP} for subsequent ROMP via cross metathesis.[139] Metal-free ROMP (MF-ROMP), an organic photoinduced method for ROMP, has also been shown to be amenable to subsequent polymerization. Because MF-ROMP can be initiated by enol ethers, latent enol ethers such as allyl ethers can be easily isomerized post-polymerization to yield the new active initiator. In one example, styrene was copolymerized with allyl ether-functionalized styrene by ATRP.[140] After polymerization, the halide chain end was removed and the allyl ether was isomerized to the active enol ether form and used to initiate MF-ROMP.

2.4.2.2 In-Situ Modification of Latent I_B

2.4.2.2.1 *In-Situ Modification of a Polymerization to Prevent Chain Transfer*

ROMP and ROP result in the ring open form of the monomers which have similar reactivities to their starting monomers and thus chain transfer can be a common problem. Chain transfer results in scrambling of the polymer sequence and makes synthesis of block copolymers difficult. For ROMP, unfunctionalized norbornene is never used in the synthesis of block copolymers due to

high rates of chain transfer. Living polymerizations with ROMP typically use norbornenes with pendant maleimides or other groups that have been shown to be too bulky or electron deficient for chain transfer.

With regards to ROP, polymerizations of cyclic monomers exist in some ring-chain equilibrium, high thermodynamic drive for the linear ring open form is necessary to prevent intramolecular chain transfer or macrocyclization. One approach to polymerize low ring strain macrolactones is to use extremely strong bases to compensate for the lack of enthalpic drive to open the ring. However, this poses a problem for the synthesis of block copolymers as strong bases also catalyze intra- and intermolecular chain transfer via transesterification, scrambling the polymer sequence. One strategy that has eliminated transesterification-induced sequence scrambling when copolymerizing low and high ring strain lactones is to first polymerize low ring strain macrolactones with a strong base, quench the active chain, and subsequently reinitiate the polymerization of a higher ring strain monomer with a weaker base.[141] The weaker base could be used to polymerize higher ring strain lactones but did not induce transesterification and the block copolymer sequence was preserved.

2.4.2.2.2 *In-Situ Modification of a Polymerization to React New Monomers*

Some polymerization systems such as RAFT have monomers of such disparate reactivities that a single chain end cannot be used to polymerize both monomers. For example, the same CTA_{RAFT} cannot be used to polymerize electron deficient vinyl acetates with more electron rich methacrylates. Although these differences in monomer reactivity may limit the ability to synthesize statistical copolymers, they can be exploited to synthesize block copolymers. The Thang group developed a switchable CTA_{RAFT} that can polymerize either methacrylates or vinyl acetates depending on its charge. A protonated pyridinyl dithiocarbamate, which polymerizes

electron rich methacrylates, can then be deprotonated by DMAP to polymerize electron deficient vinyl acetates. While control of these polymerizations varied, some copolymerizations achieved dispersities as low as 1.1 in a single pot.[142]

In situ modification of ROPs have been used to make well-defined block copolymers. *In situ* modification of a ROP iron catalyst allows for orthogonal ROP of epoxides and lactides. By switching the oxidation state of the Lewis acid catalyst either chemically[143] or electrochemically,[144] poly(cyclohexane oxide)-*block*-polylactide was synthesized in a single pot. *In situ* modification of an ROP chain end can be used to synthesize block copolymers of different cyclic ester monomers. The different reactivities of carbonates, lactones, and lactides in ROP prevent the use of a single active chain end for copolymerization. The Guo group developed a combination of different acids and bases to controllably switch the chain end and monomer reactivities to catalyze the ROP of different cyclic ester monomers.[145] In one system, the Guo group combined the use of their pH-switchable ROP and the work by the Thang group with pH-switchable RAFT CTAs.[146] With this system, these one-pot polymerizations can be taken to nearly quantitative conversion in the synthesis of tetrablock copolymers with well-defined blocks of low dispersities.

2.4.2.2.3 *The Use of Light-Controlled Orthogonal Polymerizations*

Light-controlled polymerizations allow activation and deactivation of a polymerization with temporal and spatial control. Often, these systems pair an initiating motif with an appropriate photocatalyst which generates an acid or radical to initiate the polymerization upon excitation by light.[147] Because of the many permutations of unique photocatalyst/initiator pairs, the use of different wavelengths to initiate different polymerizations can be a powerful technique in dual orthogonal polymerizations. However, despite this potential, there have been few examples of this

to date, perhaps due to limitations such as functional group incompatibility, limited mutual solubility or poor control over molecular weight.

One approach is the use of a single switchable catalyst that behaves differentially in response to different wavelengths of light. The use of a one-pot sequential polymerization of two monomers has also been explored with cationic-RAFT polymerization.[148,149] In one particularly interesting example, the Fors group was able to use different wavelengths of light to switch between pyrylium-catalyzed cationic polymerization of enol ether or $Ir(ppy)_3$-catalyzed polymerization of methyl acrylate in a single pot.[150] In another example, 550-750 nm light was used for the polymerization of methyl methacrylate and 350-380 nm light was used for photoacid generation for ROP.[151]

2.4.3 *Post-Polymerization Modification with a New Monomer Motif M_B*

This approach polymerizes a macromonomer, a polymer functionalized with a monomer motif M_B that only reacts in a subsequent polymerization (P_A-M_B). This "graft-through" approach results in a bottle-brush polymer. There are two general strategies to synthesize a macromonomer. One approach is to polymerize M_A from an inimer I_A-M_B, resulting in P_A-M_B. Another strategy is to conjugate M_B onto the polymer chain end or a monomer side chain post-polymerization.

Because of the high enthalpic drive towards norbornene polymerization and the high activity and functional group tolerance of the Grubbs metathesis catalysts, ROMP "graft-through" is a powerful strategy in the synthesis of bottle-brush polymers. Grubbs' catalyst has been shown to graft-through macromonomers as large as 8.7 kDa; smaller macromonomers with molecular weights of 2.2 kDa can be polymerized with DPs reaching upwards of 4000.[152,153] ROMP has been used to polymerize branched macromonomers with two pendants polymers, forming bottle-brush polymers.[144,145] ATRP of methacrylate-capped poly(ethylene oxide) macromonomers has also been shown to result in polymers with DPs as high as 400.[154]

2.4.3.1 Macromonomer Synthesis Starting from I_A-M_B

Macromonomer synthesis from an inimer starts similarly to the examples in section *Polymerizing an inimer M_A-I_B*. However, instead of first polymerizing the monomer and then growing a second polymer off the pendant initiator, the order is reversed. In this approach, a polymer is first grown off the initiator I_A and then a second polymerization is used to "graft through" the pendant monomer (M_B).

There are many papers that use a CTA_{RAFT}-M_{ROMP} to make bottle-brush polymers, some of which are done in a single pot.[95,155–159] In these papers, RAFT is first used to make linear macromonomers (P_{RAFT}-M_{ROMP}). The norbornene moiety (M_B) is then used to "graft through" with ROMP (Figure 2.6). However, one limitation with a one-pot approach to RAFT-ROMP polymerization is that it is important to purify away residual acrylates, as the cross metathesis of the active ROMP chain end with the acrylate results in early irreversible termination.[95] These findings have been corroborated and in fact used to functionalize ROMP polymer chain ends with acrylates.[131,160] Modified Grubbs metathesis catalysts have also been used in cyclopolymerizations of 1,6-heptadiene macromonomers with polycaprolactone tails.[161]

In a similar approach, alcohol-functionalized norbornene (I_{ROP}-M_{ROMP}) was first used for ROP of lactides and the resulting macromonomer was "grafted through" with ROMP.[162]

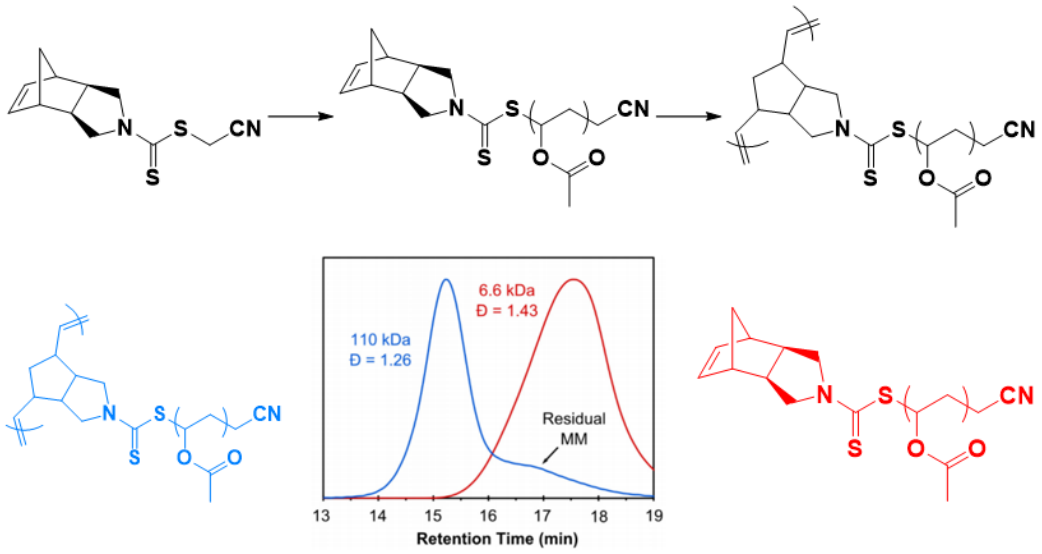

Figure 2.6. RAFT/ROMP by polymerizing a macromonomer. Reprinted from *Polymer (Guildf)*, 79, Foster, J. C., Radzinski, S. C., Lewis, S. E., Slutzker, M. B. & Matson, J. B., Norbornene-containing dithiocarbamates for use in reversible additione fragmentation chain transfer (RAFT) polymerization and ring-opening metathesis polymerization (ROMP), 205-211, Copyright 2018, with permission from Elsevier.

2.4.3.2 Macromonomer Synthesis by Post-Polymerization Functionalization of Polymer

Instead of starting with an inimer (I_A-M_B), the monomer motif can be functionalized onto the polymer post-polymerization. In one example, azide-alkyne click chemistry was used to conjugate M_{ROMP} onto a polymer and then ROMP was used to "graft through" to create bottle brush polymers with dispersities of <1.1.[162,163] Other high efficiency reactions, such as NHS ester transesterification, have been used to conjugate M_{ROMP} onto a polymer chain end.[164] This strategy was used in the development of a delivery system for doxorubicin, a small molecule chemotherapeutic.

For an example with a condensation polymerization, the Zhang group exploited the same mechanism of their polymerization to cap their polymer with a reactive end group. Poly(p-

benzamides) were synthesized by polycondensation. The phenols of the phenyl esters are good leaving groups and the aromatic amines can substitute them even at temperatures as low as -70 ˚C. While this paper shows chain end functionalization with I_{ROP} alcohol, I_{ROP} amine, an ATRP initiator, and even a click chemistry-compatible alkyne, we wanted to highlight the chain end functionalization with norbornene for subsequent ROMP.[165]

2.5 Conclusion

Major advances in polymer chemistry in the last quarter century have changed the way we conceptualize and synthesize materials. Specifically, advances in RDRP and other controlled polymerizations with "living" characteristics have unlocked many advances in biology and medicine: BCPs of novel architectures or BCPs assembled into supramolecular structures can be used for targeted delivery of therapeutics and imaging agents, and for the development of new biomaterials. We surveyed different strategies employed to synthesized BCPs via dual polymerizations, categorized into (i) use of orthogonal polymerizations (often in a single pot), (ii) post-polymerization functionalization with a new monomer motif. With this review, we hope to highlight useful synthetic strategies for the synthesis of BCPs with segmented backbones to facilitate their use in biomedical applications. As the field of polymer science and engineering grows, we expect even more creative ways to synthesize highly engineered BCPs with any permutations of backbones and side chains for biomedical applications.

There are many considerations for deciding which polymerization to use in the synthesis of a particular block. To briefly summarize a few important points: ROP can be used to synthesize polymers with biodegradable backbones but these polymerizations are sensitive to nucleophilic heteroatoms; ROMP has broad functional group tolerance and can introduce unique reactivity into the backbone but fewer ROMP monomers are commercially compared to those of other

polymerization systems. Both ATRP and RAFT produce polymers with non-degradable backbones but there are advantages unique to each. ATRP initiators are more stable towards aminolysis than CTA_{RAFT} and are easier to functionalize onto a chain end but RAFT does not require removal of the metal species used in ATRP

Combining multiple polymerization systems further expands the repertoire of potential materials by increasing diversity in the available polymer backbones but the drawbacks of each polymerization determine the optimal sequence of these polymerizations. For example, because free amines can aminolyze CTA_{RAFT}, the RAFT block is usually synthesized before amine-initiated ROP. Because ROMP can react with residual acrylates, ATRP/RAFT blocks are usually done after ROMP. We have included some experimental considerations for dual polymerization in their respective sections. As each polymerization system is investigated and improved, more limitations will be addressed, allowing more of them to be performed in a single pot.

Of the emerging polymerization techniques, we suspect that the use of light-controlled polymerizations holds many unexplored synergies with existing strategies for dual polymerizations. Because these light-controlled polymerizations can be spatially and temporally controlled, they confer new degrees of tunability in polymer synthesis with the potential to expand the complex structures available for use. New materials with varied monomer characteristics, varied backbone characteristics via multiple polymerization techniques, and varied structural characteristics via temporal and spatial control of polymerizations will enable polymers to meet the expanding materials needs in medicine.

Chapter 3. THE INTRINSIC MECHANOCHEMICAL REACTIVITY OF VINYL-ADDITION POLYNORBORNENE[4]

3.1 ABSTRACT

Herein we report the discovery of the intrinsic mechanochemical reactivity of vinyl-addition polynorbornene (VA-PNB), which has strained bicyclic ring repeat units along the polymer backbone (Figure 3.1). VA-PNBs with three different side chains were found to undergo ring-opening olefination upon sonication in dilute solutions. The sonicated polymers exhibited spectroscopic signatures consistent with conversion of the bicyclic norbornane repeat units to the ring-open isomer typical of polynorbornene made by ring-opening metathesis polymerization (ROMP-PNB). Thermal analysis and evaluation of chain scission kinetics suggest that sonication of VA-PNB results in chain segments containing a statistical mixture of vinyl-added and ROMP-type repeat units.

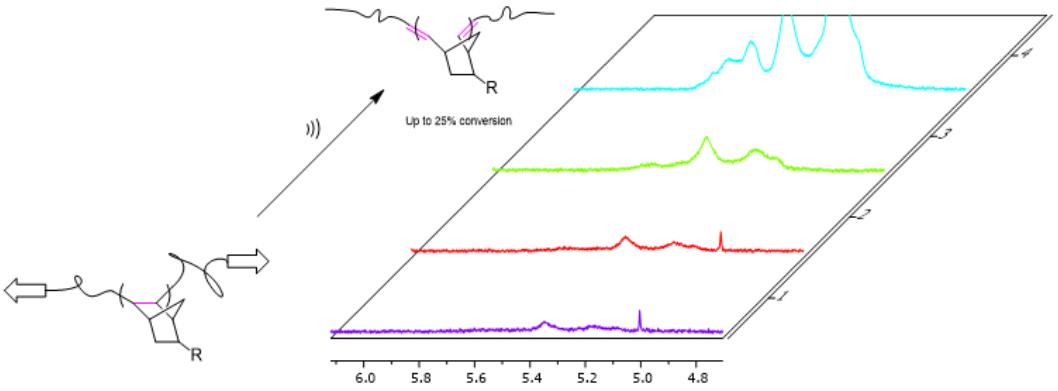

Figure 3.1. Cartoon schematic of the ring-opening olefination induced by mechanochemical activation of VA-PNB as a function of sonication time. ^{1}H NMR displayed on the right (bottom to top: 15, 30, 45, 60 min).

3.2 INTRODUCTION

Mechanoresponsive polymers that undergo chemical transformations in response to mechanical stress have been explored in many applications including force sensing,[166,167] small molecule release,[168] catalyst activation,[169] self-reinforcing materials,[170] and autonomously healable systems.[171] Macromolecular scaffolds can be designed to efficiently transduce tensile forces into particular molecular-scale geometric strain which can guide mechanophore activation.[172–176] In most cases, a single mechanophore is incorporated into the center region of the polymer main chain, and the tensile load on the polymer backbone activates the mechanophore. Mechanical manipulation of the mechanophore potential energy surface is useful for analytical and physical organic studies to elucidate novel reactions that proceed via unique pathways inaccessible by, or impractical for, thermal or photochemical input. Mechanophore activation can also be used as a synthetic strategy to lower the thermal or photochemical energy input required for known reaction pathways such as ring-opening isomerization. However, due to the low concentration of mechanophores per polymer chain, activation can be difficult to quantify and large changes in bulk material properties are typically not observed. Additionally, small deviations in mechanophore location, relative to the center of the polymer chain, may also affect activation efficiency.[177]

Incorporation of multiple mechanophores along a single polymer chain overcomes these limitations, and offers significant advantages with regard to effecting large changes in physicochemical properties. The increased concentration of mechanophores in the polymer chain can facilitate quantification of mechanophore activation, induce large changes in bulk material properties, and eliminate the need to precisely place a single mechanophore at the center of the polymer chain for activation. Examples of these custom designed multi-mechanophore polymers

include those containing strained rings along the polymer backbone, such as cyclopropanes[170,178–180] and cyclobutanes[13], which have been shown to exhibit high mechanochemical activity.

Inspired by these polymechanophores, we hypothesize that simple, commercially available cyclopolymers containing inherently strained rings might also function as intrinsic polymechanophores. We were particularly interested in polynorbornenes made by vinyl-addition polymerization (VA-PNBs), which contain norbornane repeat units having an estimated strain energy of 73.4 kJ/mol.[181] In general, VA-PNBs are easy to synthesize, offer a wide variety of side chain functionality, and display desirable mechanical and chemical properties that have thus motivated their widespread application and industrial production.[182–186] To our knowledge, the mechanochemical reactivity of VA-PNBs has not been reported. Herein, we report our initial investigations into the intrinsic mechanochemical reactivity of VA-PNBs bearing trimethylsilyl (VA-TMS), triethoxysilyl (VA-TES), and hexyl (VA-Hex) side chains, as depicted in Figure 3.2. We hypothesize that the mechanism of ring-opening olefination would be similar to that of other cyclopolymers containing strained rings,[187] and would proceed via homolytic bond scission within the norbornane rings to produce a diradical intermediate that could then propagate bidirectionally to form ROMP-type repeat units.

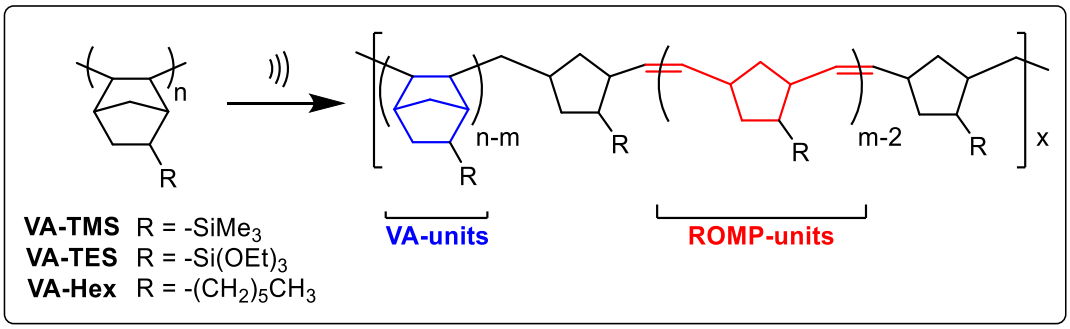

Figure 3.2. Schematic of the ring-opening olefination induced by mechanochemical activation of VA-PNB.

3.3 RESULTS

3.3.1 *Synthesis of Vinyl-Addition Polynorbornene (VA-PNB)*

High molecular weight VA-PNBs were prepared using the catalyst, *trans*-[$Ni(C_6F_5)_2(SbPh_3)_2$]. This catalyst has been shown to be highly active and applicable to a broad range of norbornyl-based monomers, including some with polar functionalities.[185] One example synthesis: In a 20 mL scintillation vial with stir bar, *trans*-[$Ni(C_6F_5)_2(SbPh_3)_2$] (5.5 mg, 5 μmol) was added to a solution of 5-trimethylsilyl-2-norbornene (0.83 g, 5 mmol) in DCM (2 mL) and stirred for 24 h. The reaction mixture was then diluted with additional DCM (8 mL) and added dropwise to stirred methanol (250 mL) causing precipitation of the polymer. The polymer was isolated via vacuum filtration, and then dried *in-vacuo* to constant weight to provide 0.30 g (37% yield) of the desired product. Lower molecular weight polymers used for sonochemical control experiments were made similarly but used the catalyst $[Pd(allyl)Cl]_2$ (1 equiv.) and activated with $AgSbF_6$ (2.1 equiv.) following literature procedures.[185] Gel permeation chromatography (GPC) analyses revealed number average molecular weight (M_n) values of 83.3, 219.7, and 185.0 kDa for the VA-TMS, VA-TES, and VA-Hex, respectively.

High molecular weight ROMP-PNBs were prepared using G2. One example synthesis: In a 20 mL scintillation vial with stir bar, G2 (7.8 mg, 0.009 mmol) was dissolved in THF (12 mL). A solution of monomer (1.005 g, 6.01 mmol) in THF (1.1 mL) was added to the solution of Grubbs II. The solution was then stirred at room temperature for 1.5 h. Conversion was monitored by ^1H NMR spectroscopy of reaction aliquots, and determined by comparison of peak areas corresponding to polymeric olefin signals versus those of monomer. After 1.5 h, the polymerization was terminated by addition of ca. 1 mL of ethyl vinyl ether, followed by stirring for 5 min. The reaction volume was then reduced under vacuum and the remaining solution was

added dropwise into an excess of ethanol, causing precipitation of the product polymer. The polymer was collected via vacuum filtration and then dried under vacuum to provide 864 mg (86% yield) of the desired product.

3.3.2 *Mechanochemical activation of VA-PNB by Sonication and Quantification*

Sonication of polymers were performed in a dry, air-free environment. A Suslick flask was oven dried and then attached to the sonicator probe. The arms of the flask were sealed with rubber septa and then the flask was purged with dry N_2. VA-PNB (50 mg) was added under N_2 atmosphere and the sample cell was flushed for 20 min with N_2. Dry THF (10 mL) was then added via syringe. The Suslick flask was then fitted with a balloon filled with N_2 to maintain positive nitrogen pressure. The polymer solution was left for 30 min to facilitate dissolution of the polymer. The polymer solution was then moved to a cold room maintained at 4-6 ℃ and stood for 30 min to allow for temperature equilibration. Polymers were sonicated at 8.5 W/cm^2 with duty cycles of 1 s on, 9 s off, for a total of 240 min of sonication on-time.

To quantify the mechanochemical activation of the VA-PNBs, aliquots were taken at 5, 10, 15, 30, 60, 120, 240 min time intervals. At each time point, an aliquot (0.5 mL of polymer solution) was taken with a needle that was oven dried and N_2 purged. The 0.5 mL solution was put under high vacuum for 16 h to remove solvent.

Conversion from VA- to ROMP-type repeat units was determined by two methods and the values averaged. First, the olefin signals in the polymer were integrated against unique proton signals in the polymer side chain as they were assumed to be unaffected by the sonication. For VA-TMS, the olefin peaks were integrated against the protons in the trimethylsilyl group (-Si-$\boldsymbol{CH_3}$, δ = -0.2 – 0.2 ppm); for VA-TES, against the triethoxysilyl group (-Si-O-$\boldsymbol{CH_2}$-CH_3, δ = 3.6 – 4 ppm); for VA-Hex, against the end of the hexyl group (-$\boldsymbol{CH_3}$, δ = 0.75 –1 ppm).

For the second method, a stock solution of 1,4-dicyanobenzene in $CDCl_3$ (106.9 mg in 100 mL) was used for ^1H NMR spectroscopy. A known mass of sonicated polymer was dissolved in this stock solution for NMR analysis. The vinyl proton signals ($\delta = 5 – 5.8$ ppm) were integrated against the 1,4-dicyanobenzene peak ($\delta = 7.8$ ppm) to determine conversion to ROMP polymer. The same mass of VA-PNB and ROMP-PNB were dissolved in the stock solution to determine 0% olefination and 100% olefination, respectively.

Each polymer displayed steadily increasing olefin content as a function of increasing sonication time, up to 60 min of sonication (Figure 3.3). Analysis of ^1H NMR spectra showed that up to 25% of the VA-TMS and VA-TES repeat units converted to ROMP-type repeat units within the first 60 min of sonication, while VA-Hex only achieved 10% olefination during the same sonication time (Figure 3.4).

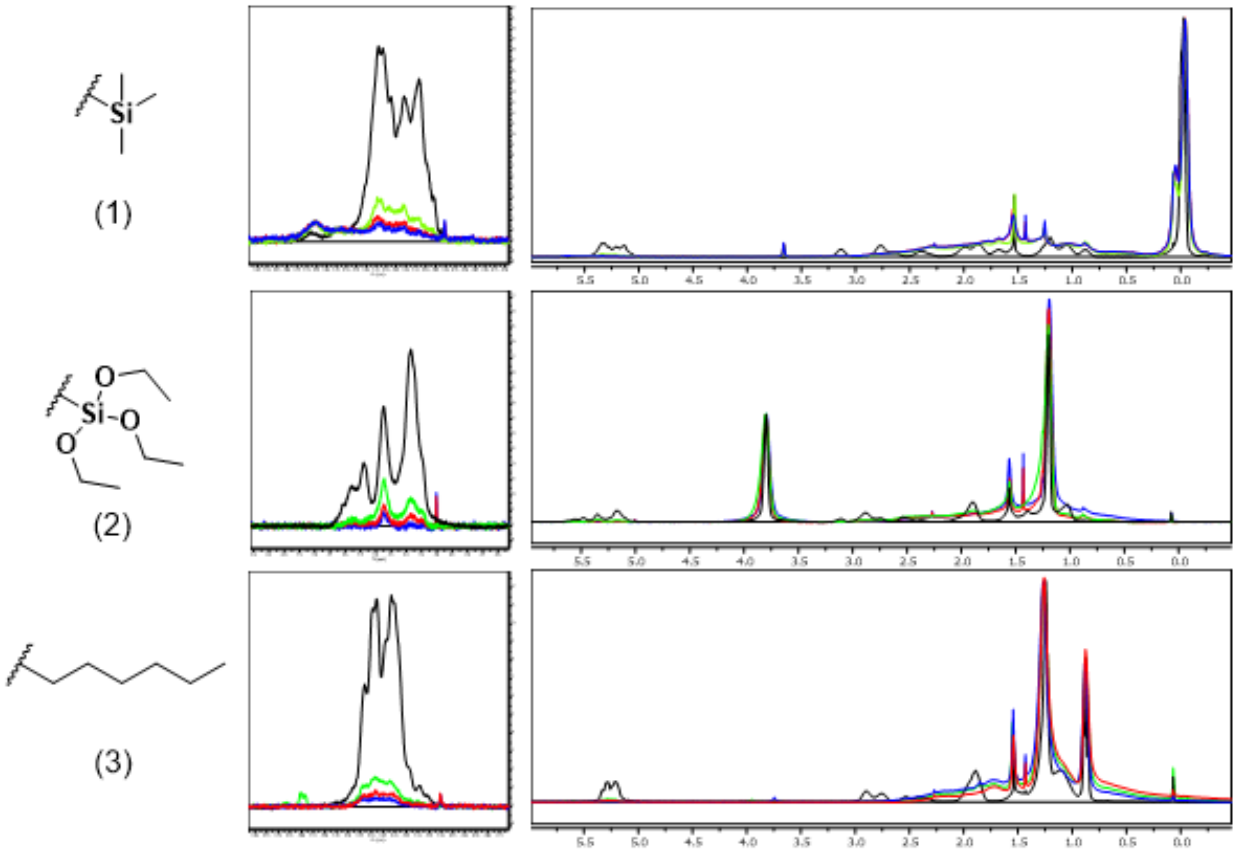

Figure 3.3. Stacked ^{1}H NMR spectra of VA-TMS (top), VA-TES (middle), VA-Hex (bottom) as a function of sonication time. t = 15 (blue), 30 (red), 240 (green) min of sonication are shown. ^{1}H NMR spectra of authentic ROMP-PNB prepared using Grubbs 2nd generation catalyst (black) is overlaid in each plot. The smaller NMR spectra on the left of each row is a zoom in on the alkene region (5-5.6 ppm). Signal intensity of polymer side chain peaks are aligned for visual aid. ^{1}H NMR ($CDCl_3$, 300 MHz): δ_H 5-5.5 (2H, broad).

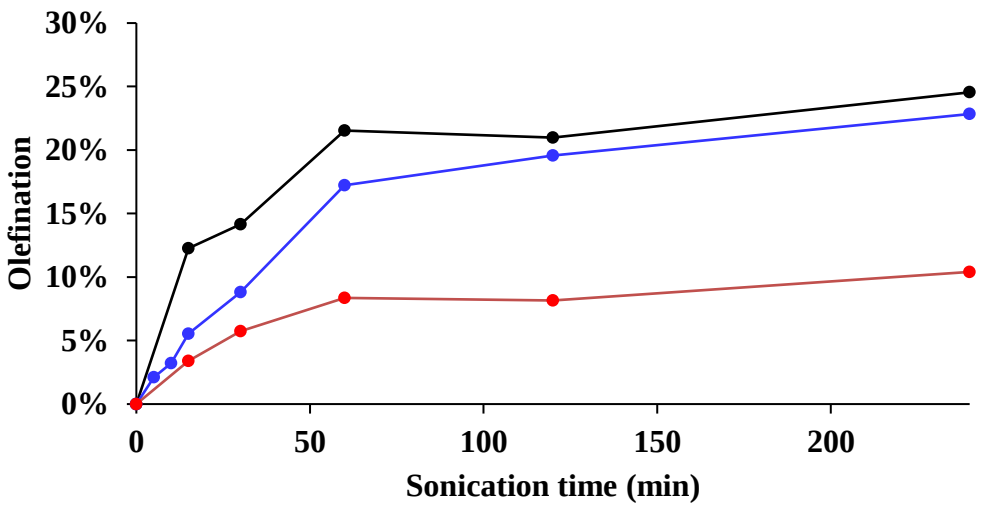

Figure 3.4. Olefination of VA-TMS (black), VA-TES (blue), VA-Hex (red) as determined by ^{1}H NMR analysis.

These differences may be due to the large impact that side chains substituents have on each polymer's solution-state conformation, relaxation dynamics, and possibly even on the mechanism for termination after ring opening. VA-TMS and VA-TES were used for further experiments due to their greater extent of olefination. To confirm that the mechanism of activation was mechanochemical and not thermal, VA-PNBs with lower molecular weights were synthesized and sonicated as negative controls (Figures 3.5 and 3.6). Sonication of the low molecular weight control VA-TES polymers did not result in any observable olefination or chain scission, which was expected as they are below the required degree of polymerization for sonication-induced cleavage.[188]

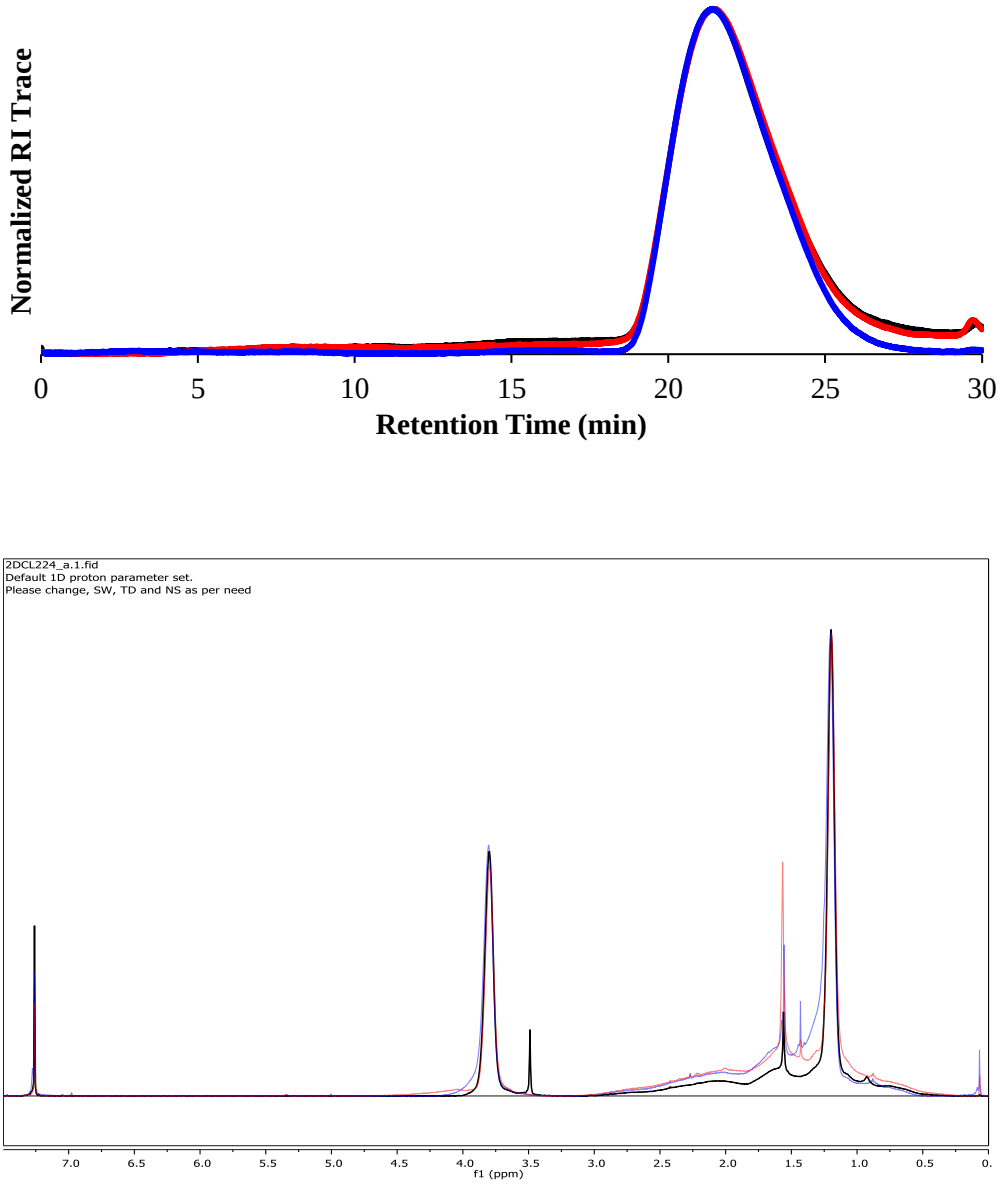

Figure 3.5. Top | Stacked GPC traces of pristine 11 kDA VA-TES (black), VA-TES sonicated for 2 h (red), and VA-TES sonicated for 4 h (blue). Bottom | Stacked ^{1}H NMR spectra of pristine 11 kDA VA-TES (black), VA-TES sonicated for 2 h (red), and VA-TES sonicated for 4 h (blue).

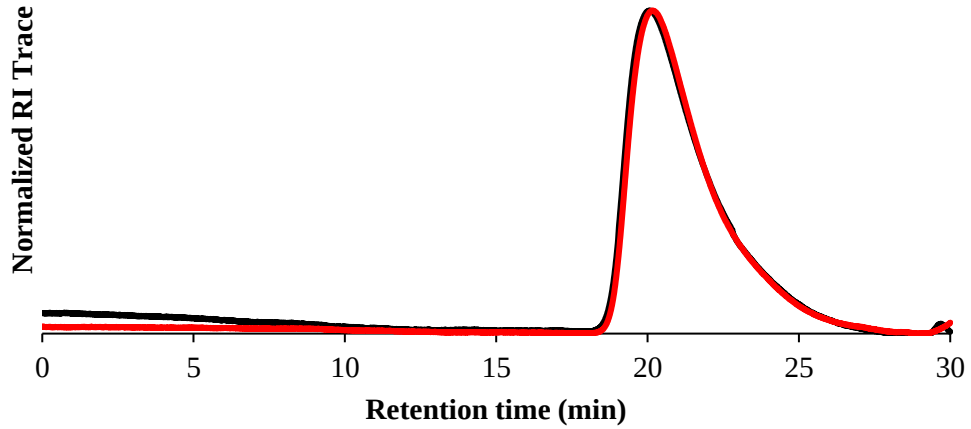

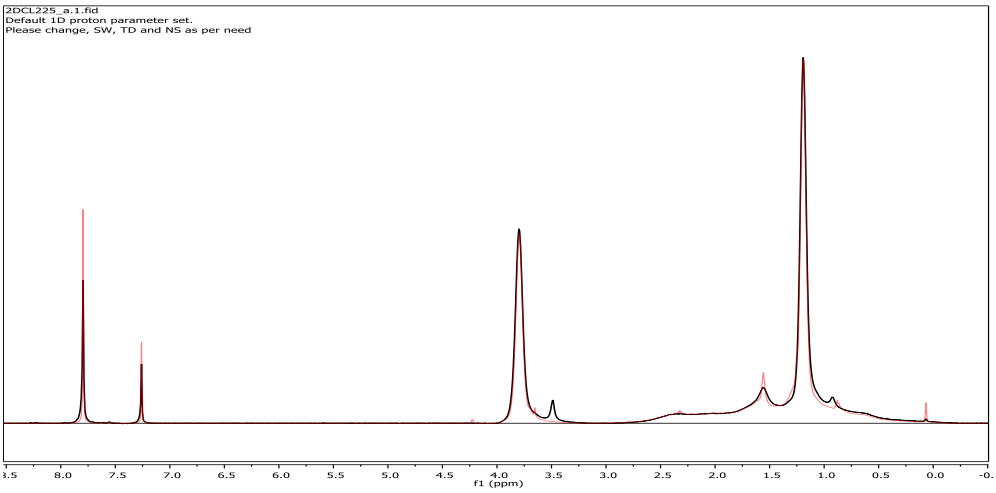

Figure 3.6. Top | Stacked GPC traces of pristine 51 kDA VA-TES (black), VA-TES sonicated for 2 h (red), and VA-TES sonicated for 4 h (blue). Bottom | Stacked ^{1}H NMR spectra of pristine 51 kDA VA-TES (black), VA-TES sonicated for 2 h (red), and VA-TES sonicated for 4 h (blue).

3.3.3 *Productive Mechanophore Activation vs. Unproductive Chain Scission*

Aliquots were also analyzed by GPC equipped with multi-angle laser light scattering detection. In all cases, the values were in good agreement and averaged to determine the percentage of repeat units having undergone ring-opening olefination (Figure 3.7). The NMR and GPC data suggest that ring-opening olefination via sonication was concurrent with chain scission, as is expected from sonication of macromolecules.[189] A representative series of GPC traces taken during sonication of VA-TES are shown in Figure 3.8 top. In general, we observed that M_n decreased with increasing sonication time and that molecular weight distributions remained monomodal, at least to the same qualitative extent as the pristine samples prior to sonication Figure 3.8 bottom. This decrease in molecular weight as a function of sonication time is plotted in Figure 3.8 for VA-TES (black) and VA-TMS (blue).

Olefination of VA-TMS

	Sonication time (min)	Olefination determined by: Side chain	Internal standard	Average
VA-TMS	15	11.0%	13.5%	12.3%
	30	12.7%	15.6%	14.2%
	60	17.8%	25.3%	21.5%
	120	18.0%	23.9%	21.0%
	240	19.3%	29.8%	24.5%

Olefination of VA-TES

	Sonication time (min)	Olefination determined by: Side chain	Internal Standard	Average
VA-TES	5	1.6%	2.7%	2.1%
	10	3.2%	3.2%	3.2%
	15	6.5%	4.6%	5.5%
	30	8.7%	8.9%	8.8%
	60	18.0%	16.4%	17.2%
	120	20.4%	18.8%	19.6%
	240	24.5%	21.2%	22.8%

Olefination of VA-Hex

	Sonication time (min)	Olefination determined by: Side chain	Internal Standard	Average
VA-Hex	15	2.7%	4.1%	3.4%
	30	4.6%	6.9%	5.7%
	60	6.7%	10.1%	8.4%
	120	6.4%	9.9%	8.2%
	240	8.3%	12.5%	10.4%

Figure 3.7. Values of olefin content as determined vs. polymer side chain and internal standard.

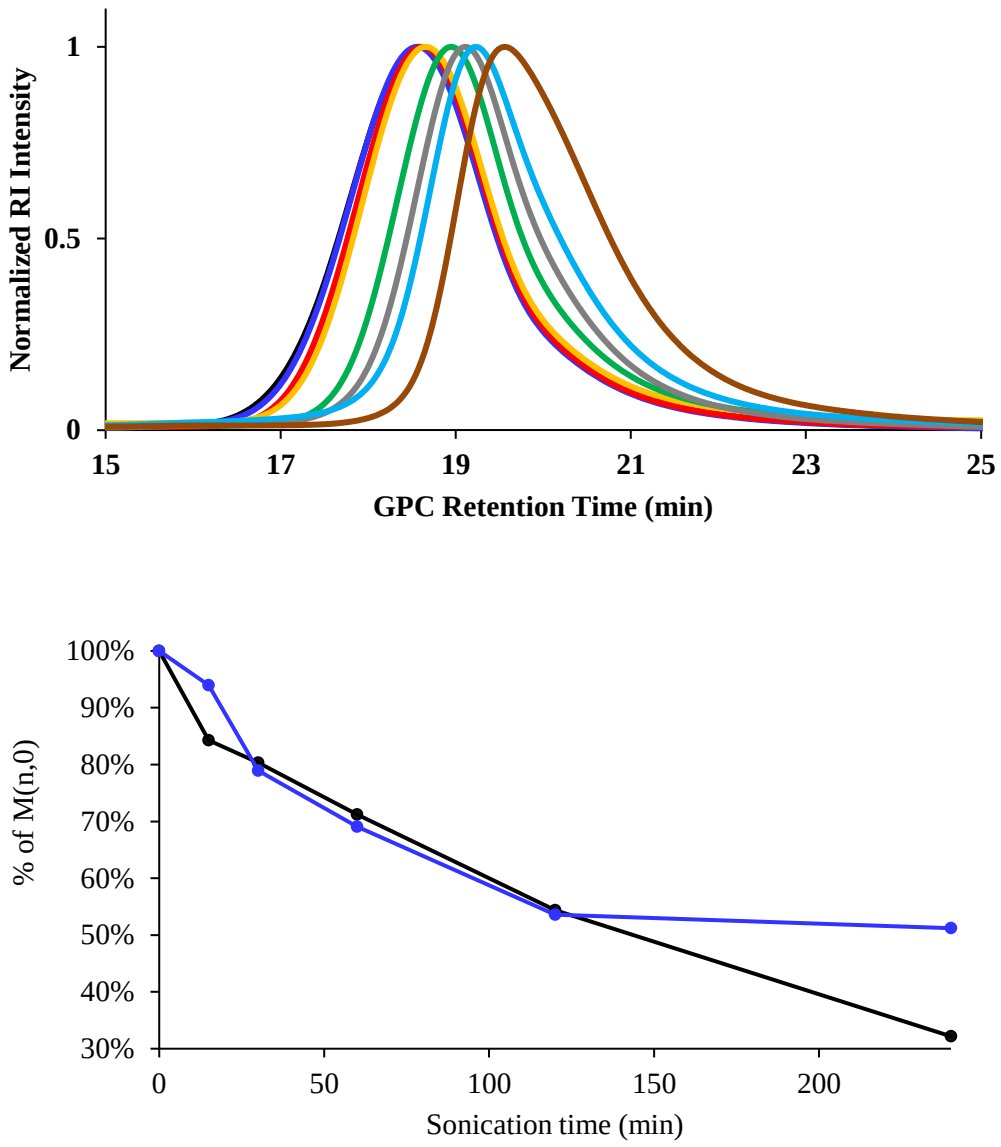

Figure 3.8. (top) GPC traces of VA-TES with increasing sonication time. GPC traces shift to lower retention times with longer sonication. Samples taken at 15, 30, 60, 120, 240 minutes of sonication on-time. (bottom) Percent of starting molecular weight ($M_{(n,0)}$) with increasing sonication time determined by GPC (VA-TES, black; VA-TMS, blue).

To better understand the competition between ring-opening olefination and secondary chain scission, the relative efficiencies of olefination compared to chain scission and the absolute rate

constants for chain scission were determined. The relative efficiencies of olefination compared to chain scission were evaluated by calculating the number of olefination events achieved before the polymer M_n was halved (i.e., extent of olefination in one scission cycle). Scission cycle (φ) was plotted against olefination and the slope was determined using linear regression (**Figure 4**). The slope of this plot (φ_1) is a useful metric to characterize the efficiency of mechanochemical activation relative to chain scission because it normalizes olefination per scission cycle to compare across polymers with different side chains and experimental conditions with indeterminant variations.[180,190] Scission cycle (φ) was calculated using the equation $\varphi = \frac{\ln(M_{n,0}) - \ln(M_{n,t})}{\ln 2}$ in which $M_{n,0}$ is the M_n at t = 0 and $M_{n,t}$ is the M_n after a given time (t) of sonication. VA-TMS exhibits φ_1 = 1.0 olefination per scission cycle and VA-TES exhibits φ_1 = 0.56. For VA-TMS, with an initial degree of polymerization (DP_0) of 500 ($M_{n,0}$ = 83.3 kDa), φ_1 = 1.0 equates to olefination of 500 repeat units per chain scission event. VA-TES, with DP_0 of 856 ($M_{n,0}$ 219.7 kDa), φ_1 = 0.56 equates to olefination of 4.8 repeat units per chain scission (Figure 3.9). The two numbers are similar, which suggests that the two side chains play similar, or perhaps generally minimal, roles in the olefination of VA-PNBs under mechanochemical activation.

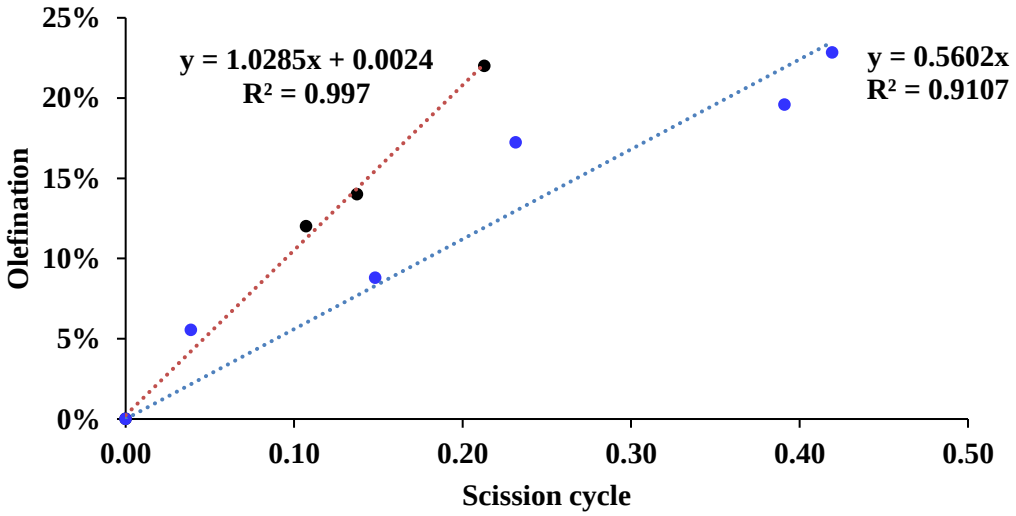

Figure 3.9. Olefination of VA-TMS (black), VA-TES (blue) plotted against scission cycle. Linear fit for olefination vs. scission cycle.

3.3.4 *Thermal and Sequence Analysis of Mechanochemically-Activated VA-PNB*

As discussed earlier, a distinguishing feature of polymechanophores is their ability to induce large changes in bulk material properties in response to mechanical force. Even at low to moderate conversions, the quantity of mechanochemical transformations far exceeds the quantity of transformations achieved by high conversions of polymers containing only a single mechanophore. As a proof of concept, DSC was used to determine changes in thermal properties of the sonicated VA-PNBs. Therein, sonicated VA-TES (26% olefination, M_n = 54.5 kDa) exhibited a T_g of 111 ºC, whereas pristine VA-TES (M_n = 219.7 kDa) did not exhibit any detectable T_g up to 350 ºC. For comparison, ROMP-TES made by Grubbs 2nd Generation catalyst (M_n = 142.6 kDa) exhibits a T_g of 11 ºC.

We initially hypothesized that the norbornane units close to the center of the chain would activate first and propagate outward, resulting in an ABA triblock structure consisting of VA-ROMP-VA repeat units before secondary scission. Assuming all olefination occurred in adjacent repeat units, the short homogenous ROMP blocks should show T_g values of ≤11 ºC according to Flory-Fox relationships of T_g and M_n.[191] Instead, the observed higher T_g of 111 ºC suggests that the mechanochemically activated region close to the center of the polymer, where ring-opening olefination is most probable, is closer to a statistical copolymer of VA- and ROMP- type repeat units rather than a homogenous ROMP block. As a result, the T_g is dominated by the VA-TES structure and reduced by sequence breaks. It is possible that termination or chain transfer events prevent the formation of homogenous blocks and the mechanism of these termination events merits future study.

3.4 CONCLUSION

In summary, we have demonstrated the intrinsic mechanochemical reactivity of VA-PNBs with conversions to ROMP-PNBs of up to 25% of the repeat units.[4] More generally, the mechanochemical activation of polymers containing strained ring repeat units is a unique method to reconfigure the molecular structure of cyclopolymers. Due to their relative ease of synthesis, high mechanophore content, and their ability to undergo changes in thermal properties and chemical group functionality upon mechnochemical activation, we envision that VA-PNBs have significant potential as functional polymechanophores.

Mechanochemistry as a field has expanded significantly in recent years and the number of new mechanophores that have been rationally designed, synthesized, and tested has risen significantly. Experimentally, the strategy of incorporating a mechanophore into a polymer backbone has remained the most popular due to its synthetic accessibility and its efficient transduction of macroscopic mechanical force into predictable molecular-scale forces. This powerful strategy is extremely useful in probing the fundamentals of mechanochemistry as well as serves as the basis of the many applications of polymeric mechanoresponsive materials.

Despite the substantial progress made in the field, there is significant potential in improving the efficiency of mechanochemical activation. Although each rationally designed mechanophore activates with extremely high efficiency, they are diluted by the inert polymer scaffold into which the mechanophore is placed; most mechanoresponsive polymers only contain 0.1-1% mechanophore by mass. The low concentration of mechanophores may be suitable for some applications such as mechanochromism, but severely hinder the adoption of mechanoresponsive polymers in other applications such as structural or self-reinforcing materials. Being able to design polymers that are mostly or entirely made of mechanochemically active repeat units would be a

breakthrough for the widespread adoption of mechanoresponsive polymers as functional materials. Other groups have also recognized the potential impact of designing mechanoresponsive polymers with multiple mechanophores and have recently reported the synthesis and mechanochemical activity of cyclopolymers with ring-strained repeat units. We further explored the use of ring strained repeat units but with cyclopolymers that were even more synthetically accessible without the need of any post-polymerization modification.

Chapter 4. SYNTHESIS AND APPLICATION OF A NEW CLASS OF ANIONIC POLY(CYCLOPENTADIENYLENE VINYLENE), A NEW CLASS OF WATER-SOLUBLE Π-CONJUGATED POLYMERS[192]

4.1 ABSTRACT

The use of π-conjugated polymers (CPs) in conductive hydrogels remains challenging due to the water-insoluble nature of most CPs. Conjugated polyelectrolytes (CPEs) are promising alternatives because they have tunable electronic properties and high water-solubility, but they are often difficult to synthesize and thus have not been widely adopted. Herein, we report the synthesis of an anionic poly(cyclopentadienylene vinylene) (aPCPV) from an insulating precursor under mild conditions and in high yield. Functionalized aPCPV is a highly water-soluble CPE that exhibits low cytotoxicity, and we found that doping hydrogels with aPCPV imparts conductivity. We also anticipate that this precursor synthetic strategy, due to its ease and high efficiency, will be widely used to create families of not-yet-explored π-conjugated vinylene polymers.

4.2 INTRODUCTION

Conductive hydrogels, water-rich networks capable of moving charge when subjected to an electric field, have significant potential for use in tissue engineering and bioelectronics. Conductive hydrogels have been used as therapeutic patches or cell scaffolds in cardiac,[193–199] neural,[200–202] and skeletomuscular applications.[203] They have also been used with electronic devices to improve the generation of ionic current and to bridge the mechanical mismatch between electronic devices and biological tissue.[204,205] Common conductive agents of CHs include metals, carbon-based nanomaterials such as carbon nanotubes, and conjugated polymers (CPs) such as

polypyrrole[206–208] and poly(3,4-ethylenedioxythiophene):poly (styrene sulfonate).[209–212] CPs are particularly attractive because the redox behavior of the material can be paired with electrolytes in solution to convert electric currents from electronic devices to ionic current for biological applications.[204]

Despite the potential of CPs in conductive hydrogels, most CPs are water-insoluble and thus require specialized fabrication techniques to incorporate them into hydrogels, including "in-gel" polymerizations and coatings,[208,213] advanced blending techniques such as dispersion or emulsification,[196,197,206,212–214] and ionic liquid exchange[211]. Despite the use of these fabrication techniques, some CPs still show limited biological integration, exhibit cytotoxicity, and induce post-implantation inflammation.[195] Additionally, due to the water-insoluble nature of most CPs, controlling conductivity without altering the mechanical properties of the gel remains an inherent challenge. Higher CP loading onto the hydrogel can increase conductivity but also impacts its hydrodynamic elasticity, affecting the survival and differentiation of encapsulated stem cells.[215,216]

Conjugated polyelectrolytes (CPEs), CPs with a high density of charged side chains, are water-soluble alternatives to hydrophobic CPs as conductive agents in conductive hydrogels.[217–219] However, the syntheses of CPEs add additional layers of complexity to the already difficult syntheses of CPs, such as solvent incompatibilities or additional deprotection steps. Additionally, commonly used aromatic monomers such as thiophenes often require high temperatures, long reaction times, and the use of air- and water-sensitive catalysts for cross-coupling chemistries. Some of these reaction conditions can be incompatible with peptides that are often incorporated in hydrogels to facilitate biological integration. Additionally, commonly used cross-coupling monomers, such as organostannanes, are toxic[220] and must be rigorously removed before medical

use.[217,221] Some CPEs are cytotoxic due to high charge density,[219,222–224] but limited synthetic accessibility of CPEs prevent rapid iterations with a wide array of side chains to develop biocompatible CPE hydrogels. Thus, there remains a critical unmet need for the synthesis of a simple CPE that can be synthesized on large-scale and formulated into biocompatible CHs without the need for advanced fabrication techniques.

One strategy to produce CPs is to synthesize a nonaromatic precursor polymer that can be transformed into a CP or CPE in a single post-polymerization modification step. In this strategy, milder synthetic conditions can be used for monomer functionalization and polymerization due to the lack of monomer aromaticity, potentially allowing for the incorporation of pendant peptides as polymer side chains. Ring-opening metathesis polymerization (ROMP) is a particularly attractive polymerization method for the synthesis of these precursor polymers because it is a well-studied living polymerization with high functional group tolerance, and the residual backbone alkenes of ROMP-based polymers can participate in π-conjugation. However, some attempts to convert a ROMP precursor into a CP or CPE require extremely high temperatures (≥200 °C) or the use of acids that are incompatible with the incorporation of peptide or protein side chains.[9,12,225–229] Additionally, many of these polymers are insoluble post-heat treatment. More recent efforts have been made to use milder acidic[9] or basic conditions[10] or even mechanochemical activation.[13,230]

Herein we report an operationally simple synthetic route to anionic poly(cyclopentadienylene vinylene) (aPCPV) via a soluble, easily accessible, and modular polymeric precursor. We synthesized a halogenated polynorbornene precursor polymer and convert this polymer into a CPE under mild conditions and in high yield (Scheme 1). The resulting polymer is negatively charged due to the deprotonation of an acidic proton from the cyclopentadiene repeat unit generated *in situ* as well as the deprotonation of the acid groups generated from imide hydrolysis. aPCPV is highly

water-soluble, displays visible light absorption up to 610 nm, is conductive, and exhibits low cytotoxicity. aPCPV is oxidized in water but can be reversed either electrochemically or chemically. Due to these properties, we believe aPCPV will be an extremely useful class of polymers for tissue engineering applications.

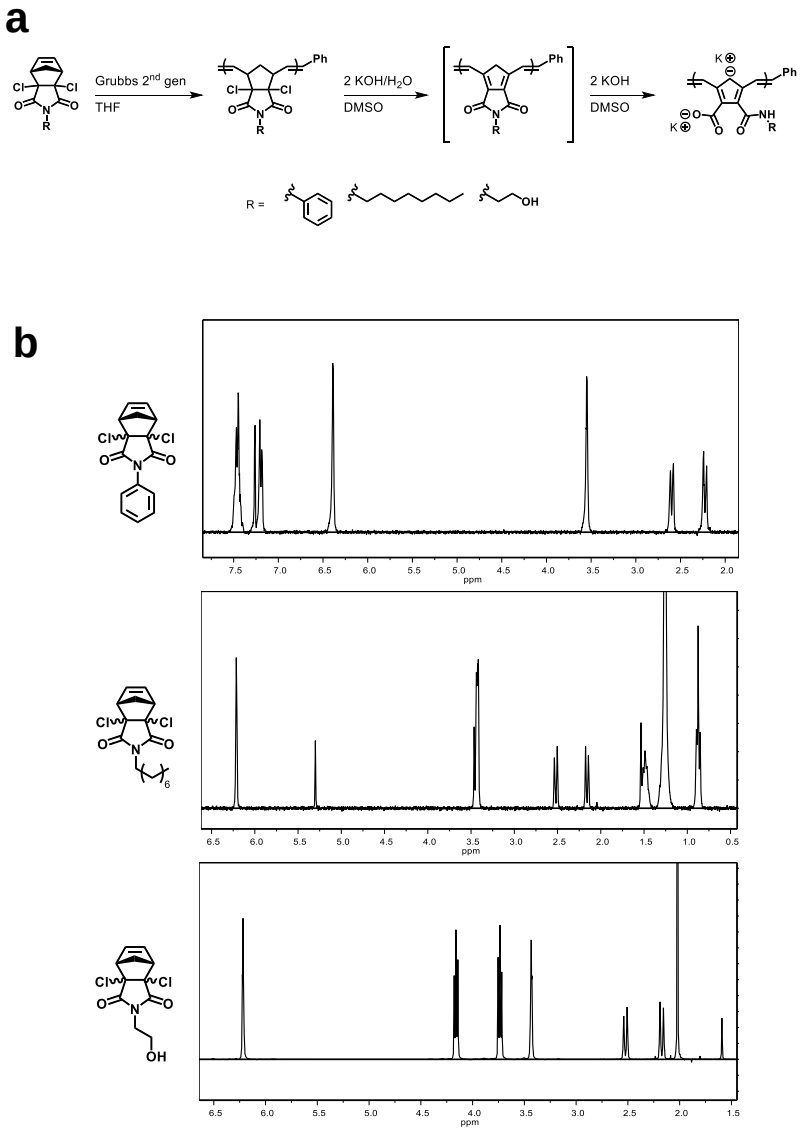

Figure 4.1. **a**, generalized synthetic scheme of poly(2). **b**, ^{1}H NMR spectra of monomers with three different side chains. Top compound: ^{1}H NMR ($CDCl_3$, 300 MHz): δ_H 7.5 (3H, m), 7.2 (2H, m), 6.4 (2H, s), 3.55 (2H, m), 2.6 (1H, d), 2.2 (1H,

d). Middle compound: ^{1}H NMR ($CDCl_3$, 300 MHz): δ_H 6.3 (2H, s), 3.5 (2H, m), 2.6 (1H, d), 2.2 (1H, d), 1.5-0.8 (15H, b). Bottom compound: ^{1}H NMR ($CDCl_3$, 300 MHz): δ_H 6.3 (2H, s), 4.3 (2H, t), 3.7 (2H, t), 3.4 (2H, s), 2.2 (1H, d).

4.3 RESULTS

4.3.1 *Synthesis of insulating precursor polymer and conversion to π-conjugated aPCPV*

We sought to synthesize a halogenated precursor polymer that could undergo dehydrohalogenation under basic conditions to yield the necessary alkenes for a π-conjugated polymer backbone. For our initial design, we hypothesized that a polymer with allylic bromines would undergo facile elimination. Thus, we synthesized an oxanorbornene monomer via a [4+2] cycloaddition with 2,5-dibromofuran as the diene. Unfortunately, we could not detect any polymerization of these oxanobornenes by ^{1}H NMR spectroscopy. We then attempted to synthesize oxanorbornene monomers with halogens one carbon further away from the alkene with furan and dihalogenated dienophiles for the [4+2] cycloaddition. However, these monomers could not be isolated in high yield. Instead, we used cyclopentadiene, a more reactive diene and were able to synthesize a panel of dihalogenated norbornene monomers on gram scale using cyclopentadiene and dichloromaleimides. In this report, we focus on three side chains of varying hydrophobicity, M(1a-c).

M(1a) was synthesized in the following manner: dichloromaleic anhydride (1 g, 6 mmol) was added to a round bottom flask with a stir bar, dissolved in 12 mL ethyl acetate, and placed in an ice bath. Freshly cracked cyclopentadiene (1 mL) was added and the reaction mixture was stirred for 16 hours. Ethyl acetate was removed by vacuum. The crude reaction mixture (0.97 g, 4.2 mmol) was redissolved in toluene and placed over an ice bath. Octylamine (0.69 mL, 4.2 mmol) and triethylamine (0.12 mL, 0.836 mmol) were added dropwise. The reaction mixture was refluxed

with a Dean-Stark trap set-up. The product was purified by column chromatography. Yield = 1 g (70%). ^{1}H NMR spectrum is presented in Fig 4.1b.

M(1b) was synthesized in the following manner: dichlorophenyl maleimide (2.3 g, 9.5 mmol) was added to a round bottom flask with a stir bar, dissolved in 50 mL acetone, and placed in an ice bath. Freshly cracked cyclopentadiene (1.6 mL) was added and the reaction mixture was stirred for 16 hours. The product was purified by column chromatography. Yield = 1.8 g (61%). H NMR spectrum is presented in Fig 4.1b.

M(1c) was synthesized in the following manner: dichloromaleic anhydride (5 g, 29.9 mmol) was added to a round bottom flask with a stir bar. The round bottom flask was placed in an ice bath and then dissolved in glacial acetic acid (30 mL, 1 molar solution). Ethanolamine (1.9 mL, 31.4 mmol) was added dropwise. The solution was refluxed for 3 hours, until conversion was complete by ^{1}H NMR analysis. Acetic acid was removed by vacuum and used without further purification. ^{1}H NMR spectrum (*dmso-d6*): δ = 4.1 (-N-***CH₂***-CH_2-OH, t, 2 H), δ = 3.7 (-N-CH_2-***CH₂***-OH, t, 2 H), δ = 3.5 (-N-CH_2-CH_2-O***H*** b, 1 H). The crude product was dissolved in 10 mL THF and placed in an ice bath. Freshly cracked cyclopentadiene (6 mL) was added and the reaction mixture was stirred for 16 hours. The crude reaction mixture was re-dissolved in methylene chloride and washed three times with 0.1 M HCl and three times with 0.1 M KOH. The product was triturated in hexanes to remove excess dicyclopentadiene. Yield = 6.4 g (77%). H NMR spectrum is presented in Fig 4.1b.

We polymerized M(1a-c) using Grubbs 2nd generation catalyst. The syntheses of only poly(1c) and poly(2c) are described here but are representative. Monomer (1c) (260.2 mg, 0.94 mmol) was added to a vial with a stir bar. The vial was cycled with vacuum and N_2 three times. Monomer (1c) was dissolved in 8.9 mL of THF obtained from a solvent purification system via syringe. In a

second vial, Grubbs 2nd generation catalyst (4 mg, 0.00472 mmol) was added and purged with N_2 for 10 minutes. A small amount of THF (0.5 mL) was used to dissolve the catalyst under air-free conditions. The solution of the catalyst was added to the solution of monomer via syringe. The polymerization conversion was monitored by ^{1}H NMR. The polymerization was terminated by addition of ca. 1 mL of ethyl vinyl ether, followed by stirring for 15 minutes. The reaction mixture was precipitated into methanol and the precipitate was collected. Yield = 239.3 mg (92%).

Complete conversion of all three norbornene monomers was observed within 90 min by ^{1}H NMR spectroscopy (Figure 4.2a) and the polymers were purified by precipitation. Due to aggregation, as determined by dynamic light scattering in dimethylformamide (DMF) and tetrahydrofuran (THF), the molecular weight of poly(1a-c) could not be determined by size exclusion chromatography with in-line multi-angle light scattering. (Figure 4.3).

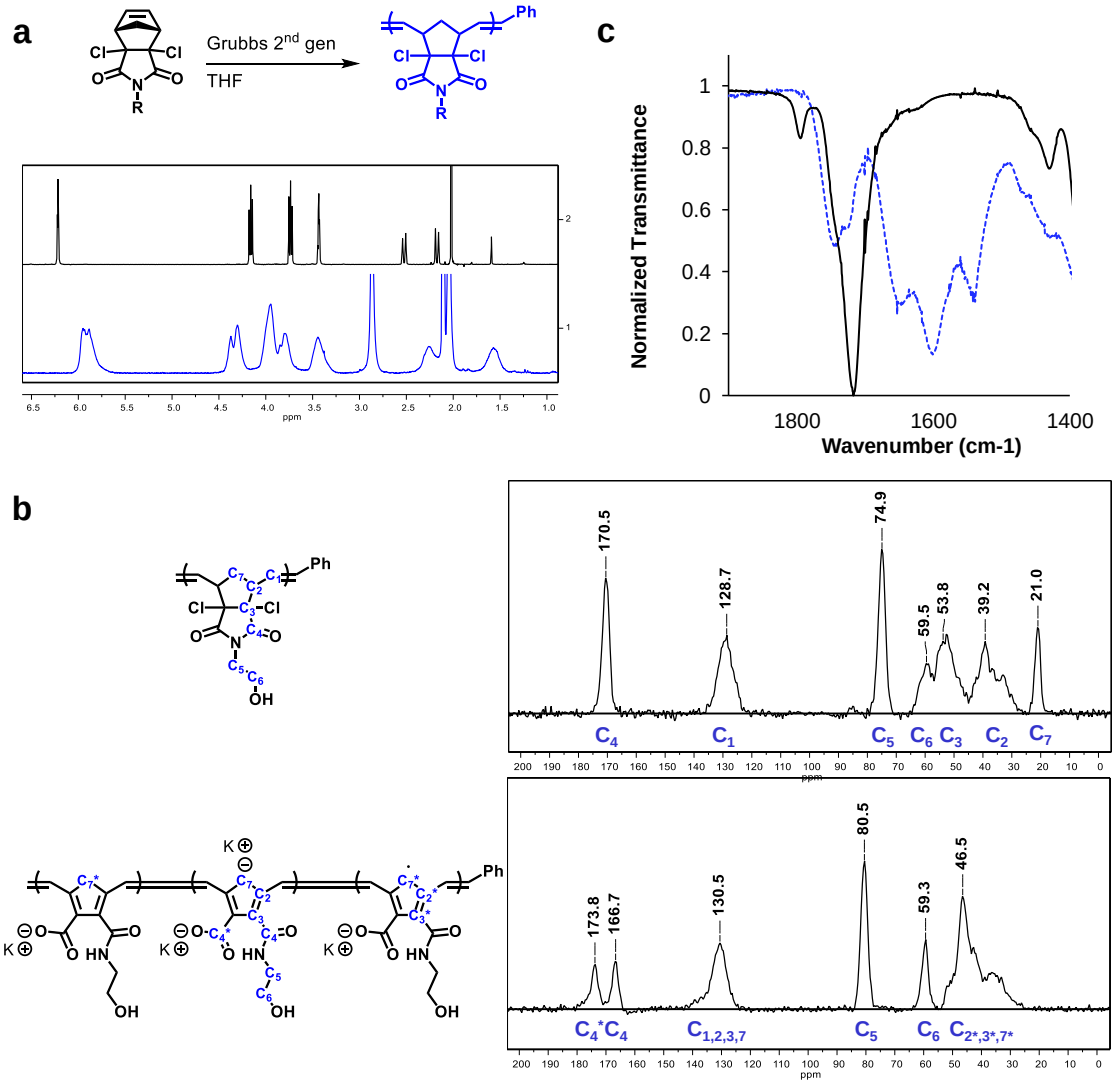

Figure 4.2. **Chemical structure identification of poly(2c).** [a]^{1}H NMR of M(1c) in $CDCl_3$ (top) and poly(1c) in acetone-*d6* (bottom). [b]Structures and CP-MAS ^{13}C NMR spectra of poly(1c) (left structure, top spectrum) and poly(2c) (right structure, bottom spectrum). [c]ATR-FTIR spectra of poly(1c) (blue) and poly(2c) (black) zoomed in on the carbonyl region.

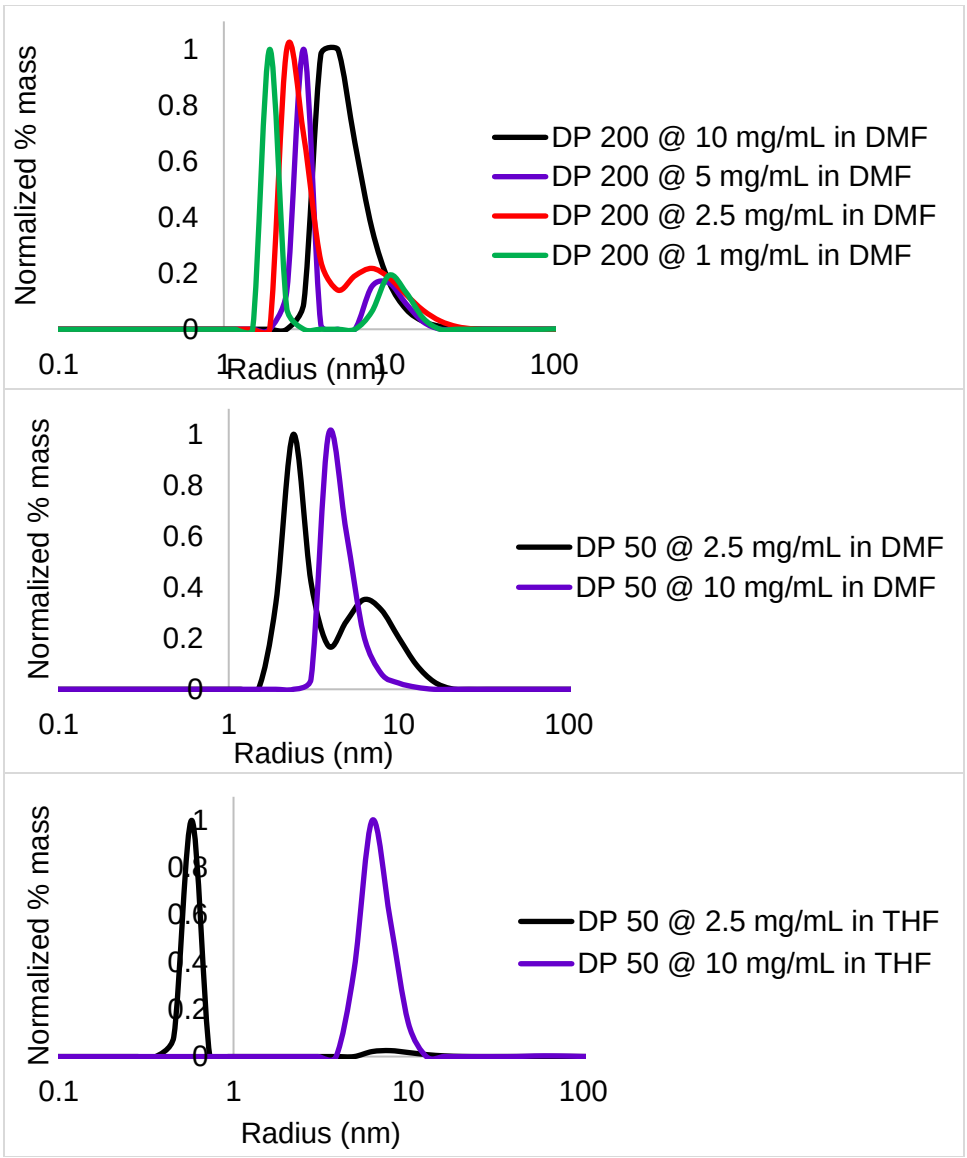

Figure 4.3. Overlapped DLS traces of poly(1c) of varying DPs and concentrations in DMF and THF. DLS of poly(1c) of DP 200 was taken in DMF (top). Lower molecular weight polymers of target DP = 50 were synthesized. DLS measurements of these DP = 50 polymers were dissolved taken at concentrations in both DMF (middle) and THF (bottom). All concentrations result in nonspecific aggregation in both solvents, even with low molecular polymers.

Poly(1a-c) were converted to their conjugated aromatic forms by the addition of base. We screened a variety of bases of varying steric bulk from tert-butoxide to sodium hydride in a variety of organic solvents. However, due to its high charge density, aPCPV exhibits limited solubility in these organic solvents. We found that slow addition of 0.1 M aqueous KOH into a solution of poly(1c) in DMSO resulted in complete conversion of poly(1c) to poly(2c) while keeping the polymer soluble during the reaction.

Poly(1c) (173 mg) was dissolved in DMSO (17.3 mL). An aqueous solution of 0.1 M KOH (18.8 mL, 1.88 mmol) was added dropwise and allowed to stir for 30 minutes. An aqueous solution of 1 M KOH (6.26 mL, 6.26 mmol) was added and allowed to stir for 1 hour. The polymers were purified by dialysis against water, lyophilized, redissolved in a small amount of water, centrifuged at 12500 rcf and the supernatant was run through a 0.45 μm PVDF filter to remove any unreacted pre-polymer. The final solution was frozen and lyophilized. The purified polymer was stored under vacuum. Yield = 138 mg (92%).

Solution ^{1}H NMR spectroscopy could not be used to monitor this reaction because both the reaction mixture and the purified polymer exhibited extreme line broadening (Figure 4.4). Therefore, we used solid state cross-polarization magic-angle spinning (CP-MAS) ^{13}C NMR analysis to confirm the structure of the final purified polymer (Figure 4.2b). CP-MAS ^{13}C NMR were taken at 273 K and a spinning rate of 15 kHz on a 700 MHz NMR spectrometer. Parameters were optimized to maximize signal intensity. For poly(1c), d1 = 8 sec, p3 = 2.5 μs, p15 = 3500 μs, pcpd2 = 4.5 μs and for poly(2c), d1 = 16 sec, p3 = 3 μs, p15 = 3500 μs, pcpd2 = 8 μs. NMR spectra were referenced to high frequency signal of adamantane. Three differences in the NMR spectra are consistent with conversion of poly(1c) to poly(2c). First, the NMR spectrum of poly(2c) shows the complete disappearance of the C_3 signals at 53.8 ppm which arises from the C-Cl bond. Second,

the spectrum of poly(2c) shows complete disappearance of alkyl signals which arises from C_7 only in poly(1c). Third, the appearance of a new peak in the carbonyl region can be attributed to a new carboxylic acid that forms from imide hydrolysis.

We further corroborated the polymer structure by ATR-FTIR spectroscopy. We observed loss of the prominent absorbance at 1714 cm^{-1}, which corresponds to the poly(1c) imide. We also observed the appearance of new absorbances from 1500-1750 cm^{-1} (Figure 4.2c). The shift into lower wavenumbers is consistent with the formation of the carboxylate from imide hydrolysis, as well as the weakening of the C-O bond via favored anionic "enolates" resonance structures which are only possible in the conjugated form.

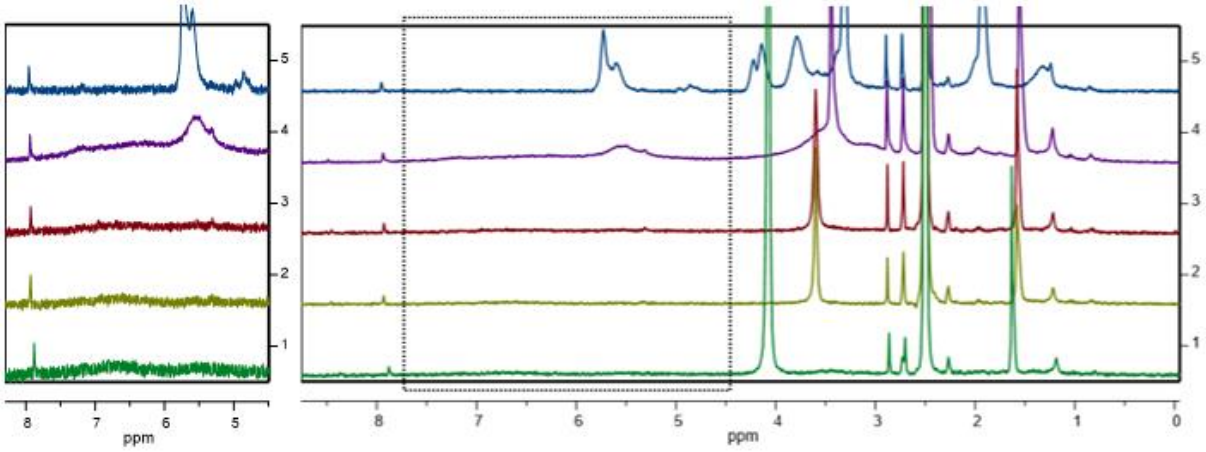

Figure 4.4. NMR scale experiment to monitor the conversion of poly(1c) to poly(2c) in DMSO-d6 by dropwise addition of KOD in D_2O. A small amount of DMF was added to act as an internal scale bar. Increasing equivalents of KOD resulted in extreme broadening and ultimately elimation of the previously well-resolved peaks of the prepolymer to the point, a phenomenon which has been previously observed with conjugated polymers.[230] Top to bottom shows different equivalents of KOD added: 0, 1, 2, 3, 10 equivalents relative to the repeat unit. Left side is a zoom in of the vinyl region.

The use of a norbornene framework offered advantages over an oxanobornene framework. In polynorbornene, the elimination of the two chlorides results in a new acidic proton *in situ* which can be deprotonated to create the cyclopentadiene anion repeat unit that can impart high water solubility without the need for water-solubilizing side chains. As expected, due to the anionic backbone and acid side chain, poly(2a-c) are all readily soluble in water despite the hydrophobic side chains in poly(2a) and poly(2b). We dissolved poly(2c) in water and found the pH to be 4-4.5 with concentrations as low as 0.15 mg/mL, consistent with the low pKa of the side chains. Poly(2a) shows expected pH-dependent solubility from the cyclopentadiene anion and carboyxlic acid group. Dissolved polymer crashes out of solution upon acidification to pH 1 with 1M HCl and redissolves upon addition of 1M KOH to pH 14 (Figure 4.5).

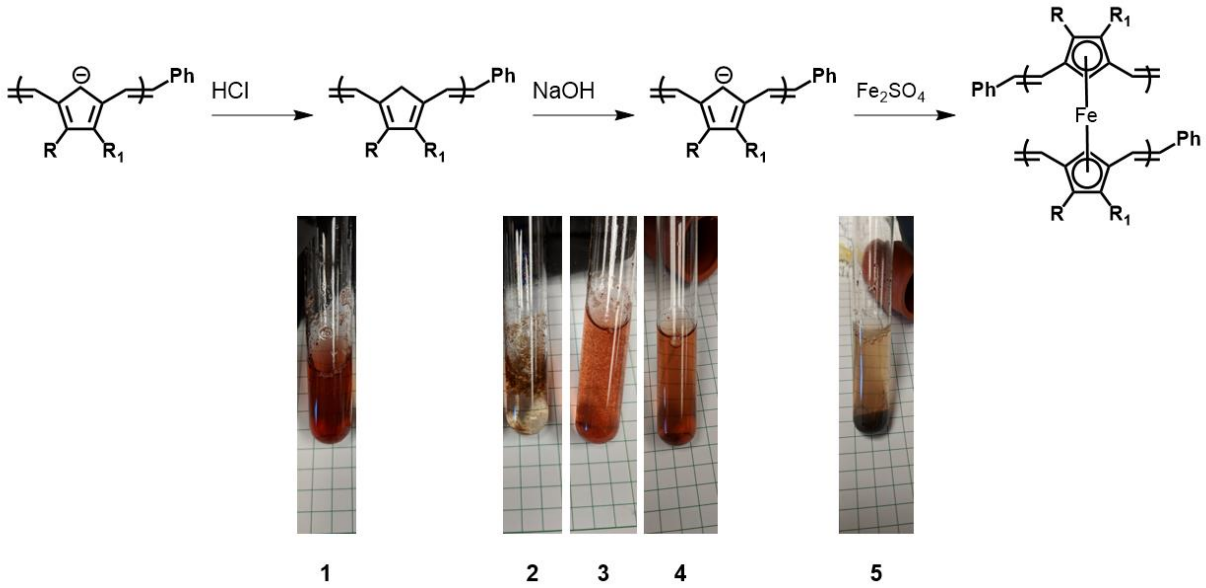

Figure 4.5. pH dependent solubility switching of aPCPV. Left to right, 1-5. Picture 1 shows the polymer fully dissolved in water. Picture 2 is the sample upon addition of HCl. Picture 3 is the sample upon addition of NaOH. Picture 4 is the same sample after 30 minutes (fully dissolved). Picture 5 shows that addition of $FeSO_4$ in solution results in precipitate formation.

4.3.2 *Characterization of the optical, electronic, and redox behavior of poly(2)*

In its fully reduced state, poly(2c) absorbs UV-Vis light up to 610 nm (Figure 4.6a), an optical band gap of 2.03 eV. The UV-Vis spectrum of poly(2c) shows 3 λ_{max} values and irradiation of the polymer at each of its three λ_{max} results in a different fluorescence wavelength (Figure 4.6a).

We attempted to monitor the conversion of poly(1c) to poly(2c) by UV-Vis spectroscopy because solution ^{1}H NMR spectroscopy proved ineffective. Although 4 equivalents of KOH are needed per repeat unit for full conversion to poly(2c), we noticed that addition of 1 equivalent of KOH resulted in UV-Vis absorption of the fully conjugated polymer. We also observed a loss of long wavelength absorption with addition of aqueous KOH (Figure 4.6b). We initially expected that as more KOH is added to the solution, poly(2c) would absorb more long-wavelength light, as more of the polymer becomes conjugated. The counterintuitive results can be explained in two parts. First, addition of 1 equivalent likely resulted in aromatization of 1/3 of the repeat units instead of elimination of one chloride from each repeat unit, and 1/3 of the polymer length exceeds the persistence length of the polymer. Elimination of one chloride from a repeat unit makes every proton on that repeat unit more acidic, resulting in accelerated aromatization. Second, the loss of long wavelength absorption is likely due to oxidation of aPCPV from water and dissolved oxygen.

We confirmed the presence of an organic radical, consistent with oxidation of the repeat unit from a (-1) state to a neutral radical, by electron spin resonance (ESR) spectroscopy (Figure 4.6c). CP-MAS ^{13}C NMR analysis corroborates oxidation of poly(2c). We originally expected there to be complete disappearance of signals in the δ = 30-50 ppm range due to the completely sp^2 hybridized carbon backbone of poly(2c). We attribute the signals at δ = 30-50 ppm to oxidation of poly(2c) under experimental conditions, which would give rise to allylic signals from $C_{1,2,3,7}$.

Cyclic voltammetry data are also consistent with the oxidized state of poly(2c). Cyclic voltammetry experiments were performed with FTO coated glass as the working electrode, Ag/AgCl as the reference electrode, and Pt as the counter electrode. The voltage was varied through the entire electrochemical window of the solvent two times at different rates from 10-100 mV/sec and the second sweep was plotted. The electrochemical activity of poly(2c) was measured in an aqueous solution at a concentration of 5 mM with respect to an idealized monomer repeat unit of 313.46 Da in a solution of 100 mM KCl as a supporting electrolyte. Poly(2c) exhibits electrochemical activity with reducing potential with the onset at -0.42 V vs. Ag/AgCl and a peak of -0.72 V vs. Ag/AgCl (Figure 4.6d).[231] However, no electrochemical oxidation current can be detected by cyclic voltammetry.

We hypothesize that the lack of electrochemical oxidation of poly(2c) is due to its facile oxidation by water, given the significant overlap between the highest occupied molecular orbital (HOMO) of poly(2c) and the lowest occupied molecular orbital (LUMO) of water. The energy level of the poly(2c) HOMO can be calculated using its reduction potential. Common n-type semiconductors become negatively charged because electron injection occurs at its LUMO; thus, the reduction potential is commonly used to determine the energy level of its LUMO. However, we believe poly(2) houses its negative charge in the aromatic cyclopentadiene anion HOMO, and that the reduction of poly(2c) at -0.72 V v. Ag/AgCl is due to an electron injection into the HOMO of poly(2c). A scan of 100 mM KCl solution without polymer shows that water is reduced at -0.75 V v. Ag/AgCl via electron injection into its LUMO. That the HOMO of poly(2c) coincides with the LUMO of water is consistent with our hypothesis that water can oxidize poly(2c).

Mechanistically, we envision that oxidation of poly(2c) results in cyclopentadiene radicals and that quickly terminate each other. But due to the resonance stabilization of the radicals, the termination is readily reversible. Two key pieces of experimental data are consistent with this. First, although we can detect the presence of an unpaired electron by ESR spectroscopy, extremely high concentrations (> 50 mg/mL) are needed to observe any signal. Although it is common to use low concentrations of organic radicals due to intermolecular quenching, poly(2) can quench itself intramolecularly and thus high concentrations only improves signal. The low concentration of radicals can be explained by the reversible radical-radical coupling between repeat units.

Second, poly(2) can be chemically reduced by sodium ascorbate under high pH conditions. Sodium ascorbate is known to be a proton-coupled electron transfer agent.[232] Poly(2c) was dissolved in 0.1 M KOH and 100 equivalents of sodium ascorbate were added. The reaction progress was monitored by following the absorption at λ = 393 nm and λ = 493 nm. Ascorbate quenches the radical on aPCPV and the bridgehead proton can be deprotonated again by hydroxide to regenerate the fully anionic polymer (Figure 4.7, top). The absorbance at 393 nm initially spikes upon addition of ascorbate due to the absorption by ascorbate (Figure 4.6e). The absorbance at λ = 393 nm continues to increase due to the re-reduction of the polymer but the monotonic decrease after 15 seconds is likely due to the degradation of the sodium ascorbate. The reduction of the polymer can be more accurately monitored by the increase in the absorption λ = 493 nm which is unique to the polymer. However, 100 equivalents of sodium ascorbate are consumed within 105 minutes and the polymer starts to oxidize again, as seen by a reduction in decrease in 493 nm absorption at 120 minutes. The increased absorption at λ = 493 nm could not be achieved in PBS 7.4 buffer, suggesting that the strong reducing power of deprotonated ascorbate and subsequent deprotonation are essential to restore the polymer. We also explored the use of other common *in-*

vivo reductants including reduced nicotinamide adenine dinucleotide, glutathione, and tris(2-carboxyethyl)phosphine. However, the other reductants did not result in any changes to the UV-Vis absorption spectrum of poly(2c) (data not shown). That a strong proton-coupled electron transfer reducing agent could reduce the polymer is consistent with our hypotheses that poly(2c) oxidation results in radicals and that the termination processes are readily reversible.

The same reducing conditions were used to determine the effect of oxidation state on the molecular weight of poly(2c). Gel permeation chromatography (GPC) analysis of poly(2c) in water "as is" showed multimodal traces and was consistent with the presence of crosslinked high molecular weight species due to interpolymer radical-radical termination events. We hypothesized that reduction of poly(2c) by sodium ascorbate under high pH conditions would result in loss of crosslinks and formation of lower molecular weight species. Poly(2c) was treated with sodium ascorbate and hydroxide and analyzed by GPC after a 15-minute incubation. As expected, the polymer was reduced and the molecular weight of poly(2c) decreased (Figure 4.7). After an additional 30 minutes, another small aliquot was taken for GPC analysis. Poly(2c) again showed the formation of high molecular weight species, consistent with reformation of crosslinks between the cyclopentadienyl radical repeat units. Light scattering (LS) traces are shown instead of differential refractive index (dRI) traces because the dRI traces are dominated by the small molecule ascorbate signal and LS ismore sensitive to the large molecular weight species.

Because poly(2c) is oxidized quickly by water, we sought alternative solvents to dissolve poly(2c). However, polar solvents such as acetonitrile, dioxane, dimethylformamide, dimethyl sulfoxide, and tetrahydrofuran could not fully dissolve poly(2c) without the addition of at least 5-10 vol% water. Thus, we decided to continue to use poly(2c) “as is.” We could not obtain a uniform film of poly(2c) for 4-point probe measurements and thus we dropcast poly(2c) onto FTO-coated

glass substrates and determined current-voltage characteristic curves by a point scan in conductive AFM (Figure 4.8a). Conductive AFM was performed on an Asylum Reserach MFP3D-Bio using gold coated contact mode AFM probes (Budget Sensors, ContGB-G).

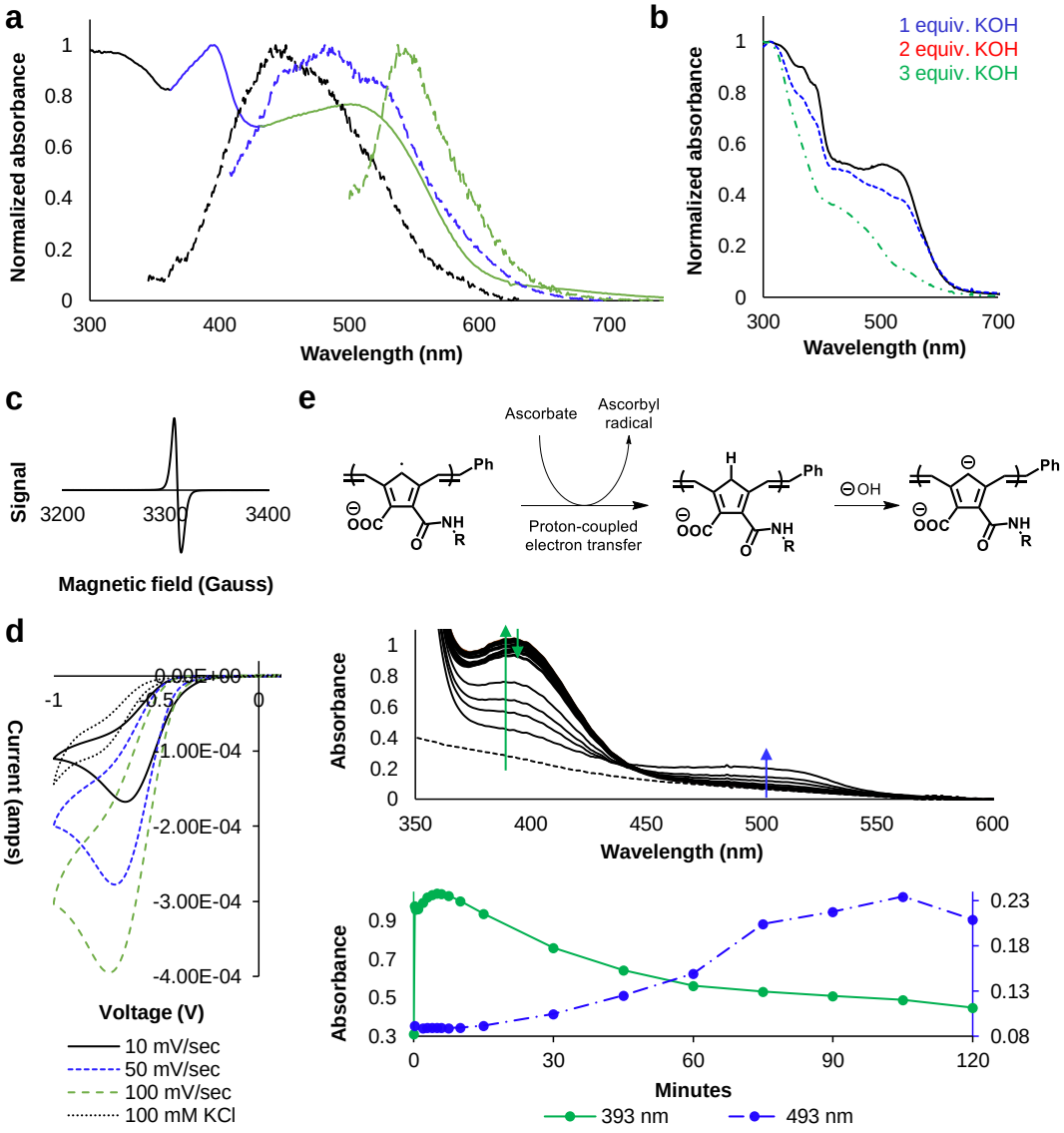

Figure 4.6. **Redox behavior of poly(2c). a,** UV-Vis and fluorescence measurements of poly(2c). Solid lines are absorbance and dotted lines are fluorescence and spectra are color coded. **b,** UV-Vis measurements of poly(2c) with 0.5 equivalents (black), 1 equivalent (blue), 2 equivalents (red), and 3 equivalents (green) of KOH supplied in a 0.1 M solution of KOH. **c**, Powder ESR spectrum of

poly(2c) shows the presence of an organic radical. **d**, CV of poly(2c) at 5 mM with respect to monomer repeat unit in a solution of 100 mM KCl. CVs were taken at different scanning speeds. Background scan of 100 mM KCl with no polymer was taken at 100 mV/sec. **e**, Reduction of aPCPV into its fully reduced form with 100 equivalents of sodium ascorbate. Top is the proposed mechanism for reduction. Middle is stacked overlay of UV-Vis spectra of a sample exposed to reducing conditions taken over 120 minutes. The polymer starting UV-Vis spectrum is a dotted. Bottom is a plot of the absorbance values at 393 nm (black) and 493 nm (blue).

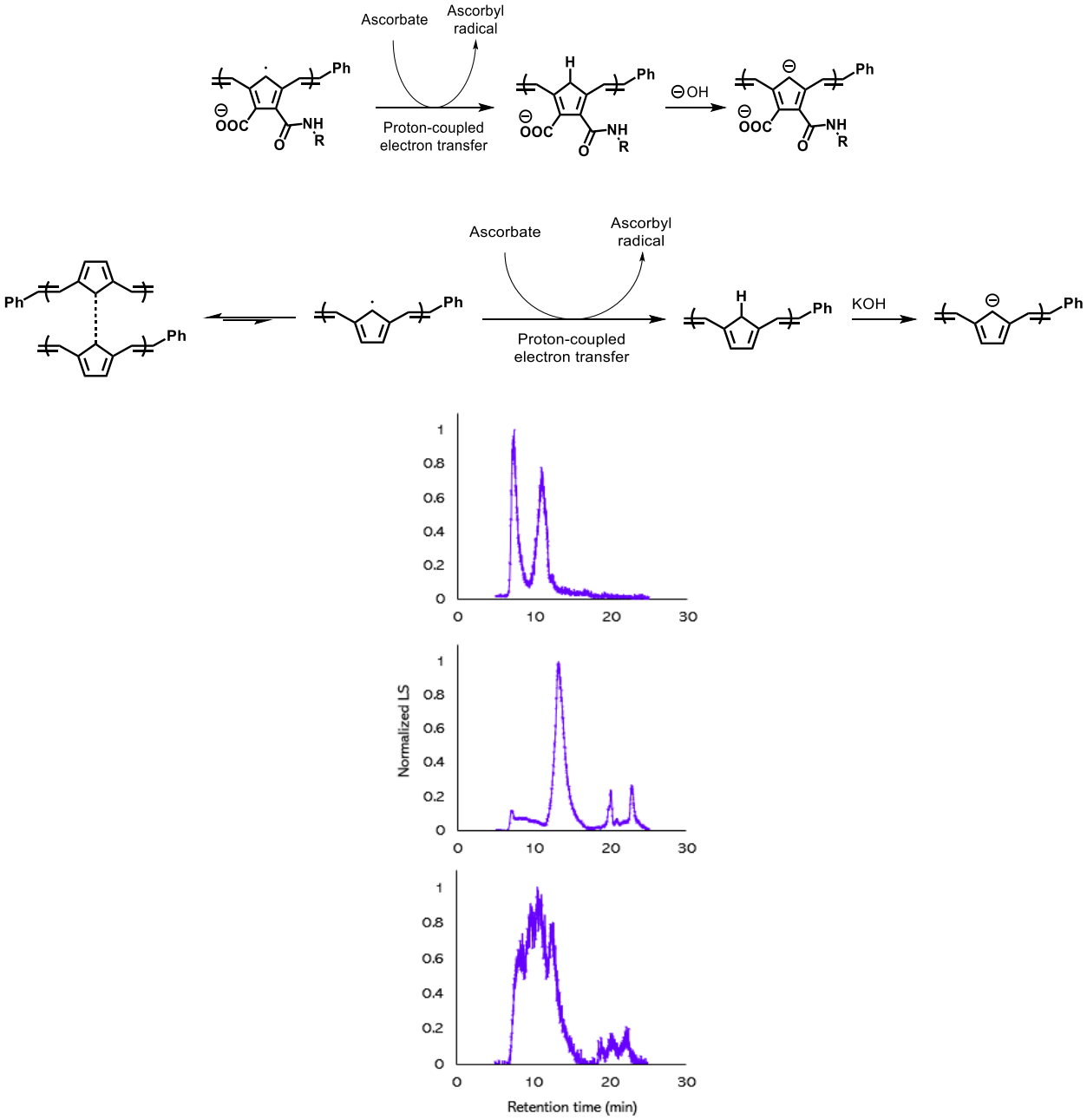

Figure 4.7. GPC LS traces of poly(2c) with the reduction by sodium ascorbate and KOH. Top is the GPC of the starting polymer. Middle is the GPC of the polymer after 15 minutes of exposure to reducing conditions. Bottom is the GPC of the polymer after 45 minutes.

4.3.3 *Preparation and characterization of conducting hydrogels for biomedical applications*

We returned to our original motivations for synthesizing a water-soluble conjugated polymer for the purposes of simplifying fabrication procedures for CHs. Because the reduced state of poly(2c) cannot be maintained in water, we used poly(2c) "as is." The polymer was formulated into 2.5 wt% agarose hydrogels in water at a final concentration of 2.5 mg/mL polymer. A stock solution of of 5%w agarose was made in Nanopure water. A stock solution of 10 mg/mL poly(2c) was made in Nanopure water. The stock solution of poly(2c) was maintained at 70 ºC to prevent cooling of the agarose gel upon mixing. The agarose stock solution was heated with a microwave until it was homogenous and could be pipetted. 3.5 mL of the agarose stock solution was added to a petri dish. 1.75 mL of the poly(2c) stock solution was added to the petri dish and in mixed thoroughly. The remaining volume was made up with 1.75 mL Nanopure water (no salt condition) or 0.7 mL 10x HBSS and 1.05 mL Nanopure water (salt condition). The Nanopure water and 10x HBSS were also maintained at 70 ºC to prevent it from cooling of the agarose gel upon mixing. 4-point probe measurements were taken with a Cascade Microtech C4S 4-point probe head connected to a Keithley 2400 multimeter. Measurements were taken 10 times per sample. Sodium polystyrene sulfonate was used as a nonconjugated polyelectrolyte control. We measured the resistances of the hydrated and dehydrated gels 10 times for each sample with a 4-point probe (Figure 4.8b). The hydrated gels showed higher conductivities than the control conditions. Interestingly, the dehydrated gels doped with poly(2c) exhibited far less resistance at a high salt concentration which suggests that ion concentration may heavily influence the electrochemical behavior of aPCPV, a commonly observed phenomenon in CPs due to their ion-charge coupling and the basis of organic electrochemical transistors.[233]

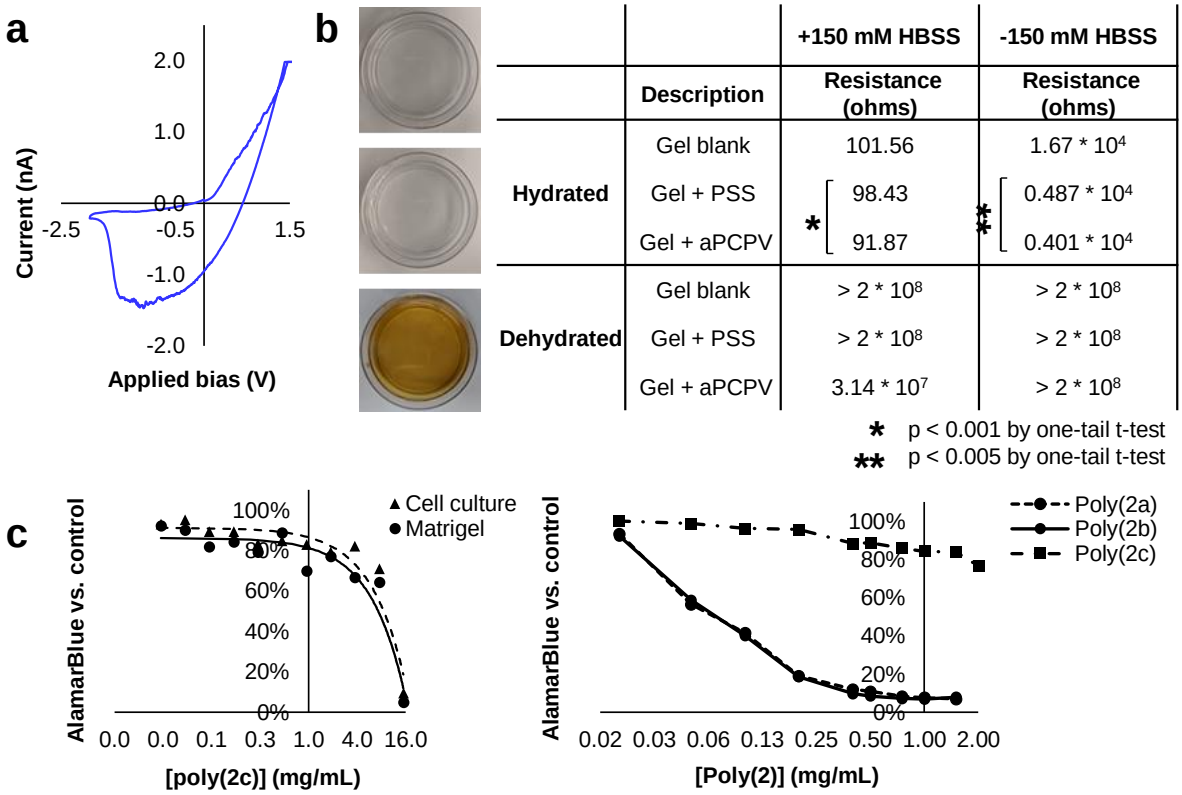

Figure 4.8. **Electrical behavior of poly(2c). a,** IV curve determined by a conductive AFM on a dropcast film on FTO functionalized glass. **b,** Representative images of hydrogels doped with poly(2c). Top, blank hydrogel; middle, hydrogel with poly(styrene sulfonate), hydrogel with poly(2c). Resistance values determined by 4-point probe of hydrated and dehydrated agarose hydrogels. **c,** cytotoxicity assays of poly(2c) determined by AlamarBlue assay in normal cell culture conditions for NIH 3T3 fibroblasts (left), and in Matrigel (right).

4.3.4 *Cytotoxicity assays for aPCPV*

The cytotoxicity of Poly(2c) was determined by AlamarBlue assay after incubating poly(2) with NIH 3T3 fibroblasts at various concentrations for 12 hours. 7500 NIH 3T3 fibroblasts were plated in a 96-well plate in triplicate. Each well was 100 uL media or 100 uL of a 1:60 dilution of Matrigel. The cells were treated with poly(2c) in a range of concentrations up to 15 mg/mL.

Polymer only conditions were also plated in triplicate. After 12 hours of incubation, 10 uL of AlamarBlue was added to the wells and allowed to incubate for 4 hours. The 96-well plate was analyzed by a plate reader (excitation: 560 nm, emission: 590 nm). The AlamarBlue absorbance and fluorescence values of the polymer only wells were subtracted from the wells with cells. The IC_{50} of poly(2c) under normal cell culture conditions was 8.4 mg/mL and in 1:60 dilution of Matrigel was 7.3 mg/mL (4.8c, left). We hypothesize that the toxicity could be due to the extremely high salt concentration from the aPCPV.

Cytotoxicity assays were repeated with poly2(a-c) on neural progenitor cells isolated from the forebrains of 8-week old mice. 15,000 mouse primary neural progenitor cells (NPCs) were plated in a 96-well plate in triplicate. NPCs were cultured with serial dilutions of poly2 (2mg/ml) in NPC growth-media (DMEM/F12, N2 supplement, 20ng/ml FGF, 20ng/ml EGF). After 20 hours, growth media was supplemented with 1/10 volume of AlamarBlue and incubated 4 hours before fluorescence analysis (excitation: 560 nm, emission: 590 nm). Poly(2c) exhibited high biocompatibility while poly(2a) and poly(2b) exhibited extreme cytotoxicity, likely due to interactions of the hydrophobic side chains with the cell membrane. (Figure 4.8c, right).

4.4 CONCLUSION

We report our initial efforts in the synthesis, characterization, and application of a new class of water-soluble conjugated polyelectrolyte. aPCPV displays UV-Vis absorption up to 610 nm, is conductive, and exhibits low cytotoxicity. Due to its high water-solubility, aPCPV can easily be mixed into hydrogel formulations without advanced fabrication techniques, and thus we believe that this new class of polymer will be readily adopted in the field of tissue engineering. Additionally, this insulating precursor approach can be used to synthesize families of not-yet-explored π-conjugated vinylene polymers from insulating precursor polymers made via ROMP.

4.5 FUTURE DIRECTIONS FOR APCPV

4.5.1 *Determining structure-function relationships of aPCPV*

4.5.1.1 Determining the effect of polymer side chains on the electrochemical activity of aPCPV

Due to the high functional group compatibility of ROMP, it is possible to synthesize aPCPV derivatives with a variety of side chains. Norbornene monomers with a variety of side chains have already been synthesized (Figure 4.9).

Because the side chain is in conjugation with the π-conjugated backbone, it is possible to use the side chains to affect the redox potential of aPCPV. The use of electron-withdrawing substituents, such as the 4-nitroaniline substituent, would make poly(2) more easy to reduce (less negative reduction potential) because of the stabilization of the negative charge on the polymer backbone.

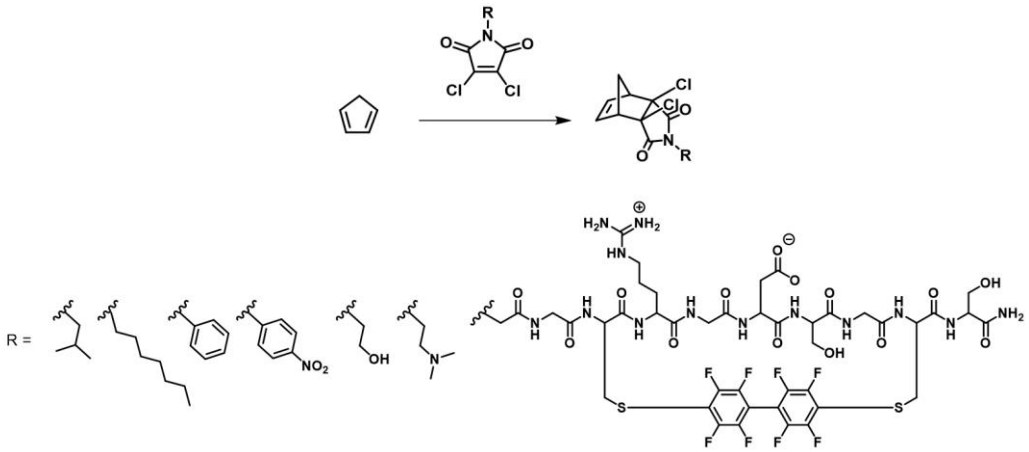

Figure 4.9. Monomers already synthesized for synthesis of poly(1) and poly(2).

4.5.1.2 Determining the effect of the cation on the electrochemical activity of aPCPV

The redox properties and doping behaviors of CPs can be modulated by the ions used to neutralize the charge injection.[233] Due to the synthesis of aPCPV, the ion-charge pairing is determined by which hydroxide counterion is used. Addition of KOH and NaOH have already been proven to result in full conversion into K^+ aPCPV and Na^+ aPCPV but the differences in the

behavior of these two polymers have not been investigated. It may also be possible to use divalent cations with the addition $CaOH_2$ and $FeOH_2$ although alternative synthetic strategies may have to be adopted due to their limited solubilities in water.

4.5.2 *aPCPV as a conductive agent in conductive hydrogels for cardiac applications*

Damage to electrically active cells such as cardiomyocytes and neurons are often catastrophic and irreparable. As of 2019, cardiovascular disease remains the leading cause of mortality in the United States, and in 2016, over 800,000 Americans died from cardiovascular disease.[234] Every year, 1.5 million cases of myocardial infarction (MI) occur and the subsequent ischemic heart damage results in irreversible damage to heart function due to formation of nonconductive scar tissue, ventricular stiffness, and altered contractibility.[235] Heart transplantation remains the only definitive treatment for ischemic heart damage but these procedures are risky and donors are limited.

Cell therapies delivered have been proposed as a regenerative medicine approach for the treatment of MI[235–237] and SCI.[238,239] However, these cell therapies have much room for improvement.[240] Cell therapies for cardiac repair can be improved by differentiating, culturing, or delivering cells in conductive hydrogels (CHs) which have been shown to benefit the culture of excitable cells.[193–197] For example, maturation of iPSCs in materials that better mimic physiological adult myocardium and with early stage electrical stimulation can serve as a useful model tissue for cardiac therapies.[198,199]

One common approach to making CHs is to dope them with π-conjugated polymers (CPs). Many reviews on the use of π-conjugated polymers (CPs) in medicine point to their potential to revolutionize the field of tissue engineering and bioelectronics. However, despite the many theorized advantages of synthetic CPs (such as tunability, post-synthetic functionalization, and

large-scale production), they have not lived up to their potential. Many CHs doped with CPs exhibit undesirable mechanical properties, limited biological integration, cytotoxicity and post-implantation inflammation.[195,196]

Preliminary experiments to determine the effect of aPCPV on the calcium transients on iPSC-derived cardiomyocytes were performed in collaboration with Eileen Brady and Prof. Kelly Stevens. iPSC-derived cardiomyocytes were encapsulated in a 1:40 dilution Matrigel with (experimental condition) or without polymer (control). Transient rises and reductions of cytosolic Ca^{2+} were studied by confocal imaging with the use of fluo-4 Ca^{2+} indicator (Figure 4.10a),[241] and the frequency of these Ca^{2+} spikes were quantified (Figure 4.10b). Cardiomyocytes cultured in the presence of aPCPV exhibited higher rate of Ca^{2+} transients (Figure 4.10c), which is consistent with other reports of CPs resulting in lower cell membrane capacitance.[242]

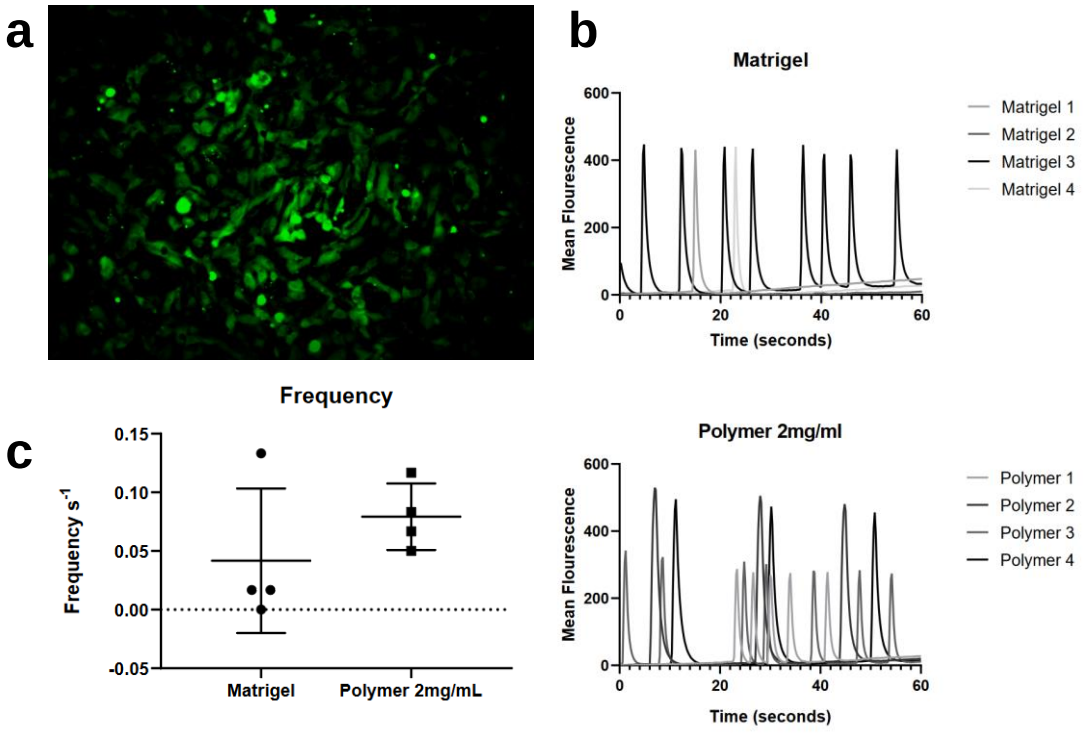

Figure 4.10. ***a***, Confocal micrsocopy image of iPSC-derived cardiomyocytes in Ca^{2+} spark detection experiment. ***b***, Fluorescence spikes due to Ca^{2+} transients for cardiomyocytes cultured in 2 mg/mL aPCPV (bottom), and without aPCPV (top). ***c***, Quantification of Ca^{2+} transient spikes. Data courtesy of Eileen Brady and (Lab of Prof. Kelly Stevens).

4.5.2.1 Strategies for incorporating aPCPV into CHs

CHs doped with aPCPV can be fabricated by direct incorporation into naturally-gelling biomaterials, by functionalizing the polymer with self-assembling gelling peptide, and by incorporation into 3D printable hydrogel formulations. Formulations with elastic moduli of around 9 kPa, similar to native myocardium, will be selected for further optimization in subsequent experiments.[243]

CPs can be doped into naturally-gelling biomaterials (e.g hyaluronic acid, collagen, alginate, agarose, and Matrigel). In this approach, we hope to maintain the mechanical properties of the natural hydrogel while only changing the conductivity of the gel, as mechanical strength of hydrogels has also been shown to affect the viability and proliferation of CM.[216,244] It is only possible to control the mechanical properties of the hydrogel independently of the conductivity because our CP is readily soluble in water. The conductivity of the final CH will be determined by 4-point probe and the mechanical properties will be measured by rheology.

It is also possible to incorporate aPCPV into existing 3D printable hydrogel formulations.[245–249] Due to its high water solubility and no need for organic co-solvents, incorporation of aPCPV may require minimal adjustments to these existing hydrogel formulations.

In our final approach, we will use the polymer itself as a gelling component by functionalizing the polymer side chains with self-assembling peptides such as FEFKFEFK.[250] This second approach is possible because ROMP polymers can easily be functionalized with peptide side chains.[88,251] The Pun lab already has experience incorporating polymers into peptide-based hydrogels formed by self-assembly of motifs such as FEFKFEFK. Although this approach does not allow for independent tuning of mechanical properties from conducting properties of the hydrogel, it allows for large amounts of the polymer to be incorporated. The conductivity of the final CH will be determined by 4-point probe and the mechanical properties will be measured by rheology.

4.5.3 *aPCPV as a conductive agent in conductive hydrogels for neural applications*

Traumatic spinal cord injuries (SCI) have devastating physical, social, and vocational consequences for patients and their families due to patients' loss of independence and increased mortality. Initial traumatic events involve mechanical disruption of the vertebral column and

damage to neurons, oligodendrocytes and nearby vasculature, and compromises the blood-brain barrier. Secondary cellular changes which include hemorrhages, influx of inflammatory cells and cytokines, result in a cascade that leads to permanent damage to the spinal cord and neurological disfunction.[238] Treatments for SCI are expensive, long in duration, and include many different approaches including surgery, electrical stimulation, and rehabilitation therapy.[238] Despite these many approaches, recovery is limited. Just as CHs have been shown to improve the cell therapies to treat MI, the use of CHs have also been shown to improve cell therapies for neural stem cell differentiation.[200–202]

Preliminary experiments were done in collaboration with Dr. Matt K. Hogan, Dr. Robert Krencik, and Dr. Philip J. Horner at Houston Methodist. We first examined whether doping Matrigel with aPCPV would alter observed spontaneous bursting activity of cultured hiPS derived neural cultures. At early timepoints, spontaneous burst rates are indicative of maturity of *in vitro* neural stem cell-derived cultures. As cortical neural cultures develop, we expect firing patterns to stabilize and complex network dynamics to inform us of synaptic and circuit level development within the cultures.[252] Oscillatory rhythmic firing patterns of organoids have been found to mimic those of developing neonates and may be informative of circuit level organization of neural ensembles within a culture.[253] Further, the relative conductive capabilities of a hydrogel formulation may serve to propagate local field potentials of neurons within the spinal cord. We propose to examine the distribution of observed neural spike amplitudes as a relative indicator of the ability of extracellular field potentials to conduct through a given formulation. As such, spontaneous burst rate, spiking amplitudes and rhythmic activity patterns will all be assessed to examine the ability of a hydrogel formulation to support and enhance development of neural cultures.

Chambers of a 6-well MEA dish were coated with Matrigel doped with 0, 0.5 and 2 mg/mL aPCPV respectively. Neurospheres were induced to form neurospheres through DOX induced upregulation of neurogenin over 15 days before neurospheres were plated onto the electrodes. Spontaneous activity was collected using a MEA2100 amplifier system and analyzed for spontaneous burst rate (Figure 4.11). After 3 days of culture, we observed significantly higher levels of spontaneous firing rates in chambers doped with aPCPV compared with controls (*p*-value = 0.039).

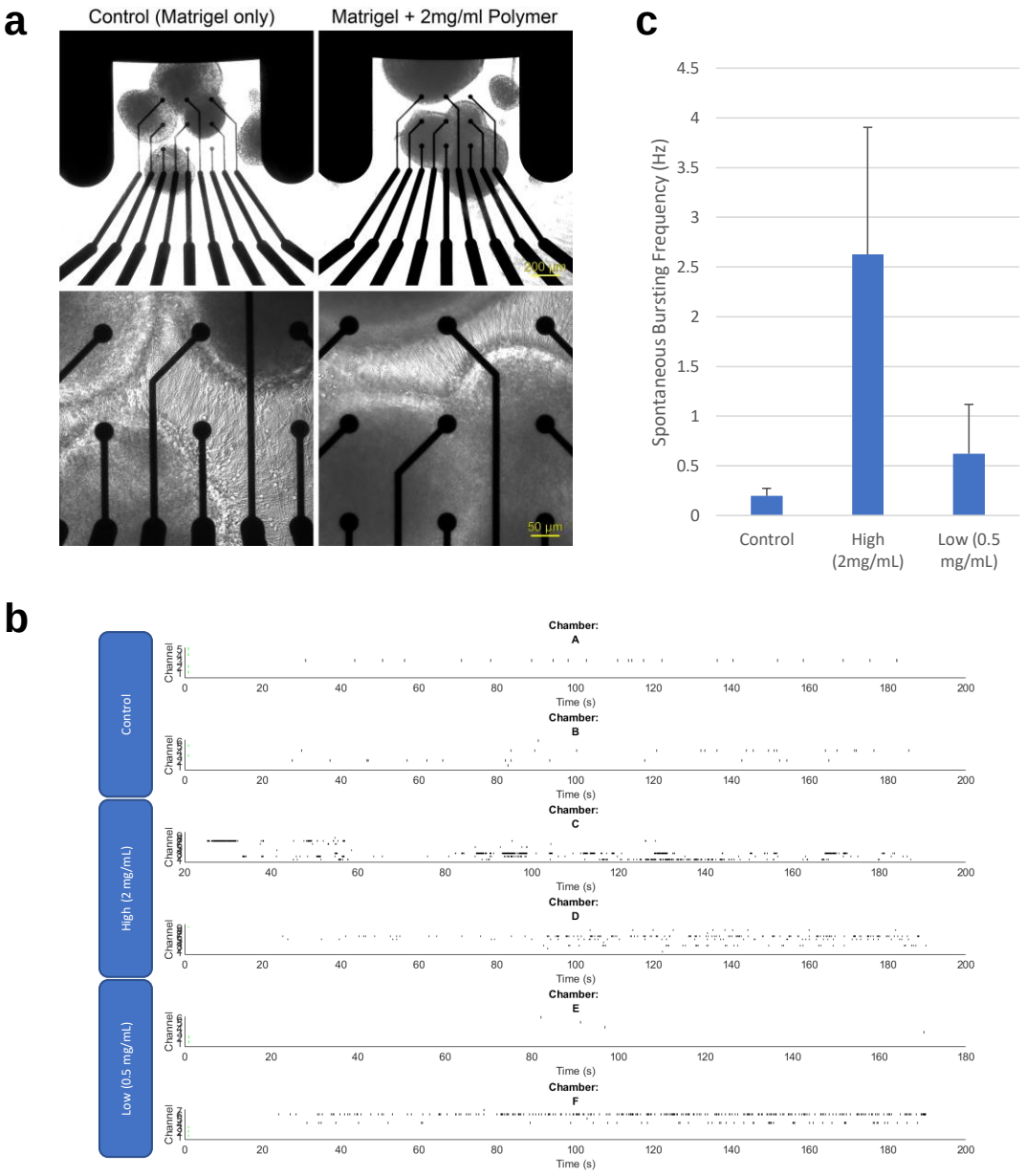

Figure 4.11. ***a***, Image of the microelectrode arrays used to monitor spontaneous activity. ***b***, Action potential activity of NPCs cultured in different concentrations of aPCPV. ***c***, Quantification of action potential activity of NPCs. Data courtesy of Dr. Matthew K. Hogan (Lab of Prof. Philip J. Horner) and Dr. Robert Krencik.

We also examined the properties of motor evoked potentials elicited from ventral cervical spinal stimulation using both aPCPV/Gelatin doped electrodes and bare uncoated electrodes. The Horner Lab developed a novel means for stimulating the cervical motor pool in rats via placement of a thin film gold electrode in the ventral epidural space. By placing electrodes geometrically closer to motor pools, we can selectively target motor associated circuitry without secondary stimulation of sensory and propriospinal circuitry. Placement of electrodes in this space requires higher currents to initiate motor recruitment due to relatively higher amounts of insulating white matter between the electrode and the circuits of interest compared with epidural dorsal and intraspinal approaches. Gold is very biocompatible, flexible and can be easily incorporated into standard flexible electronic fabrication processes, however the charge injection capacity of gold with CNS tissue is limited. Doping the electrode with a conductive hydrogel may improve the charge injection and reduce the currents needed, thus facilitating a ventral spinal approach.

Electrodes were coated in crosslinked gelatin doped with aPCPV conductive polymer. Briefly, a gelatin was prepared with EDC:NHS crosslinking at a 1:1 ratio. A 3% gelatin solution was prepared in 85% water, 15% glycerol solution and brought to 0.1M EDC and 0.1M NHS. We then added aPCPV to a concentration of 4 mg/mL while solution was kept at 45 deg C on a stir plate. After 1 hour of crosslinking, we prepared an electrode via dip coating. The electrode was allowed air dry for 1 hour and the process was repeated twice more. We examined evoked potentials in 7 muscle groups of the forelimb: Infraspinatus, Trapezius, Tricep, Bicep, Wrist Extensors, Wrist Flexors and Hand. Evoked potential thresholds were typically between 400-600 uA using unplated gold electrodes, however doped electrodes elicited potentials in all 7 muscles with less than 100 uA of injected current.

4.5.4 *aPCPV as an in-vivo magnetic resonance imaging (MRI) contrast agent*

4.5.4.1 Current MRI contrast agents

For the fundamentals of NMR, I would recommend reading *Spin Dynamics* by Malcolm H. Levitt. It starts off with a very simple vector model description of NMR that can be understood without a strong understanding of quantum mechanics. Even reading just the first few chapters has revolutionized the way I understand and take NMR spectra.

Briefly, MRI contrast agents work by shortening the T1 or T2 relaxation of surrounding water molecules. In NMR spectroscopy, a strong external magnetic field is applied along the z-axis and the bulk magnetization of the sample aligns with this magnetic field. Commonly in 1-D ^{1}H NMR spectroscopy, a 90º radio frequency pulse is applied to knock the bulk magnetization vector from being aligned with the z-axis to the x-y plane. The relaxation time for the bulk magnetization to realign with the external magnetic field is the T1 relaxation time. In addition to the very strong external magnetic field applied by the NMR instrument electromagnet, molecules themselves act as tiny, weak magnets. These small internal magnetic fields act affect the ability of the bulk magnetization vector to relax to the z-axis (T1 contrast agent) and decohere the bulk magnetization vector and causes a loss of signal according to T_2^* relaxation (T2 contrast agent). In general, MRI contrast agents are paramagnetic or superparamagnetic. The unpaired electrons of these commonly used MRI contrast agents have large magnetic susceptibilities, causing them to behave like stronger internal magnets, affecting T1 and T2 relativities. The differences in T1 and T2 are then mapped out into an image that we recognize as an MRI image.

The most common MRI contrast agents to date include paramagnetic ion complexes, superparamagnetic magnetite particles or contain lanthanide elements such as gadolinium (Gd^{3+}) and manganese (Mn^{2+}).[254] They are commonly delivered intravenously or orally (for imaging of

the gastrointestinal tract). The identities of the metal and chelating groups, and the delivery route affect the pharmacokinetics and toxicity of the MRI contrast agents. In general, however, these contrast agents accumulate in the liver, spleen and bone, and cause toxicity. Gadolinium-based contrast agents in particular, present risk for patients with chronic kidney disease, acute kidney injury, and dialysis because gadolinium-based contrast agents can cause nephrogenic systemic fibrosis.[255]

There have been a few attempts at metal-free, nitroxide based polymers as an MRI contrast agent. The Johnson group has reported the synthesis and application of nitroxide functionalized ROMP polymers.[256–258] One problem with organic radical contrast agents (ORCAs) is that they can be reduced by common in-vivo reductants such as ascorbate. The Johnson group protected the pendant TEMPO molecules by incorporating it into a sterically hindered brush structure or by burying in a cross-linked hydrophobic core of a supramolecular structure.

4.5.4.2 aPCPV as a potential ORCA polymer

aPCPV exhibits three properties which lends itself to a potential MRI contrast agent. First, it is nontoxic. Second, it itself is paramagnetic. However, electron spin resonance spectroscopy (ESR) experiments with Prof. Stefan Stoll's group (UW Department of Chemistry) for suggest that the radical concentration is extremely low. We attempted to directly image hydrogels doped with aPCPV as an MRI contrast agent in collaboration with Prof. DongHoon Lee's group, (UW Department of Radiology) but found very weak signal.

I hypothesize that the ESR and MRI signals can be improved by increasing the temperature. Our current understanding of aPCPV is that its cyclopentadiene radicals are reversibly capped by termination with another cyclopentadiene radical. It is possible that increasing the temperature will shift the equilibrium to the radical form, resulting in higher signal.

Third, aPCPV reacts quickly with sodium ascorbate and can be reoxidized in water. It may be possible to combine aPCPV and nitroxide-functionalized polymers, similarly to those synthesized previously by the Johnson group. The aPCPV can scavenge nearby ascorbate, preventing ascorbate from reducing the nitroxide.

Chapter 5. SYNTHESIS OF FOLDING POLYMERS USING MOLECULAR RECOGNITION PAIRS AZOBENZENE AND CYCLODEXTRIN[259]

5.1 INTRODUCTION

Many critical biological functions such as protein activity and DNA replication are regulated by the solution conformations of participating biopolymers. The complex 3-dimensional motion of biopolymers can be approximated as "folding," which is measured as changes in distance between labeled points along the biopolymer. Experimentally, folding has been measured by monitoring fluorescence between Förster resonance energy transfer pairs,[1] resonant frequencies between plasmonic dimers,[2,3] and electron spin resonance spectra between nitroxide spin labels.[4] More macroscopic changes in the biopolymer have been measured without labeling via circular dichroism[5] and nuclear Overhauser effect (NOE) nuclear magnetic resonance (NMR) experiments.[6]

Synthetic polymers can be made to mimic biopolymer folding by functionalizing the α- and ω- ends with high affinity molecular recognition pairs. Many of these molecular recognition pairs have been used in pioneering works that make folding polymers with hydrogen donor-acceptor pairs,[7,8] metal-ligand complexes,[9] host-guest pairs,[10,11] and even click chemistries (irreversible folding).[12] Yilmaz et al. demonstrated the use of host-guest complexes formed by β-cyclodextrin (βCD) and adamantane in a folding polymer but the polymer can only be unfolded at high temperatures.[10]

Of the available molecular recognition pairs, the azobenzene-cyclodextrin pair offers attractive features of photoreversible complexation, relative ease of synthesis and derivatization, and subsequent tunable properties.[13–15] The azobenzene moeities complex with cyclodextrin in

water to reduce the entropic penalty of water ordering around the hydrophobic azobenzenes and the hydrophobic inner core of cyclodextrin. Azobenzene-cyclodextrin pairs have been used in stimuli-responsive drug release,[15–17] material property modulation,[21,22] and supramolecular assembly.[18–20] Inoue et al. even demonstrated the use of azobenzene and βCD for folding polymers by capping 2 kDa polyethyleneglycol chains with azobenzene at one end and with βCD at the other and demonstrating their reversible solution-phase complexation.[11]

To date, most synthetic folding polymers are only responsive to a single type of stimulus. We sought to create a multi-stimuli responsive folding polymer. We were particularly interested in TMAB and β-CD as the molecular recognition pair for two reasons. First, βCD shows preferential binding of *trans*-TMAB (K_a = 1524 M^{-1}) over *cis*-TMAB (K_a = 82.1 M^{-1}).[15] Second, the cis/trans ratio of TMAB can be modulated using multiple stimuli, including heat, light, and Brønsted acids.[23] In particular, the presence of Brønsted acids catalyzes the *cis*-to-*trans* isomerization[24,25] and shifts the equilibrium to *trans*-TMAB via formation of an intramolecular hydrogen bonding 6-membered species that improves its resonance stabilization.[23] Thus, we designed a multi-stimuli responsive folding polymer by incorporating TMAB and βCD monomers into triblock copolymers within the first and third blocks, respectively.

Herein we report the synthesis and characterization of a multi-stimuli responsive high molecular weight folding polymer (**Poly1**). **Poly1** is a triblock copolymer with multiple TMAB and βCD moieties and can be reversibly unfolded by photoinduced *trans*-to-*cis* isomerization of TMAB. **Poly1** can also be irreversibly unfolded under acidic conditions; even though introduction of acids favors *trans*-TMAB, the protonated *trans*-TMAB is no longer hydrophobic and does not complex with βCD. Folding behavior was characterized by illumination-dependent extinction spectrscopy and 2-D NOE NMR experiments.

5.2 Results and Discussion

5.2.1 *Synthesis and characterization of monomers*

To incorporate TMAB moieties into a polymer made by reversible addition-fragmentation chain-transfer polymerization (RAFT), TMAB-methacrylate (TMAB-MA) and βCD-methacrylate (βCD-MA) were synthesized according to **Figure 5.1, top**. TMAB was first synthesized. A solution of 2,6-dimethoxyaniline (3.06 g, 20 mmol) in 12 mL of 6 M HCl was cooled with an ice water bath. A solution of $NaNO_2$ (2.07 g, 35 mmol) in 20 mL water was added and stirred for 30 min. Then a solution of 3,5-dimethoxyphenol (3.08 g, 20 mmol) in 20 mL in 10 w% NaOH solution was added. The reaction flask was removed from the ice bath and stirred for 12 h. The pH of the solution was then adjusted to pH 2 with the addition of conc. HCl. The precipitate was then collected by filtration and purified by column chromatography (yield = 48%).

To a flame-dried round bottom flask with a mechanical stirrer, TMAB (1.1 g, 3.5 mmol), K_2CO_3 (1.209 g, 8.75 mmol), and KI (5.8 mg, 0.035 mmol) were added. Dry DMF (17.5 mL) was then added. The reaction mixture was heated to 80 ºC and stirred for 1 h. Then bromoethanol (0.27 mL, 3.85 mmol) was added and stirred for 16 h. The reaction mixture was then allowed to cool to room temperature, diluted with dichloromethane, and washed with water to remove DMF. The organic layer was then collected, dried with brine and Na_2SO_4, and then the solvent was removed *in vacuo*. The product was used in the next step without further purification.

To a flame-dried round bottom flask with a mechanical stirrer, the product from the previous step (3.08 mmol) and triethylamine (1.5 mL, 10.78 mmol) were added. The reaction mixture was cooled with an ice bath and methacryloyl chloride (0.75 mL, 7.7 mmol) was added dropwise. The reaction was stirred for 2 h and then the solvent was removed in *vacuo*. The product was then purified by column chromatography (yield = 47%, 2 steps).

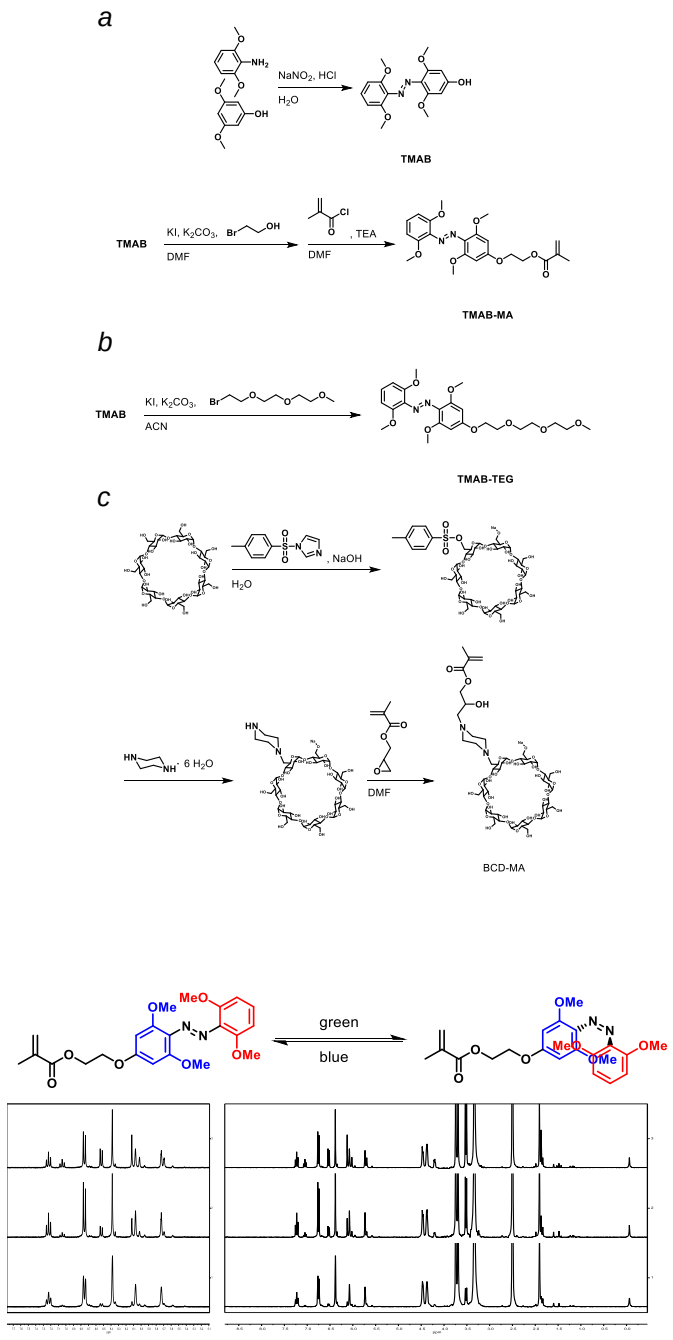

Figure 5.1. **Top**, synthetic schemes for small molecules used in this work. **Bottom**, ^{1}H NMR spectra of TMAB-MA in DMSO-*d6* as a function of green light irradiation

To synthesize BCD-MA, p-toluenesulfonyl imidazole was first synthesized and used a tosylating agent. To a 1 L flask with a mechanical stirrer, imidazole (75 g, 374 mmol), tosyl

chloride (25.5 g, 374 mmol) were dissolved in 300 mL dichloromethane. A solution of sodium bicarbonate (39 g in 500 mL water) was added. Triethylamine (5.6 mL) was added as a phase-transfer catalyst. The reaction was stirred at room temperature for 12 h. The organic layer was separated and dried with magnesium sulfate. The volume of the organic layer was reduced to 125 mL *in vacuo* and 25 mL of hexanes were added. The solution was then moved to the fridge to allow crystals to grow. The crystals were collected by filtration and washed with a cold solution of 5:1 dichloromethane:hexanes (yield = 70%).

To a 1 L reaction flask with a mechanical stirrer, βCD (20 g, 17 mL) and deionized water (450 mL) were added and heated to 60 ºC until the βCD dissolved. The solution was then allowed to cool to room temperature. Tosyl imidazole (15.5 g, 69.7 mmol), was added and stirred for 2 h. A solution of NaOH (9 g in 25 mL water) was added slowly over 20 min. NH_4Cl (24 g) was added and the solvent was removed by air-drying. The product was in the next step without further purification (yield = 150% (wet)).

To a round bottom flask with a mechanical stirrer, piperazine hexahydrate (6.4 g, 32.9 mmol) was added and melted by heating to 80 ºC. Tosylated-βCD from the previous step was added and stirred for 24 h. The reaction mixture was then precipitated into acetone and the solids were collected by centrifugation. The product was in the next step without further purification (yield = 45%).

To a round bottom flask with a mechanical stirrer, piperazine-βCD from the previous step (2.4 g, 2 mmol), GmMA (0.8 mL, 3 mmol), and DMF (25 mL) were added. The reaction mixture was sparged with N_2 for 20 min and then heated to 60 ºC for 24 h. The reaction mixture was then allowed to cool to room temperature and precipitated into 200 mL acetone. The solids were collected by filtration and the product was washed with acetone (yield = 100%).

As expected, conjugation of the MA group to TMAB preserved its photoisomerization behavior as measured by ^{1}H NMR spectroscopy in DMSO-*d6* (**Figure 5.1, bottom**).

5.2.2 *Synthesis and characterization of folding polymer (poly1)*

We aimed to synthesize a water-soluble polymer (**poly1**) with TMAB and βCD on the α- and ω- ends of the polymer, that exhibits folding and unfolding behavior in response to the isomerization and protonation state of TMAB (**Figure 5.2**). *Cis*-to-*trans* photoisomerization of pendant TMABs on **poly1** would result in TMAB-βCD interactions and subsequent polymer folding. *Trans*-to-*cis* photoisomerization of pendant TMABs on **poly1** would result in **poly1** unfolding due to the 18.6-fold lower K_a of TMAB-βCD. We also hypothesized that the reversible photoisomerization of TMAB and **poly1** folding can also be stopped via protonation of TMAB, resulting in loss of hydrophobicity and subsequent βCD inclusion.

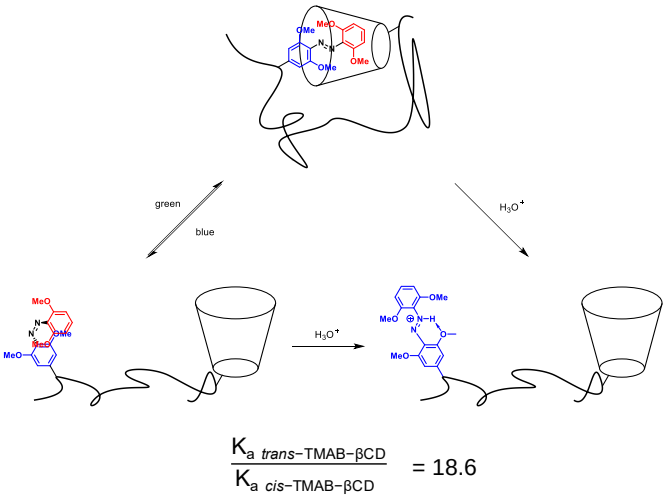

Figure 5.2. Envisioned scheme for poly(1) folding and unfolding

Specifically, we envisioned a polymer with one block that contains pendant TMABs, a second block to act as a spacer, and a third block that contains pendant βCDs (**Figure 5.3)**. Multiple goals

were kept in mind when designing the triblock copolymer. First, unlike adamantane and βCD which has a $K_a \sim 10^5\ M^{-1}$,[285] *trans*-TMAB and βCD have a lower $K_a \sim 10^3\ M^{-1}$. Thus, to improve the likelihood of folding, the first and third polymer blocks were synthesized to contain multiple TMABs and βCDs respectively. Second, first and lack blocks were copolymerized with highly water-soluble monoglycerol-methacrylate (GmMA) because a homoblock of hydrophobic TMAB or poorly water-soluble βCD could induce nonspecific aggregation. Third, βCD-MA was copolymerized with GmMA because βCD-MA shows poor homopolymerization, likely due to the steric hinderance induced by the large cyclodextrin ring.[59]

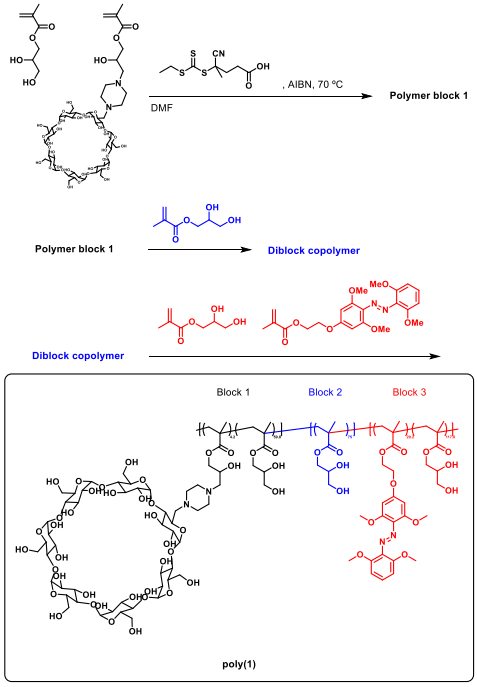

Figure 5.3. Synthetic route to poly1

Poly1 was synthesized by sequential polymerizations of macro-CTAs by reversible addition-fragmentation chain-transfer polymerization (RAFT). The polymerization of each block was stopped at 80% conversion of monomer to polymer and then the reaction mixture was subjected

to dialysis against water and was then used as a macro-CTA in the polymerization of the next block.

To a 7 mL scintillation vial with a mechanical stirrer, BCD-MA (269.1 mg, 0.2 mmol), GmMA (288.3 mg), and ECT (5.3 mg, 0.02 mmol) were added. 1 mL of a stock solution of AIBN (0.08 mg/mL, 0.001 mmol) in dry DMF was added. The reaction mixture was degassed with three freeze-pump-thaw cycles. The reaction mixture was then heated to 70 ºC for 15 h. The reaction mixture was then quenched with air exposure. The reaction mixture was then moved to 5 kDa cutoff dialysis membranes and purified by dialysis against water. Water was removed by lyophilization.

To a 7 mL scintillation vial with a mechanical stirrer, the macro-CTA from the previous step (190 mg, 0.01486 mmol) and GmMA (238 mg, 1.486 mmol) were added. 0.1 mL of a stock solutition of AIBN (1.22 mg/mL, 0.000743 mmol) in dry DMF was added. More dry DMF was added to bring the reaction mixture volume to 1.48 mL. The reaction mixture was degassed with three freeze-pump-thaw cycles. The reaction mixture was then heated to 70 ºC for 18 h. The reaction mixture was then quenched with air exposure. The reaction mixture was then moved to 5 kDa cutoff dialysis membranes and purified by dialysis against water. Water was removed by lyophilization.

To a 7 mL scintillation vial with a mechanical stirrer, the macro-CTA from the previous step (200 mg, 0.0085 mmol), TMAB-MA (42.9 mg, 0.085 mmol), and GmMA (122.7 mg, 0.766 mmol) were added. 0.851 mL of a stock solutition of AIBN (0.82 mg/mL, 0.00425 mmol) in dry DMF was added. The reaction mixture was degassed with three freeze-pump-thaw cycles. The reaction mixture was then heated to 70 ºC for 18 h. The reaction mixture was then quenched with air

exposure. The reaction mixture was then diluted with DMSO and moved to 5 kDa cutoff dialysis membranes and purified by dialysis against water. Water was removed by lyophilization.

Each block and the final poly1 exhibited monomodal molecular weight data, as analyzed by GPC (Figure 5.4).

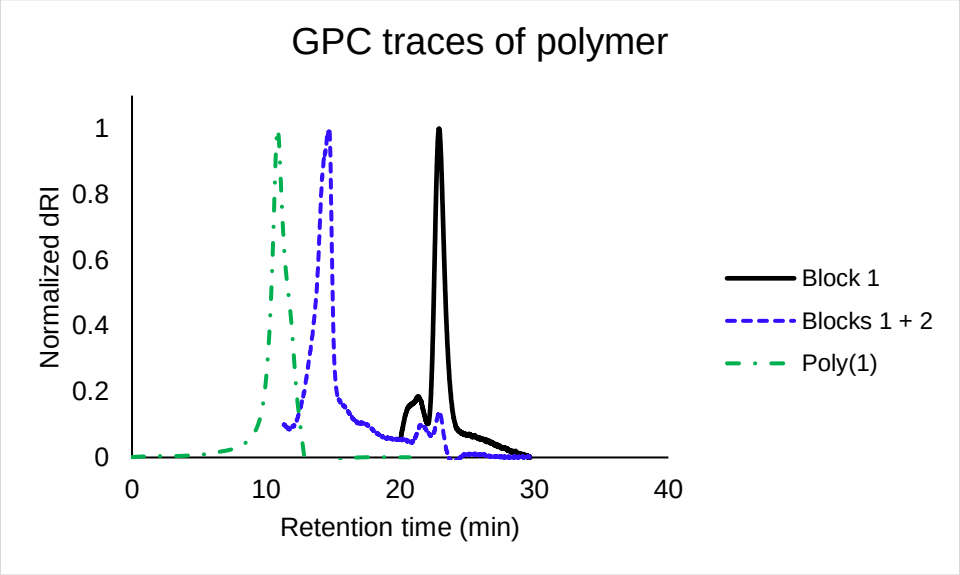

Figure 5.4. SEC chromatograms for each block of poly1

5.2.3 *Characterization of poly1 folding behavior as determined by small-angle neutron scattering (SANS)*

Small-angle neutron scattering (SANS) was first explored to determine if the radius of gyration (r_g) of **poly1** changes with the isomer-state of TMAB in a collaboration with Kacper Lachowski and Prof. Lilo Pozzo. Folded **poly1** would exhibit a lower r_g while unfolded **poly1** would exhibit a higher r_g. Samples of **poly1** at 1 and 5 mg/mL were prepared in D_2O and irradiated with green or blue light for 10 minutes. Surprisingly, we found that **poly1** existed in aggregates greater than 100 nm in diameter and these aggregates could not be disassembled by dilution in D_2O (**Figure S2**). We attribute the large aggregates of **poly1** to be due to the high insolubility of

βCD in D_2O.[286,287] Unfortunately, because deuterated solvents are essential for SANS, **poly1** folding could no longer be analyzed by SANS (Figure 5.5).

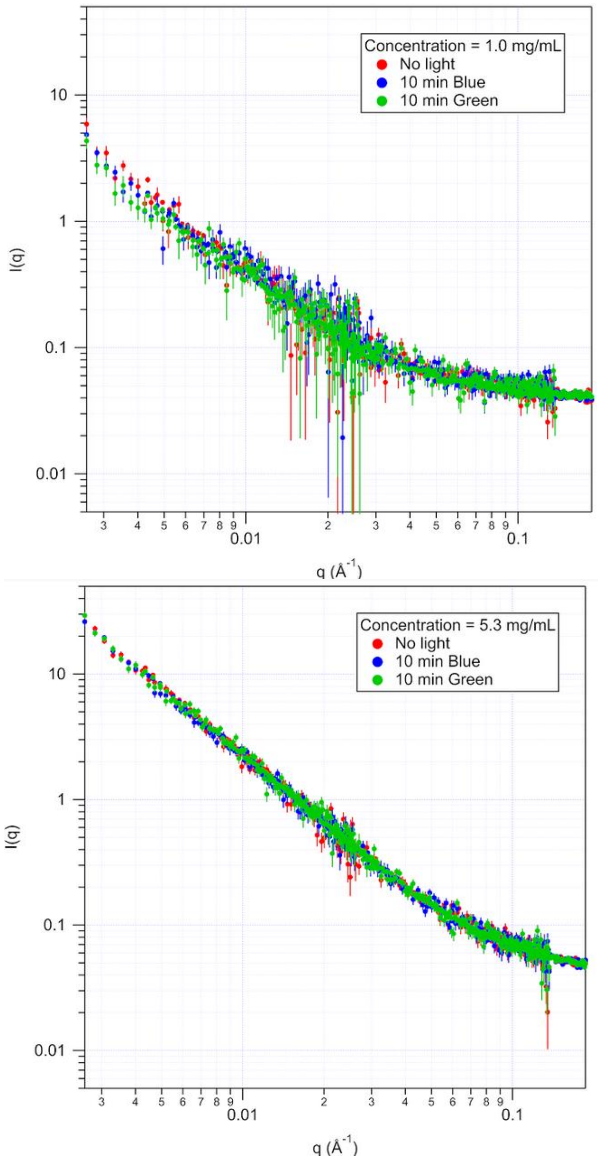

Figure 5.5. SANS data of poly1 in D_2O at various concentrations show no Guinier region. Data courtesy of Kacher Lachowski and Prof. Lilo Pozzo.

5.2.4 *Characterization of poly1 folding behavior via diffusion ordered spectroscopy (DOSY) and 2-D NOE NMR experiments (NOESY)*

We turned to NMR experiments to determine if **poly1** exhibited photoresponsive folding behavior. To determine if **poly1** exhibits photoinduced reversible folding behavior, DOSY and 2-D NOESY NMR experiments were performed. 2-D NOESY NMR experiments can be used to determine if *trans*-TMAB is in close physical proximity to βCD, consistent with folding. DOSY experiments can be used to determine if the TMAB-βCD NOE interactions are due to intrapolymer folding or interpolymer aggregation.

One drawback common to both DOSY and 2D-NOESY NMR experiments is they can take many hours. Although an NMR sample would not be exposed to light during the NMR experiment, it is possible for *cis*-azobenzene to thermally relax back into its thermodynamically more stable *trans* state. To determine the rate of *cis* to *trans* thermal relaxation in water, water-soluble TMAB-TEG was synthesized (Figure 5.1, top), and its photoisomerization and thermal relaxation were studied by ^{1}H NMR spectroscopy. TMAB-TEG shows maximum isomerization within 10 minutes of irradiation (Figure 5.6, left). When additional irradiation with colored light showed no additional TMAB isomerization, the sample was exposed to ambient light for up to 30 minutes and the *cis*-to-*trans* isomer ratio was measured again. Exposure of the TMAB-TEG sample to ambient light showed no measurable isomerization up to 30 minutes, indicating a highly photostable state. TMAB-TEG was also isomerized to its cis form with the use of green light and its relaxation to its trans state was measured at 26.1 ºC and 45 ºC by ^{1}H NMR spectroscopy (Figure 5.6, right). The thermal relaxation rate in darkness was determined to be negligible for both 26.7 ºC and 45 ºC and all further NMR experiments were done at 298 K.

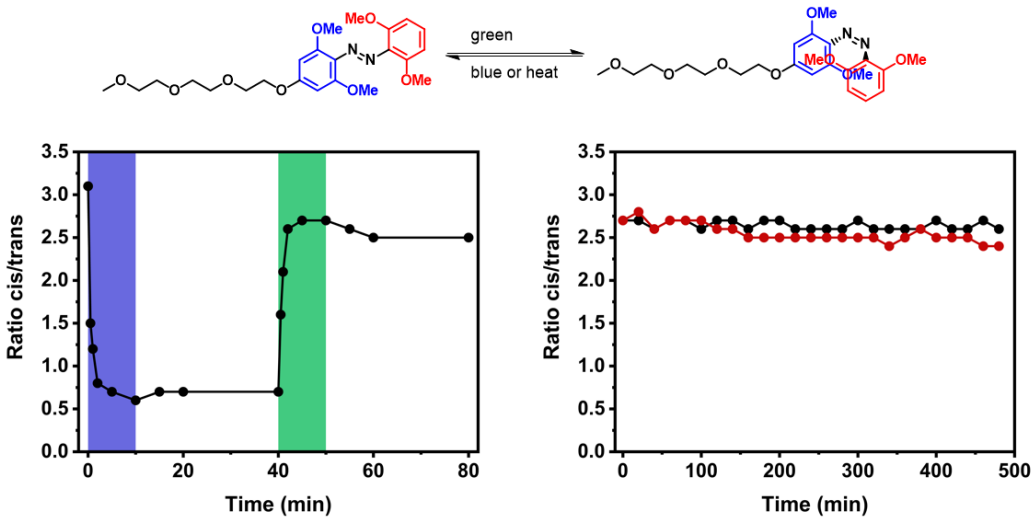

Figure 5.6. **Left**, quantification of the cis/trans ratio upon irradiation with blue and green light as determined by ^{1}H NMR spectroscopy. **Right**, quantification of the cis/trans ratio as a function of thermal relaxation as determined by ^{1}H NMR spectroscopy.

As we discovered during SANS, D_2O resulted in βCD-induced aggregation. To avoid this problem in our NMR experiments, all experiments were performed in a mixture of 90% H_2O and 10% D_2O. But due to the much higher intensity of the water signal in our NMR spectra, two different solvent suppression pulse sequences were explored. 3-9-19 *watergate* suppression did indeed suppress the water signal but also resulted in attenuation of NMR signals from the polymer. This was an important consideration because determining diffusion constants by DOSY NMR relies on signal attenuation. Instead, we used excitation sculpting *zgesgp* because it showed improved water suppression and no attenuation of NMR signals from the polymer. A custom pulse program was written in collaboration with Dr. Rajan K. Paranji to combine excitation sculpting into DOSY experiments and it was used to determine diffusion constants. The pulse program is below:

```
Water suppression and DOSY pulse program.
;ste1sesprgp.pkr
;avance-version (07/05/08)
;Pseudo-2D sequence for diffusion measurement using stimulated echo
;using 1 spoil gradient
;
;Cascaded with excitation sculpting prior to diffusion measurement
;to suppress water and measure D of solute, instead...10/4/19..pkr
;
;Adding a presat to effectively suppress H2O (use if needed)
;
;
;$CLASS=HighRes
;$DIM=1D
;$TYPE=
;$SUBTYPE=
;$COMMENT=

prosol relations=<triple>

#include <Avance.incl>
#include <Grad.incl>
#include <Delay.incl>

define list<gradient> diff=<Difframp>


"TAU=de+p1*2/3.1416+50u"
"DELTA1=d20-p1*2-p30-d16-p19-d16"

"p2=p1*2"
"d12=20u"

1 ze
2 30m
  50u pl1:f1 UNBLKGRAD
  4u pl9:f2
  d1 cw:f2 ph29
        4u do:f2
  p1 ph1

  50u UNBLKGRAD ; start excitation sculpting
  p16:gp1
  d16 pl0:f1
  (p12:sp1 ph4:r):f1
  4u
```

```
  d12 pl1:f1

  p2 ph3

  4u
  p16:gp1
  d16
  TAU
  p16:gp2
  d16 pl0:f1
  (p12:sp1 ph6:r):f1
  4u
  d12 pl1:f1

  p2 ph7

  4u
  p16:gp2
  d16   ; end excitation sculpting


  p30:gp6*diff ; grad echo start; phase encoding variable gradient
  d16
  p1 ph2
  p19:gp7
  d16
  DELTA1 ; diffusion delay
  p1 ph3
  p30:gp6*diff ; decoding variable gradient
  d16
  4u BLKGRAD
  go=2 ph31
  30m mc #0 to 2 F1QF(igrad diff)
exit


ph1= 0 0 0 0 2 2 2 2
ph2= 1 3 0 2
ph3= 1 3 0 2
ph4= 0 1 0 1
ph5= 2 3 2 3
ph6= 0 0 1 1
ph7= 2 2 3 3
ph29=0
ph31=0 0 2 2 2 2 0 0
```

```
;pl1 : f1 channel - power level for pulse (default)
;p1 : f1 channel -  high power pulse
;p19: gradient pulse 2 (spoil gradient)
;p30: gradient pulse (little DELTA)
;d1 : relaxation delay; 1-5 * T1
;d16: delay for gradient recovery
;d20: diffusion time (big DELTA)
;NS: 8 * n, total number of scans: NS * TD0
;DS: 4 * m


;use gradient ratio:    gp 6 : gp 7
;                       var  : -17.13

;for z-only gradients:
;gpz1: 31%
;gpz2: 11%
;gpz6: 1-100%
;gpz7: -17.13% (spoil)

;use gradient files:
;gpnam1: SMSQ10.100
;gpnam2: SMSQ10.100
;gpnam6: SMSQ10.100
;gpnam7: SMSQ10.100

;use AU-program dosy to calculate gradient-file Difframp


;$Id: stegp1s1d,v 1.4.6.1 2007/05/09 09:36:59 ber Exp $
```

DOSY NMR was then used to determine the concentration at which most polymers were unimeric and not intermolecular aggregates. At high concentrations, interpolymer azobenzene-cyclodextrin complexation can compete with intrapolymer folding. Because interpolymer interactions are at least second order with respect to polymer concentration and intrapolymer interactions are first order with respect to polymer concentration, the polymer solution can diluted until intrapolymer folding dominates over interpolymer aggregation. To determine the dilution

necessary, the diffusion coefficient of **poly1** was determined at different concentrations by DOSY NMR. The concentration at which the diffusion coefficient stops increasing with dilution can be determined as the maximum concentration for the single polymer regime. The polymer was determined to be in the single polymer concentration regime at <1.6 mg/mL by DOSY (Figure 5.7).

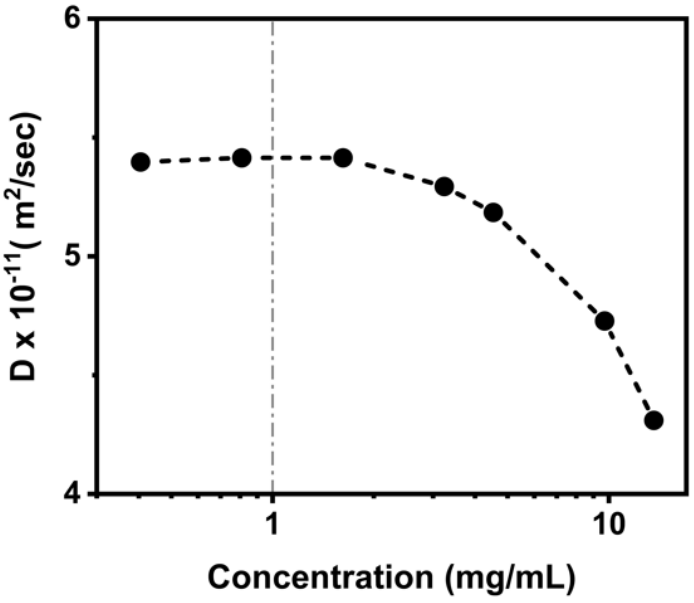

Figure 5.7. Diffusion constants determined by DOSY using 1-variable fitting.

At the single polymer regime, 2-D NOESY NMR was used to determine the through-space interaction of protons. Cross-peaks of the azobenzene and cyclodextrin should be observable during the folded state, and not in the unfolded state given a mixing time of 150 μs.[269] **Poly1** exhibited azobenzene-cyclodextrin cross-peaks when the azobenzene was in the *trans* state, and no cross-peaks when the azobenzene was isomerized to *cis* (Figure 5.8). Due to the relatively low concentration of azobenzenes and cyclodextrins per polymer, many scans were required. To limit the amount of thermal relaxation back from *cis* to *trans* azobenzene and to limit the amount of NMR instrument use time, free induction decay (FID) recordings were truncated to 20 ms because

almost all the analyte signal intensity is encoded in the first few FID points. This truncation resulted in crude NMR spectra with many truncation artifacts, but cross-peaks could still be detected.

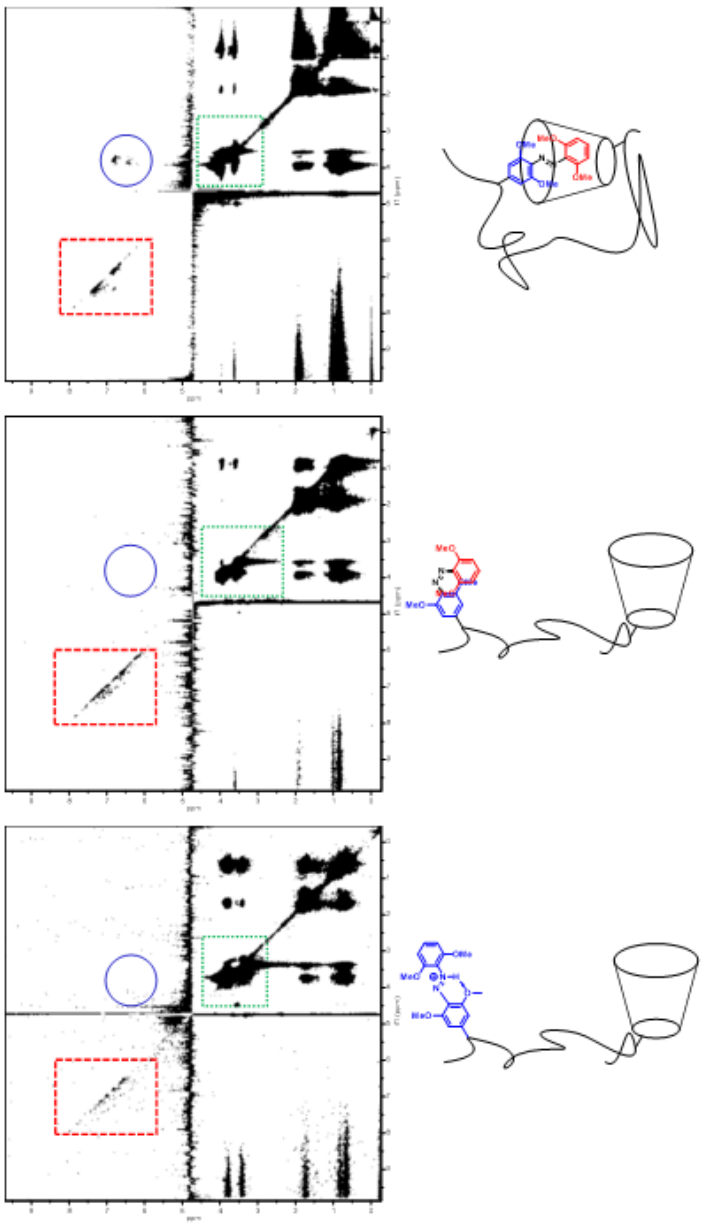

Figure 5.8. NOESY spectra shows cross-peaks between TMAB and cyclodextrin only in the unprotonated, trans-TMAB state.

5.2.5 *Characterization of poly1 folding behavior as determined by UV-Vis spectroscopy*

We then sought to confirm self-inclusion of **poly1** between TMAB and βCD by extracting relevant kinetic information of the *trans*-to-*cis* TMAB photoisomerization, in collaboration with Kathryn N. Guye and Prof. David S. Ginger. By comparing the rate and photostationary state of each sample, we gain insight about the local environment of the TMAB chromophore. Isomerization of *cis-to-trans* azobenzene is generally believed to follow a sterically unhindered inversion mechanism[288–290]. *Trans-to-cis* isomerization on the other hand, undergoes a sterically hindered rotation or hula twist, in which case, the fraction of azobenzene able to undergo a *trans-to-cis* isomerization is dependent on the local environment of the chromophore[291–293]. A more sterically crowded environment, such as on the inside of a cyclodextrin molecule, will limit the rotation of the TMAB molecule and thereby the rate and photostationary state of *trans-to-cis* isomerization.

From the ^{1}H NMR photoisomerization spectra, we determined TMAB-TEG in solution was 37% in cis-form after reaching the photostationary state with 470 nm light. As the TMAB azo-group peaks from **poly1** were obscured in its ^{1}H NMR spectrum due to overlapping polymer signal, we assumed that TMAB in **poly1** is also 37% cis in the predominantly trans photostationary state.

We then obtained the extinction spectra of **poly1** and TMAB-TEG under low 523 nm illumination fluence, 0.5 mW/cm^2. These curves are then fit to an exponential curve as

$$y_t = (y_0 - y_\infty)\exp(-Ax) + y_\infty \quad (1)$$

where y is the fraction of cis-TMAB at times t, t=0, and the final photostationary state, x is the time in seconds, and A is the rate of isomerization. As shown in Fig XXXa, the average rate of isomerization for **poly1** is 0.0027 +/- 0.00007 s^{-1}, and the fraction of cis-TMAB in the photostationary state is 0.28 +/- 0.002. TMAB, on the other hand, displays an average rate of

0.0032 +/- 0.0002 s^{-1}, and a fraction of cis-TMAB of 0.33 +/- 0.004 in the photostationary state. As predicted if **poly1** is self-folding by inclusion complexation, the *trans-to-cis* isomerization is inhibited, observed by both the reduced rate and reduced final fraction of cis-form TMAB compared to the free chromophore, TMAB-TEG, in solution.

To confirm these differences are the result of βCD inclusion of TMAB along the polymer, TMAB-TEG was then dissolved in an aqueous solution of excess (2-hydroxypropyl)-β-cyclodextrin (HP-βCD). We chose to use an excess concentration to try to mimic the high local concentration of cyclodextrin in the case of the TMAB being tethered adjacent to the cyclodextrin units. This sample was measured in the same manner, and from the fits, an average rate of 0.0026 +/- 0.0001 s^{-1} and photostationary state cis-fraction of 0.33 +/- 0.004 were extracted.

The isomerization rate of the TMAB-TEG/HP-βCD complex solution exhibited a rate similar to **poly1** (Figure 5.9), indicating a similarly sterically inhibited environment, slowing the isomerization of the free TMAB-TEG as a result of inclusion. However, the fraction of cis-TMAB at the photostationary state matches that of the free TMAB-TEG without HP-βCD. As the TMAB-TEG is not bound to the HP-βCD in this solution as it is for **poly1**, given an infinite time of illumination, such as the photostationary state is defined, the TMAB-TEG will eventually isomerize, but more importantly, separate from the HP-βCD.

As such, when included by βCD, both TMAB-TEG and **poly1** will have a similar degree of steric hindrance while being driven from *trans-to-cis* and therefore a similar rate of photoisomerization. In the photostationary state, however, both TMAB-TEG solutions should reach the same fraction of cis-form TMAB-TEG molecules as they are now independent of the cyclodextrin molecule, which is indeed observed.

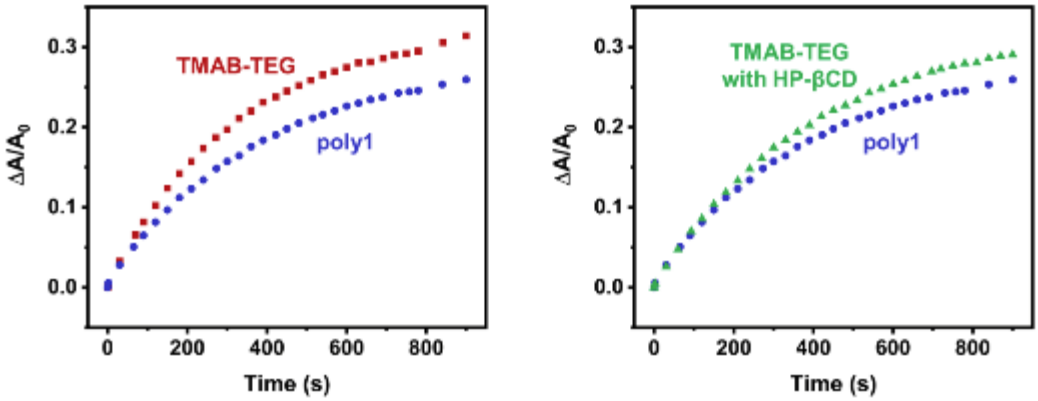

Figure 5.9. NOESY spectra shows cross-peaks between TMAB and cyclodextrin only in the unprotonated, trans-TMAB state.

5.2.6 *Determination of acid-catalyzed and acid-stabilized cis-to-trans isomerization and poly1 unfolding*

The *cis*-to-*trans* isomerization of azobenzenes has been demonstrated to be catalyzed by acids[283,284] and protonated-TMAB exhibits increased resonance stabilization in the *trans* state due to intramolecular hydrogen bonding, rendering it unable to be isomerized back into its *cis* state.[282] The effect of pH was also determined for TMAB-TEG and **poly1**. First, ^{1}H NMR spectroscopy at 26.1 ºC was used to confirm that (1) acidic protons catalyze the relaxation of TMAB from *cis* to *trans*, and (2) acidic protons stabilize the *trans* state. To prevent a large water signal from the addition of HCl in water, DCl in D_2O was used. For these experiments, TMAB-TEG was dissolved in an NMR tube and isomerized to its *cis* form with green light. DCl in D_2O was injected into the NMR tube and immediately moved into the NMR spectrometer for data acquisition. Although TMAB-TEG showed negligible thermal relaxation in D_2O, it showed complete relaxation to *trans* within 60 minutes with the addition of DCl (Figure 5.8). We then tried to photoisomerize the acidified TMAB-TEG back into its *cis* state. Irradiation with either blue or green light showed no isomerization by ^{1}H NMR spectroscopy (data not shown), likely due to the stabilization of the

planar 6-membered ring formed by the acidified TMAB-TEG. The effect of acidic conditions was determined for the folding polymer. The same NOESY experimental conditions were used and no cross-peaks were observed (Figure 5.8, bottom).

5.3 Conclusion

We report the synthesis and folding behavior of a high molecular weight polymer with multivalent TMAB and βCD moieties on the α- and ω- ends of the polymer. Folding behavior was investigated with a combination of NOESY and photoisomerization quantum efficiency calculations. The folding polymer exhibits multi-stimuli responsive behavior and can be reversibly unfolded with the use of light and irreversible folded under acidic conditions.

Chapter 6. SYNTHESIS OF CYCLIC POLYMERS VIA METAL-FREE RING EXPANSION METATHESIS POLYMERIZATION

6.1 INTRODUCTION

ROMP is a controlled polymerization that has shown great utility in newly expanding fields such as organic electronics and drug delivery. ROMP has broad functional group tolerance, high activity, tunable kinetics, good dispersity control, as well as the ability to make cyclic polymers. ROMP has broad functional group tolerance, high activity, tunable kinetics, good dispersity control, as well as the ability to make cyclic polymers. Unfortunately, transition metals like molybdenum and ruthenium are extremely expensive, making the resulting polymers expensive. Additionally, techniques to remove the transition metal initiators used for ROMP are difficult and expensive. The residual transition metals in ROMP polymers, which range from 15-400 ppm, are genotoxic and can affect their electronic and thermal properties.[11,92,294]

The desire to move away from transition metal catalysis in polymer chemistry has coincided with a growing interest in light driven reactions. Photoexcited electrons provide novel reaction pathways, allow control of stereochemistry, and temporal and spatial resolution. However, direct photoexcitation of organic molecules often requires high intensity ultraviolet range light. Organic chromophores have been used as photomediators to catalyze some of the reactions previously achieved by direct photoexcitation.[295–299] While the reaction mechanism is often not the same as that achieved by direct photoexcitation, the use of photomediators allows the use of lower light intensity in visible range. These photomediators, upon visible light excitation, will undergo photoinduced electron transfer (PET) to initiate a reaction. Organocatalyzed PET (OPET) has been applied to polymerizations to replace transition metals in atom-transfer radical polymerization

(ATRP), reversible addition-fragmentation chain transfer polymerizations (RAFT)[69,148,150,299–301] and been used in many applications including metal-free microfabrication and additive manufacturing.[302–304]

Ogawa et al. demonstrated an OPET system for the ROMP of norbornene and other common ROMP monomers.[305,306] Dubbed "metal-free ROMP" (MF-ROMP), this polymerization results in the same open ring metathesis polymers as traditional ROMP (Figure 6.1, top) but is mechanistically distinct. A photomediator, in this case a pyrylium salt, is used to oxidize an enol ether which initiates the polymerization.

MF-ROMP is a useful synthetic strategy that can potentially be adapted into metal-free ring expansion metathesis polymerization (MF-REMP) for the synthesis of cyclic polymers (CycPs). CycPs are academically interesting and have many potential applications. They have been shown to exhibit smaller hydrodynamic radii in solution, higher glass transition temperatures as bulk materials, and lower viscosities than their linear variants; they also exhibit better micelle stabilities than their linear variants.[307–309] CycPs have also been used in drug delivery: folate-functionalized sunflower polymers have been synthesized as a generalizable approach for drug carriers.[22] CycPs also have potential for organic electronics; two recent examples include the synthesis of cyclic substituted polyacetylene and the synthesis of cyclic polyphenylene ethynylene.[310,311] Interestingly, cyclic polyphenylene ethynylene has higher fluorescence quantum yield compared to its linear variant.

The full potential of CycPs has not yet been realized due to the difficulties in their syntheses, scale-up, and purification. There are two synthetic approaches to cyclic polymers. The first approach called "ring closing" are limited to <10 kDa molecular weight polymers, results in high dispersity, necessitates high dilution and often click chemistry or enzymes.[22,307,312–315] Because

these approaches require large volumes of solvent, they are impractical for scale-up. The second approach, called “ring expansion,” has limited monomer scope and results in predetermined functional groups in the polymer backbone. For example, the tin oxide initiated synthesis of cyclic polylactones, N-heterocyclic carbene initiated synthesis of polylactides, and even the thiocarbamate initiated synthesis of poly(ethylene sulfide) all predetermine the backbone functionality of the polymer.[316] The predetermined heteroatoms in backbone limit the ability for post-modification functionality, allow interconversion between the cyclic and linear conformations, and can also leave the polymer susceptible to hydrolysis. The field would be greatly advanced by the facile synthesis of purely hydrocarbon backbone cyclic polymers, which once polymerized, can access a variety of post-polymerization functionalizations, cannot undergo ring opening to be linear, and are stable to hydrolysis.

Work by Grubbs, Boydston, and Xia et al. demonstrated the use of a modified tethered Grubbs catalysts to use ring expansion metathesis polymerization (REMP) to synthesize cyclic polyoctene.[153,317,318] While these catalysts can efficiently polymerize both hydrocarbon and functionalized monomers, they are expensive, are difficult to synthesize and purify, and have poor dispersity control.[319] Additionally, these polymers are contaminated with linear polymers, and face the other limitations of traditional metal-initiated ROMP listed previously.

The use of small molecule organic initiators in MF-ROMP makes it a convenient system to adapt into MF-REMP. We hypothesize that cyclic enol ethers can be synthesized and will initiate MF-REMP (Figure 6.1, bottom).

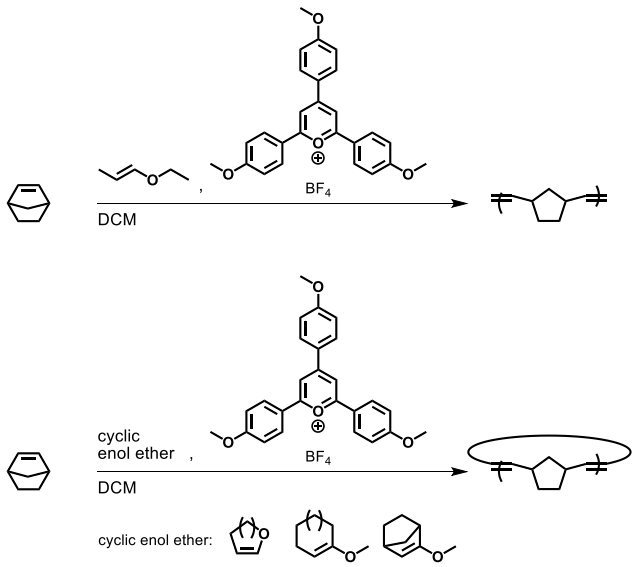

Figure 6.1. General synthetic scheme for MF-ROMP (top) and MF-REMP (bottom). Chain ends from the initiator are not shown in these figures.

6.2 SYNTHESIS AND USE OF CYCLIC ENOL ETHERS

6.2.1 *Synthesis and use of cyclic enol ethers with oxygen endocyclic to the ring (oxy-endo CycEE)*

Previous experiments done in the Boydston group showed that oxy-endo CycEEs such as commercially available dihydropyran and dihydrofuran show limited success as MF-REMP initiators, resulting in up to 20% conversion of norbornene to polynorbornene (PNB). One possible explanation for the low conversion is that the enol ether chain end undergoes acid-catalyzed hydrolysis, resulting in an inactive chain end that is unable to propagate (Figure 6.2, middle). Although linear MF-ROMP initiators such as ethyl propenyl ether can also undergo this mechanism (Figure 6.2, top), the equilibrium of the hydrolysis reaction with the oxy-endo CycEEs lies further to the right due to the more favorable ΔS term which arises from the gain in conformational entropy from ring-opening into the linear form. Another possible explanation is

that the reaction generates byproducts that react with the chain end and terminate the polymerization, as these polymerizations cannot be reinitiated with addition of fresh initiator or additional pyrylium.

One final limitation of using oxy-endo CycEEs is that hydrolysis of the enol ether into the aldehyde will result in opening the macrocycle, resulting in a linear polymer (Figure 6.2, bottom).

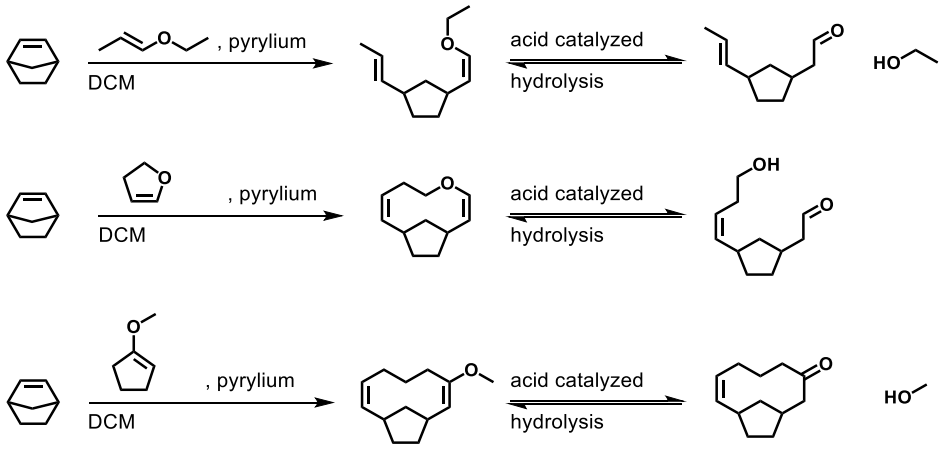

Figure 6.2. Mechanisms and products of acid catalyzed hydrolysis of the enol ether chain end in MF-ROMP. Proposed products of enol ether hydrolysis for endocyclic oxygen enol ethers (middle) and exocyclic oxygen enol ethers (bottom). The use of exocyclic oxygen enol ethers makes the resulting CycPs resistant to ring opening from acid catalyzed hydrolysis.

6.2.2 *Synthesis and use of cyclic enol ethers with oxygen exocyclic to the ring (oxy-exo CycEE)*

We hypothesized that the use of 1,1,2-trisubstituted cyclic enol ethers with the oxygen exocyclic to the ring (oxy-exo CycEEs) as MF-REMP initiators will produce hydrolytically stable CycPs. A panel of aliphatic enol ethers with exocyclic oxygens were synthesized from their corresponding ketones in >80% yield over 2 steps (Figure 6.3, top scheme).[320] Methanol was

dried by stirring over $CaSO_4$ overnight and distillation. The dry methanol was stored in a Strauss flask for future use. To a flame-dried round bottom flask containing a stir bar, the starting ketone (1 equiv.) and p-toluene sulfonic acid (1 equiv.) were added. Dry methanol (1 M solution) was added via syringe. After the ketone fully dissolved, trimethyl orthoformate (1.1 equiv.) was added dropwise via syringe. Conversion of the ketone to the methanol ketal was monitored by ^{1}H NMR spectroscopy with C_6D_6. Dissolving them in $CDCl_3$ for ^{1}H NMR analysis resulted in hydrolysis of the ketal back into the starting ketone likely due the acidic conditions of the reaction mixture and small amounts of HCl and water in the $CDCl_3$. After conversion was determined to be complete by ^{1}H NMR analysis, the reaction was quenched by addition of triethylamine by syringe (0.5 equiv.). The solvent was removed under reduced pressure and the level of residual methanol was monitored by ^{1}H NMR spectroscopy. When no more methanol could be detected by ^{1}H NMR spectroscopy, the ketal was used in the next step without further purification.

To the round bottom containing a stir bar and the ketal, N,N-diisopropylethylamine was added (1.8 equiv). Then, dry methylene chloride obtained from a solvent purification was added via syringe (0.5 M solution). When the ketal fully dissolved, the reaction flask was cooled with an ice bath and TMS-triflate was added dropwise via syringe (1.3-1.5 equiv.). The conversion was monitored by ^{1}H NMR spectroscopy in $CDCl_3$. Conversion cannot be monitored by ^{1}H NMR spectroscopy in C_6D_6 because the methylene chloride peak overlaps with the enol ether alkene proton (δ = 4-4.5 ppm). Fortunately, due to the excess amine, hydrolysis of the final product is prevented even in $CDCl_3$. When conversion was determined to be complete, the reaction was quenched by addition of 21%w sodium ethoxide in ethanol solution (1 equiv.). The final enol ether was purified by column chromatography with 1%v triethylamine, 9%v ethyl acetate, 90%v

hexanes as the running solvent. The ^{1}H NMR spectra of **oxy-exo CycEEs (1-3)** in C_6D_6 are shown in Figure 6.3, bottom.

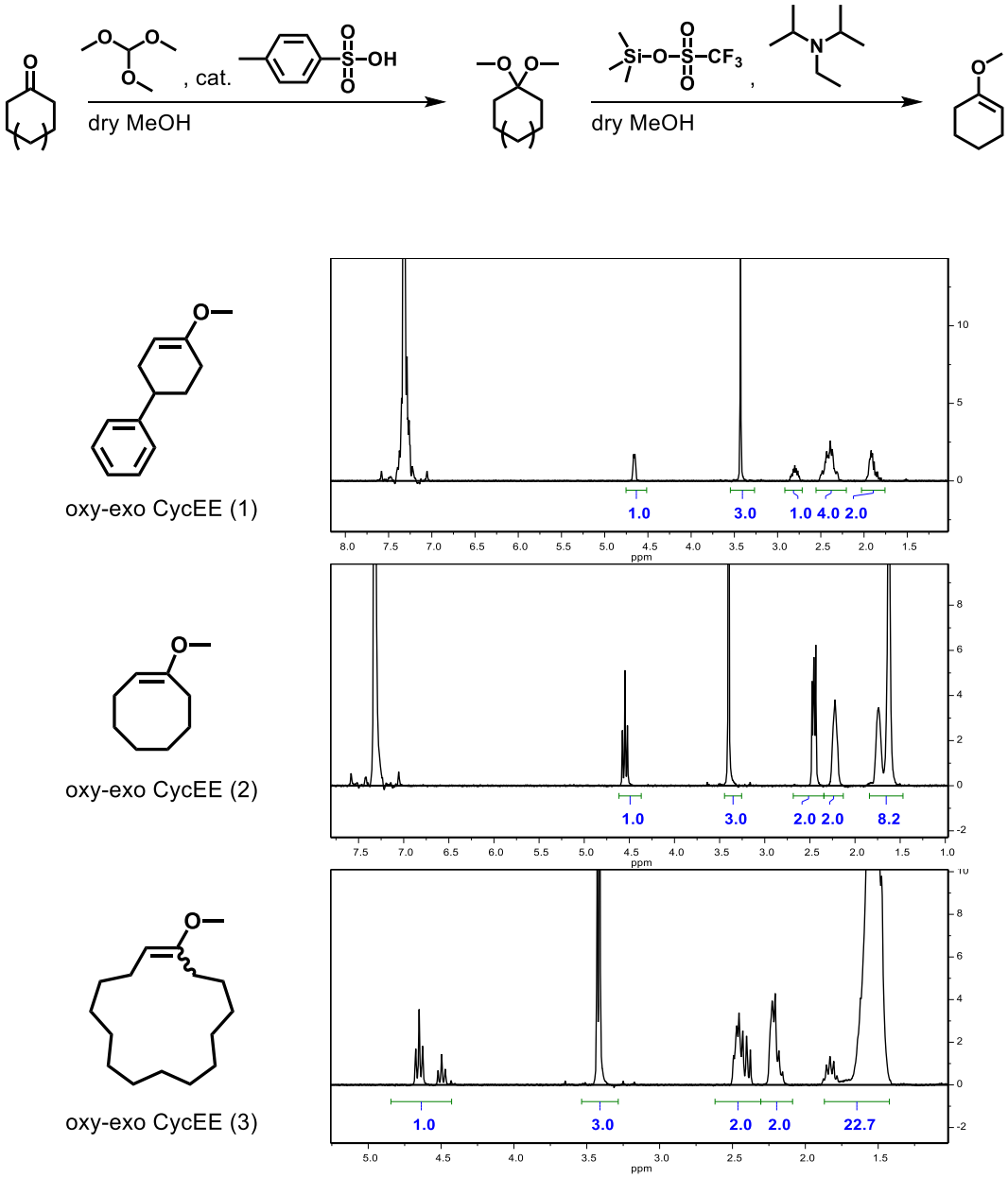

Figure 6.3. **top**, generalized synthetic scheme for the synthesis of oxy-exo CycEEs. **bottom**, NMR spectra of oxy-exo CycEEs in C_6D_6 in order of increasing ring size.

Oxy-exo CycEE (2) was synthesized first but was found to be unable to initiate MF-REMP. We hypothesized that the mixture of (*E*) and (Z) diastereomers might be important for MF-REMP and that the forced (*E*) alkene in the small 8-membered ring might limit propagation. Commercially purchased ethyl propenyl ether (EPE) which is the most used initiator in MF-ROMP exists as a mixture of 30% (*Z*) and 70% (*E*) isomers. MF-ROMP shows good initiator efficiency and oxidation by pyrylium allows for free rotation of the enol ether in EPE and thus it is likely that the (*E*) and (Z) diastereomers are equivalent for MF-ROMP. To test if the (*Z*) isomers are important in initiating MF-REMP, the **oxy-exo CycEE (3)** was synthesized. Due to the large ring size, **oxy-exo CycEE (3)** exhibited the same ratio of 30% (*Z*) and 70% (*E*) isomers as EPE. Unfortunately, **oxy-exo CycEE (3)** also failed to initiate MF-REMP.

Next, we hypothesized that these oxygen exocyclic enol ethers were too sterically hindered for MF-REMP. The increased steric crowding could raise the transition state energy of the charge transfer complex from photoexcited pyrylium, slowing the rate of enol ether oxidation and subsequent formation of an active chain end. The increased steric crowding could also raise the transition state energy of the propagation complex as norbornene approaches the active chain end, slowing the rate of propagation. All the oxy-exo CycEEs are 1,1,2-trisubstituted enol ethers, while EPE is only a 1,2-disubstituted alkene.[305] Reports of photochemical cyclobutene synthesis[321] and electrochemical enol ether metathesis[322] use only disubstituted alkenes and enol ethers as substrates. However, because the oxygen must be exocyclic to the ring, these initiators are forced to be 1,1,2-trisubstituted. To test if charge transfer to the enol ether was the rate limiting step, we synthesized **oxy-exo CycEE (1)** because the phenyl ring can act as a "redox tag" to facilitate charge transfer.[321] Unfortunately, **oxy-exo CycEE (1)** was also MF-REMP inactive.

We then hypothesized that all three cyclic enol ethers were impure or producing byproducts during MF-REMP that resulted in irreversible early termination. To test this, the cyclic enol ethers were doped into MF-ROMP initiated with EPE in a 1:1 ratio with EPE. The MF-ROMP reactions proceeded normally and resulted in normal levels of conversion, suggesting that **oxy-exo CycEEs** do not participate in this reaction.

Finally, it may be possible that charge transfer to the cyclic enol ethers was occurring, but propagation was too slow. We hypothesized that improving the stability of the oxidized enol ether and subsequent active chain end would allow for propagation by stabilizing the radical cation intermediate. Although the reaction rate is determined by the energy level of the transition state and not of the intermediate, the Hammond postulate can be used to approximate the energy of the transition state from the intermediate.

In MF-ROMP it is thought the EPE radical cation concentrates charge density on the carbon α to the oxygen and concentrates its spin density on the carbon β to the oxygen (Figure 6.4a). We synthesized **oxy-exo CycEE (4)**, which has a radical stabilizing methoxy-substitude phenyl group on the β-carbon and (Figure 6.4b). The non-styrene like product **oxy-exo CycEE (4b)** is present in 33% as an impurity and is very difficult to purify out. Fortunately, the 33% impurity is very similar to **oxy-exo CycEE (1)** which has already been shown to be MF-REMP agnostic. Control initiators **oxy-exo CycEE (5, 6)** were synthesized to determine the effect of the radical stabilizing group on the α-carbon and the substitution pattern of the electron donating methoxy group (Figure 6.4c and 6.4d).

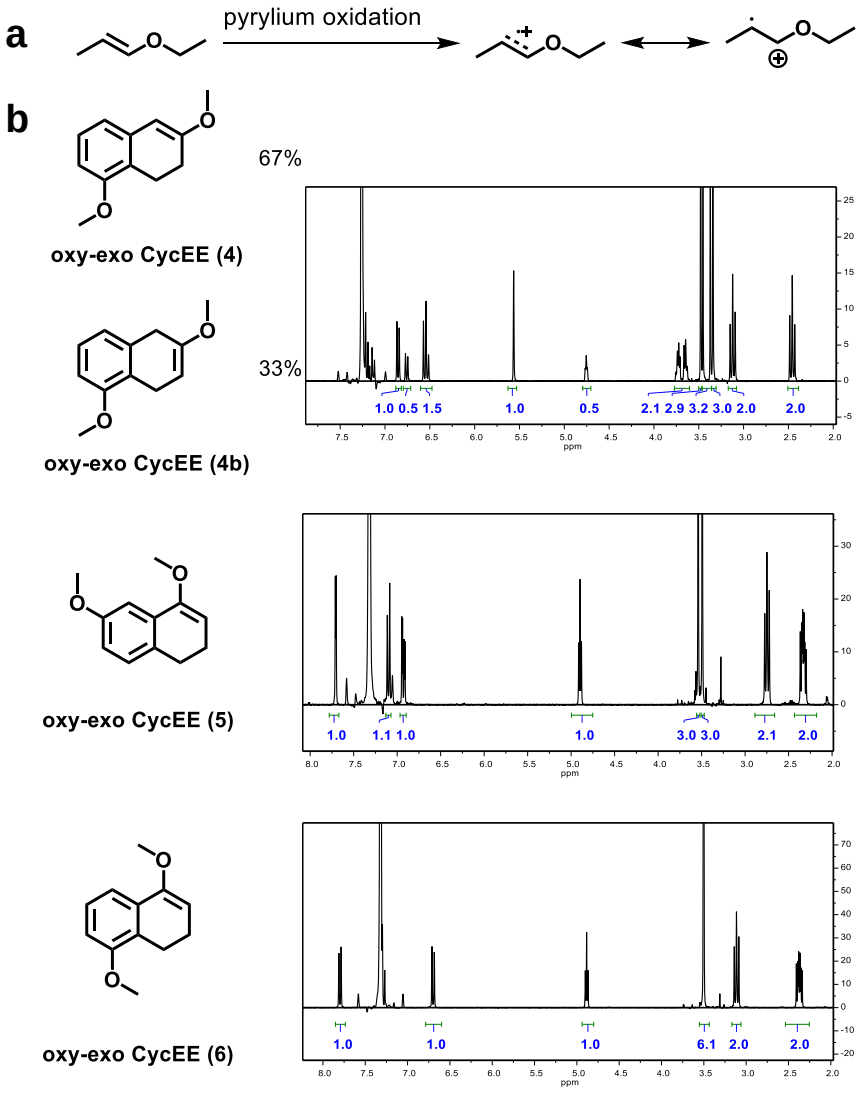

Figure 6.4. **a**, EPE oxidation by pyrylium is thought to produce a radical cation that concentrates charge density on the carbon alpha to the oxygen and the spin density on carbon beta to the oxygen. **b**, cyclic enol ether synthesized with radical stabilizing phenyl groups on the β-carbon. **c**, control cyclic enol ether synthesized to test the effect of a radical stabilizing phenyl group on the α-carbon. **d**, control cyclic enol ether synthesized to test the effect of the substitution pattern of the electron donating methoxy group on MF-REMP.

6.3 FUTURE WORK

It remains to be seen if MF-REMP with 1,1,2-trisubstituted enol ethers are viable. One experiment to test the effect of the extra substituent on MF-ROMP propagation is to use 1,2,2-trisubstituted enol ethers as initiators.

Chapter 7. RING-OPENING METATHESIS POLYMERIZATION OF A STRAINED STILBENE-BASED MACROCYCLIC MONOMER[323]

7.1 ABSTRACT

We report the synthesis of a new class of strained macrocycle that performs well in ring-opening metathesis polymerization (ROMP). The polymerization displays chain growth characteristics with evidence of secondary metathesis in the form of chain transfer. The unique structure enables access to stilbene-based polymers that are traditionally prepared *via* uncontrolled polymerizations.

7.2 INTRODUCTION

ROMP has become an indispensable synthetic technique in modern polymer chemistry and materials science.[82,324–328] The monomer landscape for ROMP is dominated largely by four highly strained monomer motifs: norbornenes, cyclobutenes, and cyclooctenes. The high amount of ring strain within these systems provides a thermodynamic driving force for ring-opening polymerizations.[13,82,329,330] In general, increasing the diversity of the backbone composition within ROMP is achieved by the polymerization of macrocycles (ring size >14 atoms), that in turn have very little ring strain and thus reduce the driving force for propagation.[331] The dichotomy exists largely between selection of monomer with high ring strain versus a macrocyclic system of greater diversity but without an enthalpic driving force.

The lack of an enthalpic driving force for the polymerization of macrocycles demands that an entropic driving force must be present for the polymerization to occur, and as such these

polymerizations are categorized as entropy-driven ring-opening metathesis polymerizations (ED-ROMPs).[331,332] ED-ROMPs are controlled by a ring-chain equilibrium that exists between macrocyclic oligomers and linear polymer. The thermodynamic drive is provided by the increase in conformational entropy as the macrocyclic oligomers become linear polymers.[331] Macrocyclic platforms for ED-ROMP have been used to synthesize polymers with many unique features including liquid crystalline polymers, poly(catenates), poly(calixarenes), and sequence-controlled polymers.[333–336] A major limitation of ED-ROMP is that when ED-ROMPs reach full equilibrium, the $Đ$ for the resulting polymer is expected to be high, around 2.0, and they will generally have remaining macrocyclic oligomer, approximately 2%.[331]

Approaches to address the challenges with ED-ROMP include designing macrocycles with high ring strain to make propagation "effectively irreversible."[337] The most common of these approaches is to synthesize highly strained macrocycles. Towards this end Miao et al. were able to utilize [2.2]paracyclophan-1-ene, a highly strained macrocycle, to synthesize a homopolymer as well as block and random co-polymers with norbornene initiated by a Schrock type catalyst.[338] Since this initial demonstration, several other cyclophanenes and cyclophanedienes have been used in ROMP to synthesize homo- and co-polymers.[339,340] In addition, a series of donor-acceptor block co-polymers have been synthesized via the ROMP of macrocycles based off of arylenevinylenes.[341] Inspired by this work, we set out to synthesize a strained macrocycle using techniques previously reported for the synthesis of highly strained cycloparaphenylenes.[342]

7.3 Results

7.3.1 *ROMP of a novel macrocycle monomer*

Macrocyclic monomer **1** was polymerized using G3 in tetrahydrofuran-d_8 ([**1**]$_0$ = 1 M) with an initial monomer to initiator ratio of 100:1 (Figure 7.11, top). With each initiator, conversion

reached >99% within 12 h at 60 °C, as determined by ^{1}H NMR spectroscopy. ^{1}H NMR spectra of the polymerization are shown in Figure 7.1, bottom. To monitor the polymerization we used 1H NMR. More specifically we compared the integrations between the benzylic ether protons of the monomer to the polymer at 5.39 and 5.48 respectively. From these experiments, we found that the molecular weight distribution of **poly(1)** was monomodal with a M_w = 107 kDa and $Đ$ of 1.7, based upon SEC analysis using multi-angle laser light scattering and refractive index detection.

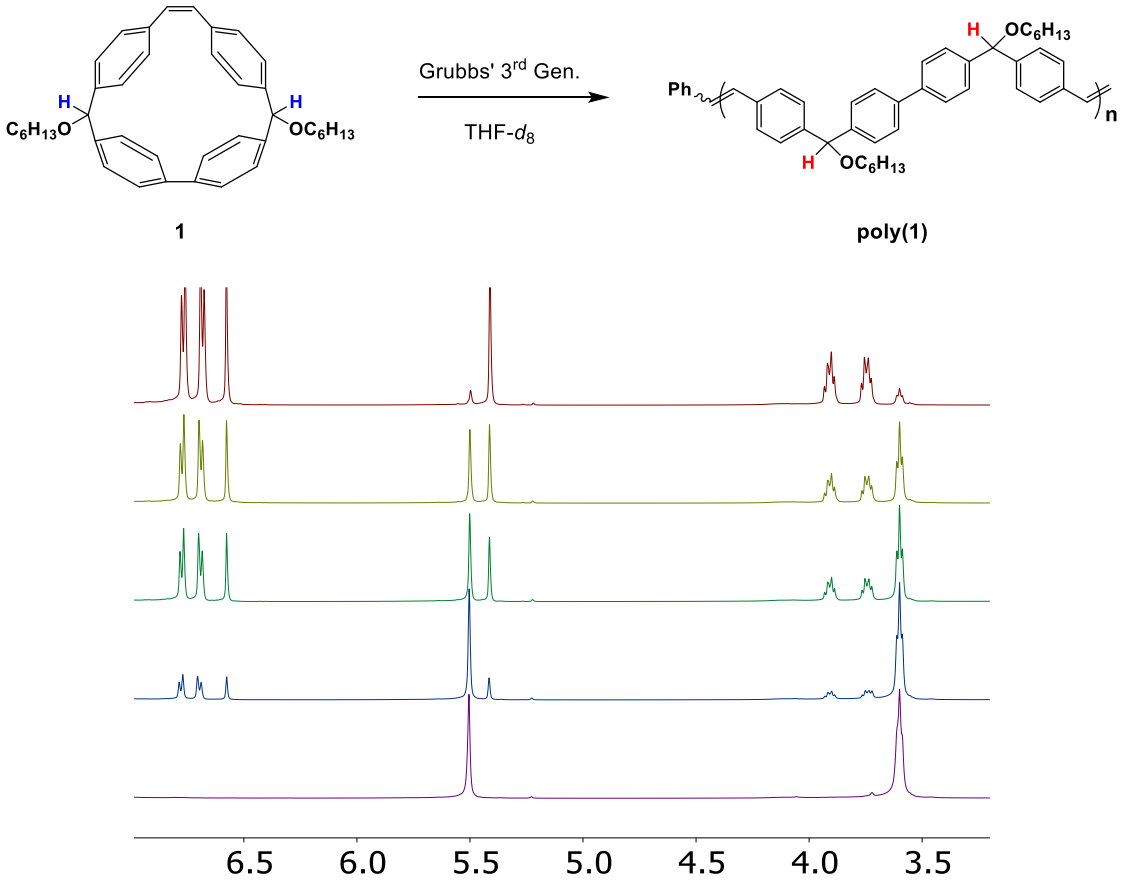

Figure 7.1. **Top**, Polymerization scheme of Monomer **1** with Grubbs catalyst. **Bottom**, Stacked ^{1}H NMR spectra of the polymerization over 12 hours. Top to bottom time points: 5, 45, 60, 135, 540 min.

The structure of **poly(1)** was confirmed by ^{1}H NMR spectroscopy and MALDI-TOF/MS. In the case of **poly(1)** there is a single vinylic signal at 7.24 ppm, consistent with a backbone of

exclusively *trans*-stilbene isomers (**Figure 7.2**).[343–345] MALDI-TOF/MS then was used to better understand the structural speciation within samples of **poly(1)** (Figure 7.3). The repeat unit for **poly(1)** has a calculated mass of 558.8 amu, which was found to be consistent with the predicted molecular weight of **1**. Notably, we did not see evidence of cyclic polymer structures from any of the analyses.

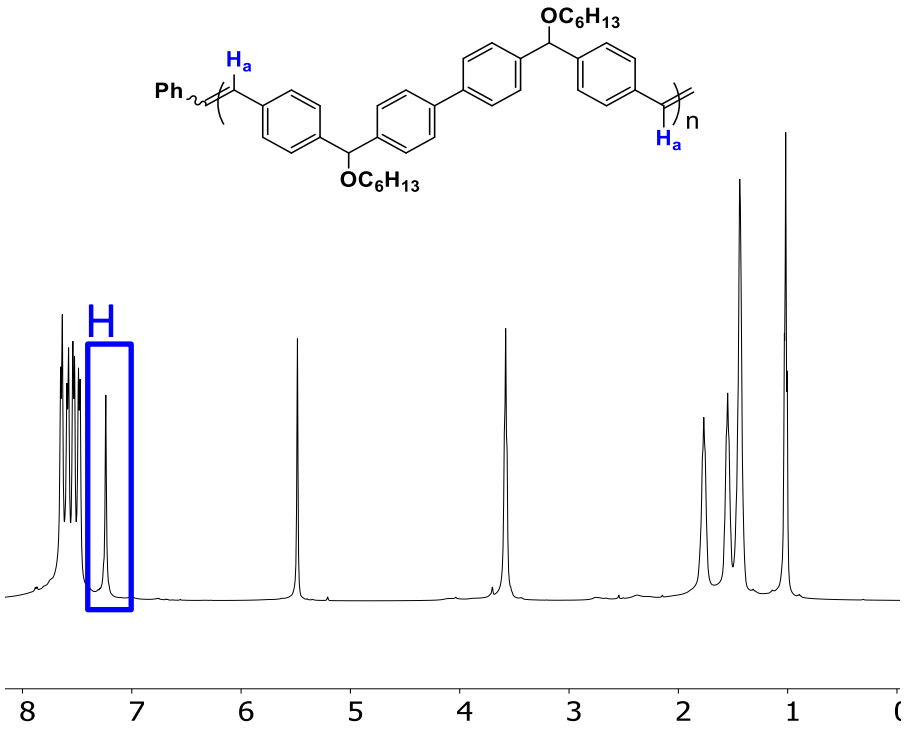

Figure 7.2. ^{1}H NMR of the final purified polymer. All of the highlighted ^{1}H on the polymer are consistent with trans protons, as compared to stillbene.

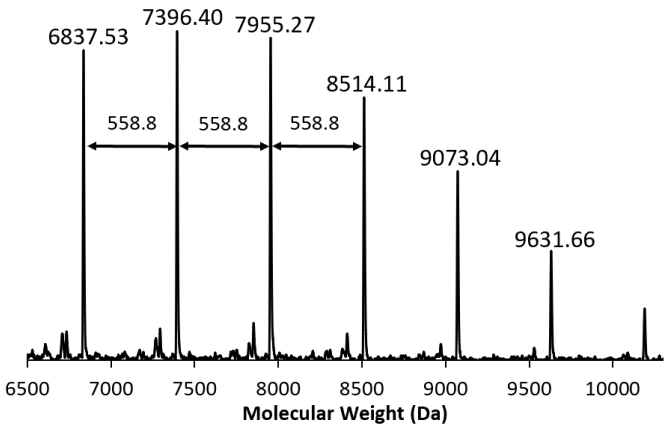

Figure 7.3. MALDI-TOF data shows the repeat unit of the polymer. End group molecular weight is consistent with linear polymers, not even larger macrocycles

The thermal properties of **poly(1**) were determine using DSC and TGA (Figure 4). The decomposition temperature (T_d) for **poly(1)** was found to be 281 °C under N_2 determined by the onset of weight loss using TGA. A glass transition temperature (T_g) for **poly(1)** was found to be 94 °C determined by differential scanning calorimetry, and no other thermal transitions were observed.

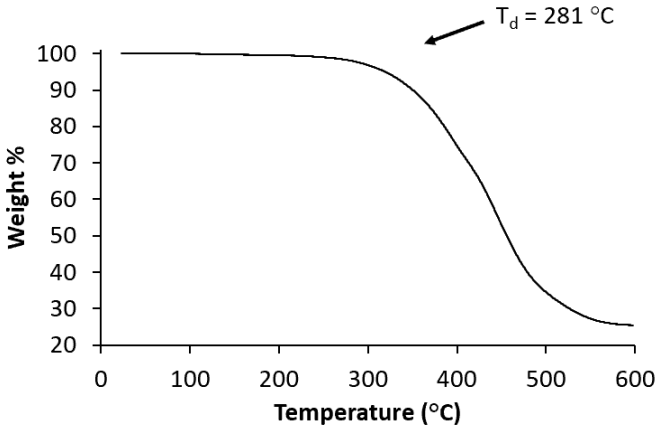

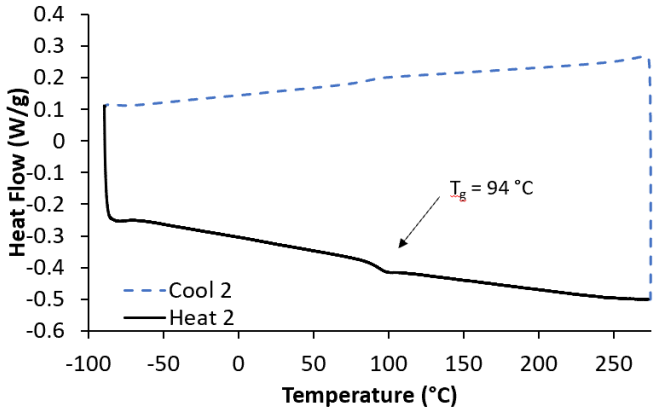

Figure 7.4. TGA (top) and DSC (bottom) data of isolated polymer.

7.3.2 *Kinetics of macrocycle ROMP and concurrent chain transfer*

Given the ring strain and expected enthalpic driving force for the ROMP of **1**, the kinetics of the polymerization were expected to be chain-growth-like, with better MW control than comparable ED-ROMP systems. To better understand the polymerization mechanism of **poly(1)**, monomer conversion was monitored by ^{1}H NMR spectroscopy using the benzylic ether hydrogen of the monomer and polymer at 5.39 ppm and 5.48 ppm, respectively. The polymerization displayed first order kinetics with respect to consumption of 1 (Figure 7.5, top), as well as, a linear correlation between M_n and conversion (Figure 7.5, bottom). During the course of the polymerization of **1** however, the $Đ$ of **poly(1)** increased from 1.0 to 1.5 further which suggested that chain transfer, not slow initiation, was the reason for the high $Đ$.

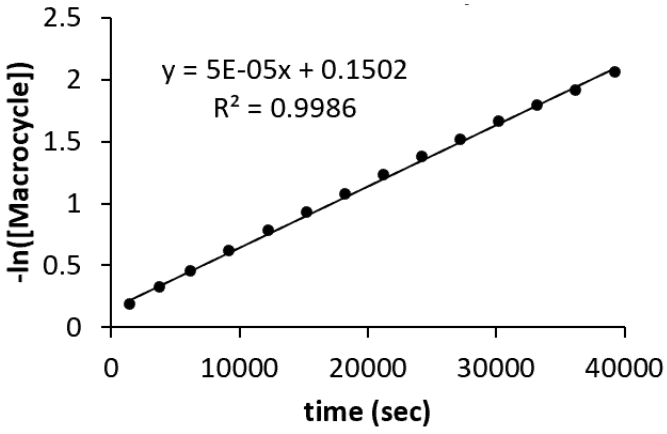

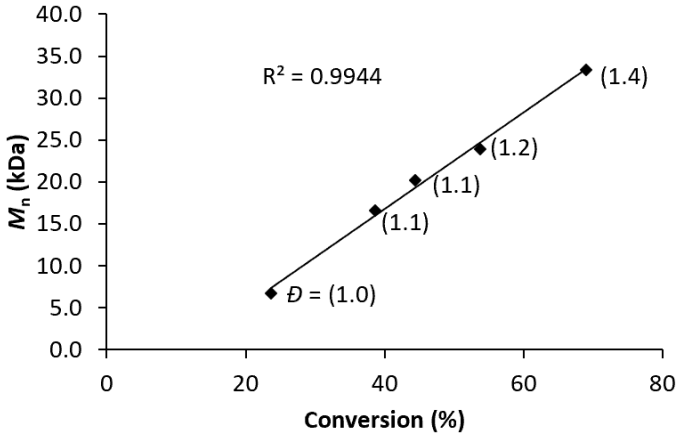

Figure 7.5. **Top**, First order kinetics plot of the disappearance of monomer **1**. **Bottom**, A plot of conversion and M_n shows a linear relationship, suggesting a chain growth mechanism.

To determine if chain transfer is indeed occuring, two molecular weigh crossover experiments were performed. In these experiments, polymers of different molecular weights are mixed together and subjected to polymerization conditions. In the first experiment, polymer of M_n = 65.2 kDa (*Đ* = 1.6) was combined with model monomer (E)-stillbene (74 equiv) and G3 in THF at 40 ºC. After 3.5 h, the polymerization was quenched with EVE and a crude reaction aliquot was taken for GPC analysis. The resulting polymer was measusred to be M_n = 16.9 (*Đ* = 1.5), suggesting that chain transfer was possible during the polymerization. In the second molecular weight crossover experiment, two polymers of different molecular weight were taken and subject to polymerization conditions (Figure 7.6, top). After 3.5 h, a crude reaction mixture aliquot was taken for GPC analysis. The resulting polymer showed an intermediate molecular weight and high dispersity (Figure 7.6, bottom).

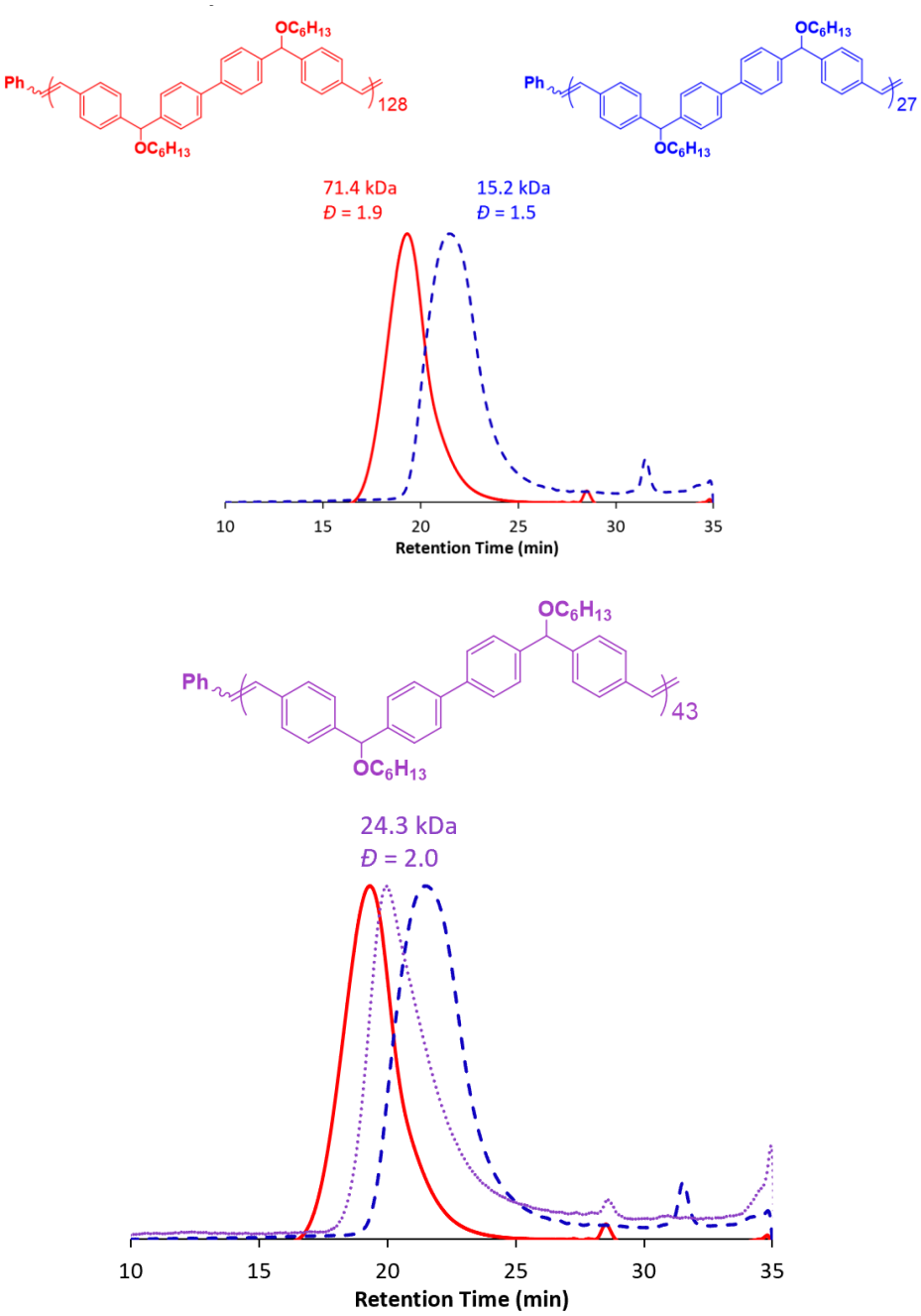

Figure 7.6. **Top**, RI traces as determined by GPC of the two starting polymers (red high MW, blue low MW) used for chain transfer experiments. **Bottom**, RI traces as determined by GPC of the two starting polymers, and the final polymer (purple mixed MW) from the chain transfer experiments.

In summary we have reported the synthesis and subsequent polymerization of strained macrocycle **1**. The polymerization of **1** demonstrated first order kinetics and a linear correlation between M_n and conversion consistent with a chain growth polymerization. The resulting linear polymer presented through this method had a T_g of 94 °C and a T_d of 281 °C. Further work is being done to use variations of **1** to make more complex polymeric materials that cannot be achieved using traditional small molecule based poly(olefins). In this way, we hope to control and modify the thermal and physical properties of these novel polymers. Ultimately, enthalpy driven ROMP of highly strained macrocyclic monomers provides an exciting avenue to create and develop new polymeric materials that would be significantly difficult to synthesize through other methods.

7.4 Conclusion

We envisioned a macrocycle (**1**) that enables predefined control of the structure of the polymer backbone based on *cis*-stilbene that would contain a high amount of ring strain. By building ring strain into the macrocycle, **poly(1)** was obtained with a low *Đ* as well as controlled molecular weight. Controlling molecular weight is inherently valuable because it heavily influences the polymer's thermal properties according to the Flory-Fox relationship between MW and T_g. The ability to synthesize potential high-performance polymers through readily accessible chain growth polymerizations, instead of step growth polymerizations, could be an exciting advancement toward more complex polymer structures that were previously thought to be unachievable.

Due to the lack of heteroatoms within the backbone, **poly(1)** would only be obtainable through a synthetically intensive step growth polymerization. We demonstrate that building ring strain into a pre-programmable macrocycle monomer is a viable synthetic strategy to make high performance polymers with better molecular weight control that might be applicable to other high performance

polymers made by polymerization macrocycle polymerization such as poly(phenylene)s, poly(phenylenevinylene)s, and poly(aryletherketone)s.

Chapter 8. FUTURE PROJECTS

8.1 FUTURE DIRECTIONS FOR APCPV

Please refer to Chapter 4.5.

8.2 ROMP FOR POLYSTAT

8.2.1 *Using ROMP for polySTAT will improve synthesis and lower costs*

PolySTAT, a water-soluble methacrylate-based polymer with multivalent fibrin-binding peptides (FBP), is a promising new biomaterial solution for hemostasis.[346] PolySTAT is synthesized by copolymerization of hydroxyethylmethacrylate (HEMA) and N-hydroxysuccinimide ester methacrylate (NHS-MA) via RAFT. The activated NHS-esters on the polymer are reacted post-polymerization with a primary amine on FBP.

One of the limitations in the synthesis of polySTAT is the less than quantitative conjugation efficiency of FBP onto the methacrylate backbone. FBP is the most expensive component of polySTAT and improving the efficiency of FBP incorporation would lower the manufacturing cost of this promising biomaterial. One alternative approach has been explored in which an FBP-methacrylate (FBP-MA) was synthesized and copolymerized with HEMA. However, this approach is limiting because RDRPs are not taken to quantitative conversion due to the increased rate of chain-chain coupling and loss of dispersity control. The unreacted monomers, including some expensive FBP-methacrylate, are then thrown away.

Using ROMP instead of RAFT to synthesize polySTAT presents several advantages. There are many methods for conjugating peptides onto ROMP monomers that can be achieved in high yield, such as reacting FBP-amine with carbic anhydride, conjugating FBP onto an acrylate and then reacting the FBP-acrylate in a [4+2] cycloaddition with cyclopentadiene or furan into a

functionalized norbornene or oxanorbornene. Additionally, ROMP monomers can be made directly by solid-phase peptide synthesis by making a norbornene-maleimide capped amino acid.[251,347] ROMP has been shown to be have high functional group tolerance, ability to ROMP peptide monomers, and can be taken to 100% conversion, resulting in no loss of expensive FBP.[251,347]

ROMP polymers, however, have residual backbone alkenes which limit the shelf-life stability of the final product. This can be addressed by hydrogenation with Pd/C and H_2, or acid catalyzed hydroxylation[84] which can impart additional water solubility.

8.2.2 *Use of ROMP for polySTAT enables the synthesis of cyclic polySTAT*

PolySTAT is primarily HEMA, which has one hydroxyl group for every 6 carbons, which is below the minimum ratio for high water-solubility (one hydroxyl for every 3 carbons). And due to its limited water-solubility, polySTAT must be administered in large volumes of liquid. The translatability of polySTAT can be greatly improved by improving its water solubility, thus allowing more concentrated formulations of polySTAT. Efforts are actively being made in the Pun Lab to improve the solubility of polySTAT by incorporating a more water-soluble monomer, GmMA into polySTAT.

An alternative approach to improve the water-solubility of polySTAT is to synthesize cyclic polySTAT. As discussed earlier, CycPs have been shown to exhibit smaller hydrodynamic radii in solution, and lower viscosities than their linear variants which may result in better water-solubility due to lower chain entanglements.[307–309] The use of ROMP for the synthesis of polySTAT will allow it to be synthesized into cyclic variants by building off the work done by ring expansion metathesis polymerization (REMP).[153,317,318]

REFERENCES

[1] D. C. Lee, A. N. Prossnitz, R. J. Lamm, A. J. Boydston, S. H. Pun, *Adv. Healthc. Mater.* **2018**, *1800861*, 1–14.
[2] C. Barner-Kowollik, *Handbook of RAFT Polymerization*, Wiley, **2008**.
[3] S. Perrier, *Macromolecules* **2017**, *50*, 7433–7447.
[4] D. C. Lee, V. Kensy, C. Maroon, B. K. Long, A. J. Boydston, *Angew. Chemie Int. Ed.* **2019**, *58*, 1–5.
[5] T. M. McGuire, C. Pérale, R. Castaing, G. Kociok-Köhn, A. Buchard, *J. Am. Chem. Soc.* **2019**, jacs.9b06259.
[6] J. B. Ravnsbæk, T. M. Swager, *ACS Macro Lett.* **2014**, *3*, 305–309.
[7] T. M. Swager, R. H. Grubbs, *J. Am. Chem. Soc.* **1987**, *109*, 894–896.
[8] T. M. Swager, R. H. Grubbs, *Synth. Met.* **1989**, *28*, 57–62.
[9] M. S. Taylor, T. M. Swager, *Angew. Chemie - Int. Ed.* **2007**, *46*, 8480–8483.
[10] J. Seo, S. Y. Lee, C. W. Bielawski, *Polym. Chem.* **2019**, *10*, 6401–6412.
[11] C. A. Jones, R. A. Lawrence, J. Martens, R. H. Friendt, D. Parker, W. J. Feast, M. L6gdlund, W. R. Salaneck, *Polymer (Guildf).* **1991**, *32*, 1200–1209.
[12] C. Road, S. Road, M. Sciences, M. Road, *Synth. Met.* **1986**, *14*, 245–269.
[13] Z. Chen, J. A. M. Mercer, X. Zhu, J. A. H. Romaniuk, R. Pfattner, L. Cegelski, T. J. Martinez, N. Z. Burns, Y. Xia, *Science (80-.).* **2017**, *357*, 475–479.
[14] C. Kang, J. Sung, K. Kim, S. H. Hong, T. Choi, *ACS Macro Lett.* **2020**, *9*, 339–343.
[15] A. Varela-Moreira, Y. Shi, M. H. A. M. Fens, T. Lammers, W. E. Hennink, R. M. Schiffelers, *Mater. Chem. Front.* **2017**, *1*, 1485–1501.
[16] R. Voelker, *JAMA* **2018**, *319*, 220.
[17] F. S. Bates, G. H. Fredrickson, *Annu. Rev. Phys. Chem.* **1990**, *41*, 525–557.
[18] M. Trollsås, J. L. Hedrick, *J. Am. Chem. Soc.* **1998**, *120*, 4644–4651.
[19] C. E. Wang, P. S. Stayton, S. H. Pun, A. J. Convertine, *J. Control. Release* **2015**, *219*, 345–354.
[20] L. Y. Qiu, Y. H. Bae, *Pharm. Res.* **2006**, *23*, 1–30.
[21] N. Nasongkia, B. Chen, N. Macaraeg, M. E. Fox, J. M. J. Fréchet, F. C. Szoka, *J. Am. Chem. Soc.* **2009**, *131*, 3842–3843.
[22] H. Wei, C. E. Wang, N. Tan, A. J. Boydston, S. H. Pun, *ACS Macro Lett.* **2015**, *4*, 938–941.
[23] P. Kesharwani, A. K. Iyer, *Drug Discov. Today* **2016**, *20*, 536–547.
[24] F. Wang, T. K. Bronich, A. V. Kabanov, R. D. Rauh, J. Roovers, *Bioconjug. Chem.* **2005**, *16*, 397–405.
[25] X. Jin, P. Sun, G. Tong, X. Zhu, *Biomaterials* **2018**, *178*, 738–750.
[26] J. Zou, Y. Yu, Y. Li, W. Ji, C.-K. Chen, W.-C. Law, P. N. Prasad, C. Cheng, *Biomater. Sci.* **2015**, *3*, 1078–1084.
[27] W. Wu, W. Dai, X. Zhao, J. Zhang, Y. Zhao, *Polym. Chem.* **2018**, *9*, 1947–1960.
[28] J. M. Benns, J. S. Choi, R. I. Mahato, J. S. Park, Sung Wan Kim, *Bioconjug. Chem.* **2000**, *11*, 637–645.
[29] D. S. H. Chu, J. G. Schellinger, J. Shi, A. J. Convertine, P. S. Stayton, S. H. Pun, *Acc. Chem. Res.* **2012**, *45*, 1089–1099.
[30] C. E. Wang, H. Wei, N. Tan, A. J. Boydston, S. H. Pun, *Biomacromolecules* **2016**, *17*, 69–75.

[31] Y. Cheng, H. Wei, J. K. Y. Tan, D. J. Peeler, D. O. Maris, D. L. Sellers, P. J. Horner, S. H. Pun, *Small* **2016**, *12*, 2750–2758.
[32] H. Wei, X. Zhang, C. Cheng, S. X. Cheng, R. X. Zhuo, *Biomaterials* **2007**, *28*, 99–107.
[33] M. R. Nabid, S. J. Tabatabaei Rezaei, R. Sedghi, H. Niknejad, A. A. Entezami, H. A. Oskooie, M. M. Heravi, *Polymer (Guildf).* **2011**, *52*, 2799–2809.
[34] K. Kataoka, A. Harada, Y. Nagasaki, *Adv. Drug Deliv. Rev.* **2001**, *47*, 113–131.
[35] M. Harada, I. Bobe, H. Saito, N. Shibata, R. Tanaka, T. Hayashi, Y. Kato, *Cancer Sci.* **2011**, *102*, 192–199.
[36] C. J. Rijcken, C. J. Snel, R. M. Schiffelers, C. F. van Nostrum, W. E. Hennink, *Biomaterials* **2007**, *28*, 5581–5593.
[37] V. S. Trubetskoy, *Adv. Drug Deliv. Rev.* **1999**, *37*, 81–88.
[38] J. Park, G. Von Maltzahn, E. Ruoslahti, S. N. Bhatia, M. J. Sailor, *Angew. Chem.* **2008**, *120*, 7394–7398.
[39] B. M. Discher, Y. Won, D. S. Ege, J. C. Lee, F. S. Bates, D. E. Discher, D. A. Hammer, *Adv. Sci.* **2012**, *284*, 1143–1146.
[40] F. Ahmed, R. I. Pakunlu, A. Brannan, F. Bates, T. Minko, D. E. Discher, *J. Control. Release* **2006**, *116*, 150–158.
[41] H. Lomas, I. Canton, S. MacNeil, J. Du, S. P. Armes, A. J. Ryan, A. L. Lewis, G. Battaglia, *Adv. Mater.* **2007**, *19*, 4238–4243.
[42] Y. Wang, L. Wang, B. Li, Y. Cheng, D. Zhou, X. Chen, X. Jing, Y. Huang, *ACS Macro Lett.* **2017**, *6*, 1186–1190.
[43] N. Maurer, D. B. Fenske, P. R. Cullis, *Expert Opin. Biol. Ther.* **2001**, *1*, 923–47.
[44] D. E. Discher, F. Ahmed, *Annu. Rev. Biomed. Eng.* **2006**, *8*, 323–341.
[45] K. M. Park, D. W. Lee, B. Sarkar, H. Jung, J. Kim, Y. H. Ko, K. E. Lee, H. Jeon, K. Kim, *Small* **2010**, *6*, 1430–1441.
[46] F. Meng, Z. Zhong, J. Feijen, *Biomacromolecules* **2009**, *10*, 197–209.
[47] R. Cheng, F. Feng, F. Meng, C. Deng, J. Feijen, Z. Zhong, *J. Control. Release* **2011**, *152*, 2–12.
[48] R. Cheng, F. Meng, C. Deng, H. A. Klok, Z. Zhong, *Biomaterials* **2013**, *34*, 3647–3657.
[49] J. Leong, J. Y. Teo, V. K. Aakalu, Y. Y. Yang, H. Kong, *Adv. Healthc. Mater.* **2018**, *7*, 1–27.
[50] W. S. Shim, J. S. Yoo, Y. H. Bae, D. S. Lee, *Biomacromolecules* **2005**, *6*, 2930–2934.
[51] B. Jeong, Y. H. Bae, D. S. Lee, S. W. Kim, *Nature* **1997**, *388*, 860–862.
[52] A. Bose, S. Jana, A. Saha, T. K. Mandal, *Polym. (United Kingdom)* **2017**, *110*, 12–24.
[53] J. M. Sarapas, C. M. Backlund, B. M. deRonde, L. M. Minter, G. N. Tew, *Chem. - A Eur. J.* **2017**, *23*, 6858–6863.
[54] H. Wei, J. G. Schellinger, D. S. H. Chu, S. H. Pun, *J. Am. Chem. Soc.* **2012**, *134*, 16554–16557.
[55] X. Sui, Z. Zhang, S. Guan, Y. Xu, C. Li, Y. Lv, A. Chen, L. Yang, L. Gao, *Polym. Chem.* **2015**, *6*, 2777–2782.
[56] C. Boyer, N. A. Corrigan, K. Jung, D. Nguyen, T. K. Nguyen, N. N. M. Adnan, S. Oliver, S. Shanmugam, J. Yeow, *Chem. Rev.* **2016**, *116*, 1803–1949.
[57] J. S. Wang, K. Matyjaszewski, *J. Am. Chem. Soc.* **1995**, *117*, 5614–5615.
[58] K. Matyjaszewski, *Macromolecules* **2012**, *45*, 4015–4039.
[59] M. Zhang, Q. Xiong, W. Shen, Q. Zhang, *RSC Adv.* **2014**, *4*, 30566–30572.
[60] M. Fantin, A. A. Isse, A. Gennaro, K. Matyjaszewski, *Macromolecules* **2015**, *48*, 6862–

6875.
[61] M. Fantin, A. A. Isse, A. Venzo, A. Gennaro, K. Matyjaszewski, *J. Am. Chem. Soc.* **2016**, *138*, 7216–7219.
[62] P. Z. Elias, G. W. Liu, H. Wei, M. C. Jensen, P. J. Horner, S. H. Pun, *J. Control. Release* **2015**, *208*, 76–84.
[63] X. Pan, M. Fantin, F. Yuan, K. Matyjaszewski, *Chem. Soc. Rev.* **2018**, *47*, 5457–5490.
[64] M. R. Hill, R. N. Carmean, B. S. Sumerlin, *Macromolecules* **2015**, *48*, 5459–5469.
[65] J. Chiefari, Y. K. B. Chong, F. Ercole, J. Krstina, J. Jeffery, T. P. T. Le, R. T. A. Mayadunne, G. F. Meijs, C. L. Moad, G. Moad, et al., *Macromolecules* **1998**, *31*, 5559–5562.
[66] B. Apostolovic, S. P. E. Deacon, R. Duncan, H.-A. Klok, *Biomacromolecules* **2010**, *11*, 1187–1195.
[67] R. N. Johnson, R. S. Burke, A. J. Convertine, A. S. Hoffman, P. S. Stayton, S. H. Pun, *Biomacromolecules* **2010**, *11*, 3007–13.
[68] D. S. H. Chu, J. G. Schellinger, M. J. Bocek, R. N. Johnson, S. H. Pun, *Biomaterials* **2013**, *34*, 9632–9637.
[69] J. Niu, D. J. Lunn, A. Pusuluri, J. I. Yoo, M. A. O 'malley, S. Mitragotri, H. T. Soh, C. J. Hawker, *Nat. Chem.* **2017**, *9*, 537–545.
[70] D. K. Schneiderman, J. M. Ting, A. A. Purchel, R. Miranda, M. V. Tirrell, T. M. Reineke, S. J. Rowan, *ACS Macro Lett.* **2018**, 406–411.
[71] D. B. Thomas, A. J. Convertine, R. D. Hester, A. B. Lowe, C. L. Mccormick, *Macromolecules* **2004**, *37*, 1735–1741.
[72] A.-C. Albertsson, I. K. Varma, *Biomacromolecules* **2003**, *4*, 1466–1486.
[73] O. Dechy-cabaret, B. Martin-vaca, D. Bourissou, O. Dechy-cabaret, B. Martin-vaca, D. Bourissou, *Chem. Rev.* **2004**, *104*, 6147–6176.
[74] N. Hadjichristidis, H. Iatrou, M. Pitsikalis, G. Sakellariou, *Chem. Rev.* **2009**, *109*, 5528–5578.
[75] K. Makiguchi, T. Satoh, T. Kakuchi, *Macromolecules* **2011**, *44*, 1999–2005.
[76] N. E. Kamber, W. Jeong, R. M. Waymouth, R. C. Pratt, B. G. G. Lohmeijer, J. L. Hedrick, *Chem. Rev.* **2007**, *107*, 5813–5840.
[77] H. R. Kricheldorf, *Angew. Chemie - Int. Ed.* **2006**, *45*, 5752–5784.
[78] J. Cheng, T. J. Deming, in (Ed.: T. Deming), Springer Berlin Heidelberg, Berlin, Heidelberg, **2012**, pp. 1–26.
[79] S. Kobayashi, S. Kobayashi, H. Uyama, H. Uyama, S. Kimura, S. Kimura, *Chem. Rev.* **2001**, *101*, 3793–3818.
[80] R. Tong, J. Cheng, *Macromolecules* **2012**, *45*, 2225–2232.
[81] S. Lv, Y. Wu, J. Dang, Z. Tang, Z. Song, S. Ma, X. Wang, X. Chen, J. Cheng, L. Yin, *Polym. Chem.* **2017**, *8*, DOI 10.1039/c6py02230h.
[82] C. W. Bielawski, R. H. Grubbs, *Prog. Polym. Sci.* **2007**, *32*, 1–29.
[83] B. C. W., G. R. H., in *Control. Living Polym.*, Wiley-Blackwell, **2010**, pp. 297–342.
[84] M. Wathier, S. S. Stoddart, M. J. Sheehy, M. W. Grinstaff, *J. Am. Chem. Soc.* **2010**, *132*, 15887–15889.
[85] E. K. Riga, D. Boschert, M. Vöhringer, V. T. Widyaya, M. Kurowska, W. Hartleb, K. Lienkamp, *Macromol. Chem. Phys.* **2017**, *218*, 1700273.
[86] A. E. Madkour, A. H. R. Koch, K. Lienkamp, G. N. Tew, *Macromolecules* **2010**, *43*, 4557–4561.

[87] R. M. Conrad, R. H. Grubbs, *Angew. Chemie Int. Ed.* **2009**, *48*, 8328–8330.
[88] J. K. Kammeyer, A. P. Blum, L. Adamiak, M. E. Hahn, N. C. Gianneschi, *Polym. Chem.* **2013**, *4*, 3929.
[89] D. C. Church, S. Nourian, C.-U. Lee, N. A. Yakelis, J. P. Toscano, A. J. Boydston, *ACS Macro Lett.* **2017**, *6*, 46–49.
[90] K. Grela, *Olefin Metathesis : Theory and Practice*, John Wiley & Sons, **2014**.
[91] C. S. Higman, J. A. M. Lummiss, D. E. Fogg, *Angew. Chemie - Int. Ed.* **2016**, *55*, 3552–3565.
[92] P. Wheeler, J. H. Phillips, R. L. Pederson, *Org. Process Res. Dev.* **2016**, *20*, 1182–1190.
[93] R. Verduzco, X. Li, S. L. Pesek, G. E. Stein, *Chem. Soc. Rev.* **2015**, *44*, 2405–2420.
[94] I. conference on Harmonization, *Guideline for Elemental Impurities Q3D*, **2014**.
[95] A. Li, J. Ma, G. Sun, Z. Li, S. Cho, C. Clark, K. L. Wooley, *Polym. Chem.* **2012**, *50*, 1681–1688.
[96] K. V Bernaerts, F. E. Du Prez, *Prog. Polym. Sci* **2006**, *31*, 671–722.
[97] H. U. Kang, Y. C. Yu, S. J. Shin, J. H. Youk, *J. Polym. Sci. Part A Polym. Chem.* **2013**, *51*, 774–779.
[98] S. Jin Shin, Y. Chang Yu, J. Deok Seo, S. Ju Cho, J. Ho Youk, C. to, J. H. Youk, *J. Polym. Sci., Part A Polym. Chem* **2014**, *52*, 1607–1613.
[99] E. Themistou, G. Battaglia, S. P. Armes, *Polym. Chem.* **2014**, *5*, 1405.
[100] Y. Zheng, W. Turner, M. Zong, D. J. Irvine, S. M. Howdle, K. J. Thurecht, *Macromolecules* **2011**, *44*, 1347–1354.
[101] T. Oztürk, M. Göktas, B. Hazer, *J Appl Polym Sci* **2010**, *117*, 1638–1645.
[102] X. Zhang, J. Li, W. Li, A. Zhang, *Biomacromolecules* **2007**, *8*, 3557–3567.
[103] V. A. Piunova, H. W. Horn, G. O. Jones, J. E. Rice, R. D. Miller, *J. Polym. Sci. Part A Polym. Chem.* **2016**, *54*, 563–569.
[104] C. Aydogan, C. Kutahya, A. Allushi, G. Yilmaz, Y. Yagci, *Polym. Chem.* **2017**, *8*, DOI 10.1039/c7py00069c.
[105] Z. Tong, Y. Li, H. Xu, H. Chen, W. Yu, W. Zhuo, R. Zhang, G. Jiang, *ACS Macro Lett.* **2016**, *5*, 867–872.
[106] J. Zhou, H. Xu, Z. Tong, Y. Yang, G. Jiang, *Mater. Sci. Eng. C* **2018**, *89*, 237–244.
[107] B. K. Sourkohi, A. Cunningham, Q. Zhang, J. K. Oh, B. Khorsand Sourkohi, A. Cunningham, Q. Zhang, J. K. Oh, *Biomacromolecules* **2011**, *12*, 3819–3825.
[108] C.-F. Huang, S.-W. Kuo, H.-F. Lee, F.-C. Chang, *Polymer (Guildf).* **2005**, *46*, 1561–1565.
[109] W. Jakubowski, K. Matyjaszewski, *Macromolecules* **2005**, *38*, 4139–4146.
[110] L. Lei, F. Li, H. Zhao, Y. Wang, *Polym. Chem.* **2018**, *56*, 699–704.
[111] J. Song, J. Xu, S. Pispas, G. Zhang, *RSC Adv.* **2015**, *5*, 38243.
[112] M. De Geus, L. Schormans, A. R. A. Palmans, C. E. Koning, A. Heise, *J. Polym. Sci. Part A Polym. Chem.* **2006**, *44*, 4290–4297.
[113] J. Peeters, A. R. A. Palmans, M. Veld, F. Scheijen, A. Heise, E. W. Meijer, J. Peeters, A. R. A. Palmans, M. Veld, F. Scheijen, et al., *Biomacromolecules* **2004**, *5*, 1862–1868.
[114] Y. Wang, M. Fantin, K. Matyjaszewski, Y. Wang, M. Fantin, K. Matyjaszewski, *Macromol. Rapid Commun.* **2018**, 1800221.
[115] J. C. Theriot, G. M. Miyake, C. A. Boyer, *ACS Macro Lett.* **2018**, *7*, 662–666.
[116] C.-F. Huang, Y.-A. Hsieh, S.-C. Hsu, K. Matyjaszewski, *Polymer (Guildf).* **2014**, *55*, 6051–6057.
[117] C.-F. Huang, R. Nicolay, Y. Kwak, F.-C. Chang, K. Matyjaszewski, *Macromolecules*

2009, *42*, 8198–8210.
[118] C. W. Bielawski, J. Louie, R. H. Grubbs, M. Beckman, Christopher W. Bielawski, A. Janis Louie, R. H. Grubbs*, *J. Am. Chem. Soc.* **2000**, *122*, 12872–12873.
[119] M. B. Runge, S. Dutta, N. B. Bowden, *Macromolecules* **2006**, *39*, 498–508.
[120] G. Chen, D. Huynh, P. L. Felgner, Z. Guan, *J. Am. Chem. Soc.* **2006**, *128*, 4298–4302.
[121] M. Xie, J. Dang, H. Han, W. Wang, J. Liu, X. He, Y. Zhang, *Macromolecules* **2008**, *41*, 9004–9010.
[122] J. Cuthbert, A. Beziau, E. Gottlieb, L. Fu, R. Yuan, A. C. Balazs, T. Kowalewski, K. Matyjaszewski, *Macromolecules* **2018**, *51*, 3808–3817.
[123] D. Zehm, A. E. Laschewsky, H. Liang, J. Urgen, P. Rabe, J. P. Rabe, *Macromolecules* **2011**, *44*, 9635–9641.
[124] J. Bolton, J. Rzayev, *ACS Macro Lett.* **2012**, *1*, 15–18.
[125] S. Boisse, M. A. Kryuchkov, N.-D. Tien, C. G. Bazuin, R. E. Prud'homme, *Macromolecules* **2016**, *49*, 6973–6986.
[126] M. A. Kryuchkov, C. Detrembleur, R. J. Jerome, R. E. Prud 'homme, C. G. Bazuin, *Macromolecules* **2011**, *44*, 5209–5217.
[127] M. Spasova, L. Mespouille, O. Coulembier, D. Paneva, N. Manolova, I. Rashkov, P. Dubois, *Biomacromolecules* **2009**, *10*, 1217–1223.
[128] X. Cao, W. Mao, Y. Mai, L. Han, S. Che, *Macromolecules* **2018**, *51*, 4381–4396.
[129] H. Cheng, X. Fan, C. Wu, X. Wang, L.-J. Wang, X. J. Loh, Z. Li, Y.-L. Wu, *Macromol. Rapid Commun.* **2018**, *1800207*, 1–7.
[130] W. Zhu, A. Nese, K. Matyjaszewski, *J. Polym. Sci. Part A Polym. Chem.* **2011**, *49*, 1942–1952.
[131] J. B. Matson, R. H. Grubbs, *Macromolecules* **2008**, *41*, 5626–5631.
[132] G. Fuks, R. M. Talom, F. Gauffre, *Chem. Soc. Rev. Chem. Soc. Rev* **2011**, *40*, 2475–2493.
[133] L. Wang, R. Zeng, C. Li, R. Qiao, *Colloids Surfaces B Biointerfaces* **2009**, *74*, 284–292.
[134] H. Kukula, H. Schlaad, M. Antonietti, S. Fö, *J. Am. Chem. Soc.* **2002**, *124*, 1658–1663.
[135] J. Babin, C. Leroy, S. Lecommandoux, R. Borsali, Y. Gnanou, D. Taton, *Chem. Commun.* **2005**, 1993–1995.
[136] J. Babin, D. Taton, M. Brinkmann, S. Lecommandoux, *Macromolecules* **2008**, *41*, 1384–1392.
[137] K. R. Brzezinska, T. J. Deming, *Macromol. Biosci.* **2004**, *4*, 566–569.
[138] C.-J. Huang, F.-C. Chang, *Macromolecules* **2008**, *41*, 7041–7052.
[139] T. C. Castle, E. Khosravi, L. R. Hutchings, *Macromolecules* **2006**, *39*, 5639–5645.
[140] P. Lu, N. M. Alrashdi, A. J. Boydston, *J. Polym. Sci. Part A Polym. Chem.* **2017**, *55*, 2977–2982.
[141] V. Ladelta, J. D. Kim, P. Bilalis, Y. Gnanou, N. Hadjichristidis, *Macromolecules* **2018**, *51*, 2428–2436.
[142] M. Benaglia, J. Chiefari, Y. K. Chong, G. Moad, E. Rizzardo, S. H. Thang, *J. Am. Chem. Soc.* **2009**, *131*, 6914–6915.
[143] A. B. Biernesser, K. R. D. Chiaie, J. B. Curley, J. A. Byers, *Angew. Chemie - Int. Ed.* **2016**, *55*, 5251–5254.
[144] M. Qi, Q. Dong, D. Wang, J. A. Byers, *J. Am. Chem. Soc* **2018**, *140*, 48.
[145] P. Zhenjiang Li, K. Guo, X. Wang, J. Liu, S. Xu, J. Xu, X. Pan, J. Liu, S. Cui, Z. Li, *Polym. Chem* **2016**, *7*, 6281–6424.
[146] H. Dong, Y. Zhu, Z. Li, J. Xu, J. Liu, S. Xu, H. Wang, Y. Gao, K. Guo, *Macromolecules*

2017, *50*, 9295–9306.
[147] A. J. Teator, D. N. Lastovickova, C. W. Bielawski, *Chem. Rev.* **2016**, *116*, 1969–1992.
[148] Q. Michaudel, V. Kottisch, B. P. Fors, *Angew. Chem. Int. Ed.* **2017**, *56*, 9670–9679.
[149] K. Satoh, H. Hashimoto, S. Kumagai, H. Aoshima, M. Uchiyama, R. Ishibashi, Y. Fujiki, M. Kamigaito, *Polym. Chem.* **2017**, *8*, 4891–5254.
[150] V. Kottisch, Q. Michaudel, B. P. Fors, *J. Am. Chem. Soc.* **2017**, *139*, 10665–10668.
[151] A. Ohtsuki, L. Lei, M. Tanishima, A. Goto, H. Kaji, *J. Am. Chem. Soc.* **2015**, *137*, 5610–5617.
[152] Y. Xia, J. A. Kornfield, R. H. Grubbs, *Macromolecules* **2009**, *42*, 3761–3766.
[153] Y. Xia, A. J. Boydston, R. H. Grubbs, *Angew. Chemie - Int. Ed.* **2011**, *50*, 5882–5885.
[154] D. Neugebauer, Y. Zhang, T. Pakula, S. S. Sheiko, K. Matyjaszewski, *Macromolecules* **2003**, *36*, 6746–6755.
[155] J. C. Foster, S. C. Radzinski, S. E. Lewis, M. B. Slutzker, J. B. Matson, *Polymer (Guildf).* **2015**, *79*, 205–211.
[156] S. L. Pesek, X. Li, B. Hammouda, K. Hong, R. Verduzco, *Macromolecules* **2013**, *46*, 6998–7005.
[157] Z. Li, J. Ma, N. S. Lee, K. L. Wooley, *J. Am. Chem. Soc* **2011**, *133*, 1228–1231.
[158] H. Zhou, J. A. Johnson, *Angew. Chemie - Int. Ed.* **2013**, *52*, 2235–2238.
[159] Y. Li, E. Themistou, J. Zou, B. P. Das, M. Tsianou, C. Cheng, *ACS Macro Lett.* **2012**, *1*, 52–56.
[160] C. Lexer, R. Saf, C. Slugovc, *J. Polym. Sci., Part A Polym. Chem.* **2009**, *47*, 299–305.
[161] E.-H. Kang, I.-H. Lee, T.-L. Choi, *ACS Macro Lett.* **2012**, *1*, 1098–1102.
[162] Y. Xia, B. D. Olsen, J. A. Kornfield, R. H. Grubbs, *J. Am. Chem. Soc.* **2009**, *131*, 18525–18532.
[163] K. Kawamoto, M. Zhong, K. R. Gadelrab, L.-C. Cheng, C. A. Ross, A. Alexander-Katz, J. A. Johnson, *J. Am. Chem. Soc.* **2016**, *138*, 11501–11504.
[164] J. A. Johnson, Y. Y. Lu, A. O. Burts, Y.-H. Lim, M. G. Finn, J. T. Koberstein, N. J. Turro, D. A. Tirrell, R. H. Grubbs, *J. Am. Chem. Soc.* **2011**, *133*, 559–566.
[165] M. Alizadeh, A. F. M. Kilbinger, *Macromolecules* **2018**, *51*, 4363–4369.
[166] G. R. Gossweiler, G. B. Hewage, G. Soriano, Q. Wang, G. W. Welshofer, X. Zhao, S. L. Craig, *ACS Macro Lett.* **2014**, *3*, 216–219.
[167] Y. Chen, A. J. H. Spiering, S. Karthikeyan, G. W. M. Peters, E. W. Meijer, R. P. Sijbesma, **2012**, DOI 10.1038/NCHEM.1358.
[168] B. Cao, N. Boechler, A. J. Boydston, *Polymer (Guildf).* **2018**, *152*, 4–8.
[169] A. Piermattei, S. Karthikeyan, R. P. Sijbesma, *Nat. Chem.* **2009**, *1*, 133–137.
[170] A. L. B. Ramirez, Z. S. Kean, J. A. Orlicki, M. Champhekar, S. M. Elsakr, W. E. Krause, S. L. Craig, *Nat. Chem.* **2013**, *5*, 757–761.
[171] D. W. R. Balkenende, S. Coulibaly, S. Balog, Y. C. Simon, G. L. Fiore, C. Weder, *J. Am. Chem. Soc.* **2014**, *136*, 10493–10498.
[172] J. Li, C. Nagamani, J. S. Moore, S. Moore, *Acc. Chem. Res.* **2015**, *48*, 2181–2190.
[173] M. B. Larsen, A. J. Boydston, *J. Am. Chem. Soc.* **2013**, *135*, 8189–8192.
[174] B. H. Bowser, S. L. Craig, *Polym. Chem.* **2018**, *9*, 3583–3593.
[175] M. J. Kryger, A. M. Munaretto, S. Moore, *J. Am. Chem. Soc.* **2011**, *133*, 18992–18998.
[176] M. T. Ong, J. Leiding, H. Tao, A. M. Virshup, T. J. Martı, **2009**, *9*, 6377–6379.
[177] Z. S. Kean, G. R. Gossweiler, T. B. Kouznetsova, G. B. Hewage, S. L. Craig, *Chem. Commun.* **2015**, *51*, 9157–9160.

[178] J. M. Lenhardt, A. L. Black, S. L. Craig, *J. Am. Chem. Soc.* **2009**, *131*, 10818–10819.
[179] B. Lee, Z. Niu, J. Wang, C. Slebodnick, S. L. Craig, *J. Am. Chem. Soc.* **2015**, *137*, 10826–10832.
[180] J. M. Lenhardt, A. L. Black Ramirez, B. Lee, T. B. Kouznetsova, S. L. Craig, *Macromolecules* **2015**, *48*, 6396–6403.
[181] P. V. R. Schleyer, J. E. Wiliiams, K. R. Blanchard, *J. Am. Chem. Soc.* **1970**, *92*, 2377–2386.
[182] B. H. T. Etsuka, Ã. K. I. Sobe, M. H. Agiwara, *Polym. J.* **2009**, *41*, 643–649.
[183] K. H. Park, R. J. Twieg, R. Ravikiran, L. F. Rhodes, R. A. Shick, D. Yankelevich, A. Knoesen, *Macromolecules* **2004**, *37*, 5163–5178.
[184] B. Liu, Y. Li, A. S. Mathews, Y. Wang, W. Yan, S. Abraham, C. S. Ha, D. W. Park, I. Kim, *React. Funct. Polym.* **2008**, *68*, 1619–1624.
[185] K. R. Gmernicki, E. Hong, C. R. Maroon, S. M. Mahurin, A. P. Sokolov, T. Saito, B. K. Long, *ACS Macro Lett.* **2016**, *5*, 879–883.
[186] N. Belov, R. Nikiforov, L. Starannikova, K. R. Gmernicki, C. R. Maroon, B. K. Long, V. Shantarovich, Y. Yampolskii, *Eur. Polym. J.* **2017**, *93*, 602–611.
[187] J. M. Lenhardt, M. T. Ong, R. Choe, C. R. Evenhuis, T. J. Martinez, S. L. Craig, *Science (80-.).* **2010**, *329*, 1057–60.
[188] P. A. May, N. F. Munaretto, M. B. Hamoy, M. J. Robb, J. S. Moore, *ACS Macro Lett.* **2016**, *5*, 177–180.
[189] M. W. A. Kuijpers, P. D. Iedema, M. F. Kemmere, J. T. F. Keurentjes, *Polymer (Guildf).* **2004**, *45*, 6461–6467.
[190] J. M. Lenhardt, J. W. Ogle, M. T. Ong, R. Choe, T. J. Martinez, S. L. Craig, *J. Am. Chem. Soc.* **2011**, *133*, 3222–3225.
[191] T. G. Fox, P. J. Flory, *J. Appl. Phys.* **1950**, *21*, 581–591.
[192] D. C. Lee, D. L. Sellers, F. Liu, A. J. Boydston, S. H. Pun, **n.d.**
[193] J. Zhou, J. Chen, H. Sun, X. Qiu, Y. Mou, Z. Liu, Y. Zhao, X. Li, Y. Han, C. Duan, et al., *Sci. Rep.* **2014**, *4*, 1–11.
[194] A. M. Martins, G. Eng, S. G. Caridade, F. Mano, R. L. Reis, G. Vunjak-Novakovic, *Biomacromolecules* **2014**, *15*, 635–643.
[195] R. Balint, N. J. Cassidy, S. H. Cartmell, *Acta Biomater.* **2014**, *10*, 2341–2353.
[196] A. Borriello, V. Guarino, L. Schiavo, M. A. Alvarez-Perez, L. Ambrosio, *J. Mater. Sci. Mater Med* **2011**, *22*, 1053–1062.
[197] B. Liu, *Biomacromolecules* **2018**, *19*, 1783–1803.
[198] K. Ronaldson-Bouchard, S. P. Ma, K. Yeager, T. Chen, L. Song, D. Sirabella, K. Morikawa, D. Teles, M. Yazawa, G. Vunjak-Novakovic, *Nature* **2018**, *556*, 239–243.
[199] S. Yoshida, K. Sumomozawa, K. Nagamine, M. Nishizawa, *Macromol. Biosci.* **2019**, *1900060*, 1900060.
[200] B. Xu, T. Bai, A. Sinclair, W. Wang, Q. Wu, F. Gao, H. Jia, S. Jiang, W. Liu, *Mater. Today Chem.* **2016**, *1–2*, 15–22.
[201] A. N. Koppes, K. W. Keating, A. L. McGregor, R. A. Koppes, K. R. Kearns, A. M. Ziemba, C. A. McKay, J. M. Zuidema, C. J. Rivet, R. J. Gilbert, et al., *Acta Biomater.* **2016**, *39*, 34–43.
[202] L. Zhou, L. Fan, X. Yi, Z. Zhou, C. Liu, R. Fu, C. Dai, Z. Wang, X. Chen, P. Yu, et al., *ACS Nano* **2018**, *12*, 10957–10967.
[203] S. Sirivisoot, R. Pareta, B. S. Harrison, *Interface Focus* **2014**, *4*, DOI

10.1098/rsfs.2013.0050.
[204] H. Yuk, B. Lu, X. Zhao, *Chem. Soc. Rev.* **2019**, *48*, 1642–1667.
[205] M. R. Abidian, D. C. Martin, *Adv. Funct. Mater.* **2009**, *19*, 573–585.
[206] M. Liu, N. Xu, W. Liu, Z. Xie, *RSC Adv.* **2016**, *6*, 84269–84275.
[207] J. H. Collier, J. P. Camp, T. W. Hudson, C. E. Schmidt, *J. Biomed. Mater. Res.* **2000**, *50*, 574–84.
[208] A. Mihic, Z. Cui, J. Wu, G. Vlacic, Y. Miyagi, S. H. Li, S. Lu, H. W. Sung, R. D. Weisel, R. K. Li, *Circulation* **2015**, *132*, 772–784.
[209] B. Lu, H. Yuk, S. Lin, N. Jian, K. Qu, J. Xu, X. Zhao, *Nat. Commun.* **2019**, *10*, DOI 10.1038/s41467-019-09003-5.
[210] B. Zhu, S. C. Luo, H. Zhao, H. A. Lin, J. Sekine, A. Nakao, C. Chen, Y. Yamashita, H. H. Yu, *Nat. Commun.* **2014**, *5*, 1–9.
[211] Y. Liu, J. Liu, S. Chen, T. Lei, Y. Kim, S. Niu, H. Wang, X. Wang, A. M. Foudeh, J. B. H. Tok, et al., *Nat. Biomed. Eng.* **2019**, *3*, 58–68.
[212] V. R. Feig, H. Tran, M. Lee, Z. Bao, *Nat. Commun.* **2018**, *9*, 1–9.
[213] J. Y. Lee, C. A. Bashur, A. S. Goldstein, C. E. Schmidt, *Biomaterials* **2009**, *30*, 4325–4335.
[214] J. Han, Q. Wu, Y. Xia, M. B. Wagner, C. Xu, *Stem Cell Res.* **2016**, *16*, 740–750.
[215] A. J. Engler, S. Sen, H. L. Sweeney, D. E. Discher, *Cell* **2006**, *126*, 677–689.
[216] M. E. Jeffords, J. Wu, M. Shah, Y. Hong, G. Zhang, *ACS Appl. Mater. Interfaces* **2015**, *7*, 11053–11061.
[217] C. Zhu, L. Liu, Q. Yang, F. Lv, S. Wang, *Chem. Rev.* **2012**, *112*, 4687–4735.
[218] D. Wang, X. Gong, P. S. Heeger, F. Rininsland, G. C. Bazan, A. J. Heeger, *Proc. Natl. Acad. Sci.* **2002**, *99*, 49–53.
[219] B. Liu, G. C. Bazan, *Chem. Mater.* **2004**, *16*, 4467–4476.
[220] D. Lowe, "A Farewell to Tin | In the Pipeline," can be found under http://blogs.sciencemag.org/pipeline/archives/2007/07/22/a_farewell_to_tin, **2007**.
[221] S. Das, D. P. Chatterjee, R. Ghosh, A. K. Nandi, *RSC Adv.* **2015**, *5*, 20160–20177.
[222] E. Mendez, J. H. Moon, *Chem. Commun.* **2013**, *49*, 6048–6050.
[223] J. Lee, M. Twomey, C. Machado, G. Gomez, M. Doshi, A. J. Gesquiere, J. H. Moon, *Macromol. Biosci.* **2013**, *13*, 913–920.
[224] L. P. Fernando, P. K. Kandel, J. Yu, J. Mcneill, P. Christine, K. a Christensen, *Biomacromolecules* **2011**, *11*, 2675–2682.
[225] D. C. Bott, C. S. Brown, C. K. Chai, N. S. Walker, W. J. Feast, P. J. S Foot, P. D. Calvert, N. C. Billingham, R. H. Friend, *Synth. Met.* **1986**, *14*, 245–269.
[226] P. J. S. Foot, P. D. Calvert, N. C. Billingham, C. S. Brown, N. S. Walker, D. I. James, *Polymer (Guildf).* **1986**, *27*, 448–454.
[227] W. Fischer, F. Stelzer, C. Heller, G. Leising, *Synth. Met.* **1993**, *55–57*, 815–820.
[228] M. Schimetta, F. Stelzer, *Macromolecules* **1994**, *27*, 3769–3772.
[229] M. Schimetta, G. Leising, F. Stelzer, *Synth. Met.* **1995**, *74*, 99–102.
[230] J. Yang, M. Horst, J. A. H. Romaniuk, Z. Jin, L. Cegelski, Y. Xia, *J. Am. Chem. Soc.* **2019**, *141*, 6479–6483.
[231] C. Creutz, *Inorg. Chem.* **1981**, *20*, 4449–4452.
[232] J. J. Warren, T. A. Tronic, J. M. Mayer, *Chem. Rev.* **2010**, *110*, 6961–7001.
[233] L. Q. Flagg, R. Giridharagopal, J. Guo, D. S. Ginger, *Chem. Mater.* **2018**, *30*, 5380–5389.
[234] E. J. Benjamin, P. Muntner, A. Alonso, M. S. Bittencourt, C. W. Callaway, A. P. Carson,

A. M. Chamberlain, A. R. Chang, S. Cheng, S. R. Das, et al., *Heart Disease and Stroke Statistics-2019 Update: A Report From the American Heart Association*, **2019**.
[235] M. Madigan, R. Atoui, *Bioengineering* **2018**, *5*, 1–18.
[236] S. Dimmeler, J. Burchfield, A. M. Zeiher, *Arterioscler. Thromb. Vasc. Biol.* **2008**, *28*, 208–216.
[237] A. Higuchi, N. J. Ku, Y. C. Tseng, C. H. Pan, H. F. Li, S. S. Kumar, Q. D. Ling, Y. Chang, A. A. Alarfaj, M. A. Munusamy, et al., *Lab. Investig.* **2017**, *97*, 1167–1179.
[238] C. S. Ahuja, J. R. Wilson, S. Nori, M. R. N. Kotter, C. Druschel, A. Curt, M. G. Fehlings, *Nat. Rev. Dis. Prim.* **2017**, *3*, DOI 10.1038/nrdp.2017.18.
[239] M. Gazdic, V. Volarevic, C. Randall Harrell, C. Fellabaum, N. Jovicic, N. Arsenijevic, M. Stojkovic, *Int. J. Mol. Sci.* **2018**, *19*, 1–14.
[240] L. Jiang, Y. Wang, Z. Liu, C. Ma, H. Yan, N. Xu, F. Gang, X. Wang, L. Zhao, X. Sun, *Tissue Eng. - Part B Rev.* **2019**, *25*, 398–411.
[241] V. Pinho, F. M. Coelho, G. B. Menezes, D. C. Cara, *Intravital Microscopy to Study Leukocyte Recruitment in Vivo.*, **2011**.
[242] J. Liu, Y. S. Kim, C. E. Richardson, A. Tom, C. Ramakrishnan, F. Birey, T. Katsumata, S. Chen, C. Wang, X. Wang, et al., *Science (80-.).* **2020**, *367*, 1372–1376.
[243] Y. Xi, J. G. Jacot, J. Sun, J. D. Myers, R. M. Nieto, S. Pok, J. Cheng, S. D. Boothe, *Cell Biochem. Biophys.* **2016**, *74*, 527–535.
[244] A. Hasan, A. Khattab, M. A. Islam, K. A. Hweij, J. Zeitouny, R. Waters, M. Sayegh, M. Hossain, A. Paul, *Adv. Sci* **2015**, *2*, DOI 10.1002/advs.201500122.
[245] B. Grigoryan, S. J. Paulsen, D. C. Corbett, D. W. Sazer, C. L. Fortin, A. J. Zaita, P. T. Greenfield, N. J. Calafat, J. P. Gounley, A. H. Ta, et al., *Science (80-.).* **2019**, *364*, 458–464.
[246] A. Saha, T. G. Johnston, R. T. Shafranek, C. J. Goodman, J. G. Zalatan, D. W. Storti, M. A. Ganter, A. Nelson, *ACS Appl. Mater. Interfaces* **2018**, *10*, 13373–13380.
[247] K. Dubbin, Y. Hori, K. K. Lewis, S. C. Heilshorn, *Adv. Healthc. Mater.* **2016**, *5*, 2488–2492.
[248] C. B. Highley, C. B. Rodell, J. A. Burdick, *Adv. Mater.* **2015**, *27*, 5075–5079.
[249] U. N. Lee, J. H. Day, A. J. Haack, R. C. Bretherton, W. Lu, C. A. DeForest, A. B. Theberge, E. Berthier, *Lab Chip* **2020**, DOI 10.1039/c9lc00621d.
[250] A. Saiani, A. Mohammed, H. Frielinghaus, R. Collins, N. Hodson, C. M. Kielty, M. J. Sherratt, A. F. Miller, *Soft Matter* **2009**, *5*, 193–202.
[251] P. R. Patel, R. C. Kiser, Y. Y. Lu, E. Fong, W. C. Ho, D. A. Tirrell, R. H. Grubbs, *Biomacromolecules* **2012**, *13*, 2546–2553.
[252] P. Charlesworth, E. Cotterill, A. Morton, S. G. N. Grant, S. J. Eglen, *Neural Dev.* **2015**, *10*, 1.
[253] C. A. Trujillo, R. Gao, P. D. Negraes, J. Gu, J. Buchanan, S. Preissl, A. Wang, W. Wu, G. G. Haddad, I. A. Chaim, *Cell Stem Cell* **2019**.
[254] Y. D. Xiao, R. Paudel, J. Liu, C. Ma, Z. S. Zhang, S. K. Zhou, *Int. J. Mol. Med.* **2016**, *38*, 1319–1326.
[255] N. Schieda, J. I. Blaichman, A. F. Costa, R. Glikstein, C. Hurrell, M. James, P. Jabehdar Maralani, W. Shabana, A. Tang, A. Tsampalieros, et al., *Can. J. Kidney Heal. Dis.* **2018**, *5*, DOI 10.1177/2054358118778573.
[256] H. V. T. Nguyen, A. Detappe, N. M. Gallagher, H. Zhang, P. Harvey, C. Yan, C. Mathieu, M. R. Golder, Y. Jiang, M. F. Ottaviani, et al., *ACS Nano* **2018**, *12*, 11343–11354.

[257] H. V. T. Nguyen, Q. Chen, J. T. Paletta, P. Harvey, Y. Jiang, H. Zhang, M. D. Boska, M. F. Ottaviani, A. Jasanoff, A. Rajca, et al., *ACS Cent. Sci.* **2017**, *3*, 800–811.
[258] M. A. Sowers, J. R. Mccombs, Y. Wang, J. T. Paletta, S. W. Morton, E. C. Dreaden, M. D. Boska, M. Francesca Ottaviani, P. T. Hammond, A. Rajca, et al., *Nat. Commun.* **2014**, *5*, 1–9.
[259] D. C. Lee, K. N. Guye, R. K. Paranji, D. S. Ginger, S. H. Pun, **n.d.**
[260] B. Schuler, W. A. Eaton, *Curr. Opin. Struct. Biol.* **2008**, *18*, 16–26.
[261] J. I. L. Chen, Y. Chen, D. S. Ginger, *J. Am. Chem. Soc.* **2010**, *132*, 9600–9601.
[262] J. I. L. Chen, H. Durkee, B. Traxler, D. S. Ginger, *Small* **2011**, *7*, 1993–1997.
[263] M. Gränz, N. Erlenbach, P. Spindler, D. B. Gophane, L. S. Stelzl, S. T. Sigurdsson, T. F. Prisner, *Angew. Chemie - Int. Ed.* **2018**, *57*, 10540–10543.
[264] S. M. Kelly, C. Price, Nicholas, *Biochim. Biophys. Acta* **1997**, *1338*, 161–185.
[265] S. M. V. Freund, K. B. Wong, A. R. Fersht, *Proc. Natl. Acad. Sci. U. S. A.* **1996**, *93*, 10600–10603.
[266] O. Altintas, P. Gerstel, N. Dingenouts, C. Barner-Kowollik, *Chem. Commun.* **2010**, *46*, 6291–6293.
[267] N. Hosono, M. A. J. Gillissen, Y. Li, S. S. Sheiko, A. R. A. Palmans, E. W. Meijer, *J. Am. Chem. Soc.* **2013**, *135*, 501–510.
[268] J. Willenbacher, O. Altintas, P. W. Roesky, C. Barner-Kowollik, *Macromol. Rapid Commun.* **2014**, *35*, 45–51.
[269] G. Yilmaz, V. Uzunova, R. Napier, C. Remzi Becer, *Biomacromolecules* **2018**, *19*, 3040–3047.
[270] Y. Inoue, P. Kuad, Y. Okumura, Y. Takashima, H. Yamaguchi, A. Harada, *J. Am. Chem. Soc.* **2007**, *129*, 6396–6397.
[271] B. V. K. J. Schmidt, N. Fechler, J. Falkenhagen, J. F. Lutz, *Nat. Chem.* **2011**, *3*, 234–238.
[272] S. Jia, W.-K. Fong, B. Graham, B. J. Boyd, *Chem. Mater.* **2018**, *30*, 2873–2887.
[273] H. M. D. Bandara, S. C. Burdette, *Chem. Soc. Rev.* **2012**, *41*, 1809–1825.
[274] D. Wang, M. Wagner, H. J. Butt, S. Wu, *Soft Matter* **2015**, *11*, 7656–7662.
[275] Y. Wang, N. Ma, Z. Wang, X. Zhang, *Angew. Chemie - Int. Ed.* **2007**, *46*, 2823–2826.
[276] H. Asanuma, X. Liang, H. Nishioka, D. Matsunaga, M. Liu, M. Komiyama, *Nat. Protoc.* **2007**, *2*, 203–212.
[277] D. Tarn, D. P. Ferris, J. C. Barnes, M. W. Ambrogio, J. F. Stoddart, J. I. Zink, *Nanoscale* **2014**, *6*, 3335.
[278] D. P. Ferris, Y.-L. Zhao, N. M. Khashab, H. A. Khatib, J. F. Stoddart, J. I. Zink, *J. Am. Chem. Soc.* **2009**, *131*, 1686–1688.
[279] Q. Bian, S. Chen, Y. Xing, D. Yuan, L. Lv, G. Wang, *Acta Biomater.* **2018**, *76*, 39–45.
[280] S. Ito, H. Akiyama, M. Mori, M. Yoshida, H. Kihara, *Macromol. Chem. Phys.* **2019**, *1900105*, 1900105.
[281] I. Tomatsu, A. Hashidzume, A. Harada, *Macromolecules* **2005**, *38*, 5223–5227.
[282] S. Samanta, A. Babalhavaeji, M. X. Dong, G. A. Woolley, *Angew. Chemie - Int. Ed.* **2013**, *52*, 14127–14130.
[283] A. M. Sanchez, M. Barra, R. H. De Rossi, *J. Org. Chem.* **1999**, *64*, 1604–1609.
[284] M. Azuki, K. Morihashi, T. Watanabe, O. Takahashi, O. Kikuchi, *J. Mol. Struct. THEOCHEM* **2001**, *542*, 255–262.
[285] H. J. Lee, P. T. Le, H. J. Kwon, K. D. Park, *J. Mater. Chem. B* **2019**, *7*, 3374–3382.
[286] E. Sabadini, T. Cosgrove, F. do C. Egídio, *Carbohydr. Res.* **2006**, *341*, 270–274.

[287] H.-J. Schneider, F. Hacket, V. Rüdiger, H. Ikeda, *Chem. Rev.* **1998**, *98*, 1755–1785.
[288] E. R. Talaty, J. C. Fargo, *Chem. Commun.* **1967**, 65–66.
[289] H. Rau, E. Lüddecke, *J. Am. Chem. Soc.* **1982**, *104*, 1616–1620.
[290] T. Ikegami, N. Kurita, H. Sekino, Y. Ishikawa, *J. Phys. Chem. A* **2003**, *107*, 4555–4562.
[291] S. Samai, D. J. Bradley, T. L. Y. Choi, Y. Yan, D. S. Ginger, *J. Phys. Chem. C* **2017**, *121*, 6997–7004.
[292] Y. Yan, X. Wang, J. I. L. Chen, D. S. Ginger, *J. Am. Chem. Soc.* **2013**, *135*, 8382–8387.
[293] P. Bortolus, S. Monti, *J. Phys. Chem.* **1987**, *91*, 5046–5050.
[294] P. D. Townsend, R. H. Friend, *Phys. Rev. B* **1989**, *40*, 3112–3120.
[295] S. Blanc, T. Pigot, C. Cugnet, R. Brown, S. Lacombe, T. Miyashi, E. Oliveros, C. Cantau, P. Saint-Cricq, *Phys. Chem. Chem. Phys.* **2010**, *12*, 11280.
[296] L. Pascual, D. Dunford, A. Goetz, K. Ogawa, A. Boydston, *Synlett* **2016**, *27*, 759–762.
[297] S. S. Jayanthi, P. Ramamurthy, *Phys. Chem. Chem. Phys.* **1999**, *1*, 4751–4757.
[298] D. P. Hari, B. König, *Chem. Commun.* **2014**, *50*, 6688–6699.
[299] Y. Du, R. M. Pearson, C.-H. Lim, S. M. Sartor, M. D. Ryan, H. Yang, N. H. Damrauer, G. M. Miyake, *Chem. - A Eur. J.* **2017**, DOI 10.1002/chem.201702926.
[300] J. C. Theriot, B. G. McCarthy, C. Lim, G. M. Miyake, *Macromol. Rapid Commun.* **2017**, *201700040*, 1–12.
[301] V. Kottisch, Q. Michaudel, B. P. Fors, *J. Am. Chem. Soc* **2016**, *138*, 15535–15538.
[302] G. I. Peterson, J. J. Schwartz, D. Zhang, B. M. Weiss, M. A. Ganter, D. W. Storti, A. J. Boydston, *ACS Appl. Mater. Interfaces* **2016**, 29037–29043.
[303] B. Adzima, C. Kloxin, C. DeForest, K. Anseth, C. Bowman, *Macromol. Rapid Commun.* **2012**, 1–5.
[304] J. Tan, D. Liu, Y. Bai, C. Huang, X. Li, J. He, Q. Xu, L. Zhang, *Macromolecules* **n.d.**, DOI 10.1021/acs.macromol.7b01219.
[305] K. A. Ogawa, A. E. Goetz, A. J. Boydston, *J. Am. Chem. Soc.* **2015**, *137*, 1400–1403.
[306] A. E. Goetz, A. J. Boydston, *J. Am. Chem. Soc.* **2015**, *137*, 7572–7575.
[307] S. Honda, T. Yamamoto, Y. Tezuka, *J. Am. Chem. Soc.* **2010**, *132*, 10251–10253.
[308] E. Minatti, P. Viville, R. Borsali, M. Schappacher, A. Deffieux, R. Lazzaroni, *Macromolecules* **2003**, *36*, 4125–4133.
[309] D. J. Orrah, J. A. Semlyen, S. B. Ross-Murphy, *Polymer (Guildf).* **1988**, *29*, 1455–1458.
[310] C. D. Roland, H. Li, K. A. Abboud, K. B. Wagener, A. S. Veige, *Nat. Chem.* **2016**, *8*, 791–796.
[311] S. von Kugelgen, D. E. Bellone, R. R. Cloke, W. S. Perkins, F. R. Fischer, *J. Am. Chem. Soc.* **2016**, *138*, 6234–6239.
[312] Q. Tang, Y. Wu, P. Sun, Y. Chen, K. Zhang, *Macromolecules* **2014**, *47*, 3775–3781.
[313] F. Kopp, M. A. Marahiel, *Nat. Prod. Rep.* **2007**, *24*, 735–749.
[314] D. Ye, A. J. Shuhendler, L. Cui, L. Tong, S. S. Tee, G. Tikhomirov, D. W. Felsher, J. Rao, *Nat. Chem.* **2014**, *6*, 519–526.
[315] M. Zhang, Y. Wu, Z. Liu, J. Li, L. Huang, K. Zhang, *Macromol. Rapid Commun.* **2019**, *1900598*, 1–6.
[316] Z. Jia, M. J. Monteiro, *J. Polym. Sci., Part A Polym. Chem.* **2012**, *50*, 2025–2097.
[317] C. Bielawski, D. Benitez, R. Grubbs, *Sci. Mag.* **2002**, *297*, 2041–2044.
[318] A. J. Boydston, Y. Xia, J. A. Kornfield, I. A. Gorodetskaya, R. H. Grubbs, *J. Am. Chem. Soc.* **2008**, *130*, 12775–12782.
[319] A. J. Boydston, T. W. Holcombe, D. A. Unruh, J. M. J Fré chet, R. H. Grubbs, M.

Beckman, *J. Am. Chem. Soc.* **2009**, *131*, 5388–5389.
[320] P. G. Gassman, S. J. Burns, K. B. Pfister, *J. Org. Chem.* **1993**, *58*, 1449–1457.
[321] M. Riener, D. A. Nicewicz, *Chem. Sci.* **2013**, *4*, 2625–2629.
[322] T. Miura, S. Kim, Y. Kitano, M. Tada, K. Chiba, *Angew. Chemie - Int. Ed.* **2006**, *45*, 1461–1463.
[323] B. E. Lynde, R. L. Maust, P. Li, D. C. Lee, R. Jasti, A. J. Boydston, *Mater. Chem. Front.* **2020**, *4*, 252–256.
[324] O. Nuyken, S. D. Pask, *Polymers (Basel).* **2013**, *5*, 361–403.
[325] H. Unsal, S. Onbulak, F. Calik, M. Er-Rafik, M. Schmutz, A. Sanyal, J. Rzayev, *Macromolecules* **2017**, *50*, 1342–1352.
[326] J. A. Johnson, Y. Y. Lu, A. O. Burts, Y. Xia, A. C. Durrell, D. A. Tirrell, R. H. Grubbs, *Macromolecules* **2010**, *43*, 10326–10335.
[327] Y. Hu, X. Li, A. W. Lang, Y. Zhang, S. R. Nutt, *Polym. Degrad. Stab.* **2016**, *124*, 35–42.
[328] Y. Wang, L. Zhang, J. Sun, J. B. Bao, Z. Wang, L. Ni, *Ind. Eng. Chem. Res.* **2017**, *56*, 4750–4757.
[329] H. Martinez, N. Ren, M. E. Matta, M. A. Hillmyer, *Polym. Chem.* **2014**, *5*, 3507–3532.
[330] B. R. Elling, J. K. Su, Y. Xia, *Chem. Commun.* **2016**, *52*, 9097–9100.
[331] P. Hodge, *Chem. Rev.* **2014**, *114*, 2278–2312.
[332] C. Y. Tastard, P. Hodge, A. Ben-Haida, M. Dobinson, *React. Funct. Polym.* **2006**, *66*, 93–107.
[333] J. H. Swisher, J. A. Nowalk, T. Y. Meyer, *Polym. Chem.* **2019**, *10*, 244–252.
[334] J. A. Berrocal, L. M. Pitet, M. M. L. Nieuwenhuizen, L. Mandolini, E. W. Meijer, S. Di Stefano, *Macromolecules* **2015**, *48*, 1358–1363.
[335] L.-L. Deng, L.-X. Guo, B.-P. Lin, X.-Q. Zhang, Y. Sun, H. Yang, *Polym. Chem.* **2016**, *7*, 5265–5272.
[336] Y. Yang, T. M. Swager, *Macromolecules* **2007**, *40*, 7437–7440.
[337] W. R. Gutekunst, C. J. Hawker, *J. Am. Chem. Soc.* **2015**, *137*, 8038–8041.
[338] Y.-J. Miao, G. C. Bazan, *Macromolecules* **1994**, *27*, 1063–1064.
[339] A. M. Spring, C.-Y. Yu, M. Horie, M. L. Turner, *Chem. Commun.* **2009**, 2676–2678.
[340] C.-Y. Yu, J. W. Kingsley, D. G. Lidzey, M. L. Turner, *Macromol. Rapid Commun.* **2009**, *30*, 1889–1892.
[341] S.-W. Chang, M. Horie, *Chem. Commun.* **2015**, *51*, 9113–9116.
[342] E. R. Darzi, B. M. White, L. K. Loventhal, L. N. Zakharov, R. Jasti, *J . Am. Chem. Soc.* **2017**, *139*, 3106–3114.
[343] Y. Xu, W. L. Xu, M. D. Smith, L. S. Shimizu, *RSC Adv.* **2014**, *4*, 1675–1682.
[344] D. Maker, C. Maier, K. Brodner, U. Bunz, D. Mäker, C. Maier, K. Brödner, U. Bunz, *ACS Macro Lett.* **2014**, *3*, 415–418.
[345] R. Adhikary, C. A. Barnes, R. L. Trampel, S. J. Wallace, T. W. Kee, J. W. Petrich, *J. Phys. Chem. B* **2011**, *115*, 10707–10714.
[346] L. W. Chan, X. Wang, H. Wei, L. D. Pozzo, N. J. White, S. H. Pun, *Sci. Transl. Med.* **2015**, *7*, DOI 10.1126/scitranslmed.3010383.
[347] J. K. Kammeyer, A. P. Blum, L. Adamiak, M. E. Hahn, N. C. Gianneschi, *Polym. Chem.* **2013**, *4*, 3929–3933.

VITA

After coming to the United States from South Korea when he was 5, Daniel was raised in New York City. He later attended Cornell University where he received a BA in chemistry and psychology. For his undergraduate research, he studied the effects of different allosteric modulators on the single channel kinetics of glutamate receptors with Prof. Linda Nowak. He then moved to New Orleans to work as a chemist in the petrochemical industry for two years before starting his PhD with Prof. AJ Boydston in Autumn 2016. Starting in 2018, Dan continued his Ph. D. under Prof. Suzie H. Pun. Outside of lab, Daniel plays volleyball, coaches policy debate at UW, and enjoys traveling.